HYDROGEOMORPHIC CONTROLS ON BENTHIC LIGHT AVAILABILITY IN RIVERS

Jason Paul Julian

A dissertation submitted to the faculty of the University of North Carolina at Chapel Hill in partial fulfillment of the requirements for the degree of Doctor of Philosophy in the Department of Geography.

Chapel Hill
2007

Approved by:

Martin W. Doyle

Lawrence E. Band

Peter J. Robinson

Emily H. Stanley

Stephen C. Whalen

ABSTRACT

Julian, J.P., Ph.D., University of North Carolina at Chapel Hill, August 2007.
Hydrogeomorphic Controls on Light Availability in Rivers
(Under the direction of Martin W. Doyle)

Light is vital to the dynamics of aquatic ecosystems. It drives photosynthesis and photochemical reactions, affects thermal structure, and influences the behavior of aquatic biota. While the influence of hydrology and geomorphology on other ecosystem-limiting factors have been well studied (e.g., habitat, nutrient cycling), the more fundamental limitation of light availability has received much less attention. In this thesis, I analyzed and quantified the hydrogeomorphic controls on benthic (or riverbed) light availability using a combination of meta-analyses, field studies, laboratory studies, and model simulations. I developed a benthic light availability model (BLAM) that predicts photosynthetically active radiation (PAR) at the riverbed (E_{bed}) by calculating the amount of above-canopy PAR that is attenuated by all five hydrogeomorphic controls: topography, riparian vegetation, channel geometry, optical water quality, and hydrologic regime. This model was used to assess and characterize broad spatial patterns of E_{bed} and temporal variations associated with variable flow conditions for a wide range of rivers. BLAM was also used to assess the effects of riparian deforestation and degraded optical water quality associated with agriculturalization on E_{bed}. BLAM is the first model to quantify E_{bed} using all five hydrogeomorphic controls, and thus provides a new tool that can be used to investigate the role of light in river ecosystem dynamics and establish light

availability targets in water resource management. BLAM also provides a framework for future models to characterize spatiotemporal variations of ultraviolet and infrared radiation in rivers.

To Victoria, who has shared my love for rivers and has supported me in everyway possible.

ACKNOWLEDGEMENTS

This research was primarily funded by the National Research Initiative of the USDA Cooperative State Research, Education, and Extension Service (CSREES grant # 2004-35102-14793). Additional support was provided by NSF grant DEB-0321559US, U.S. Fish and Wildlife Service, and Restoration Systems, LLC. Special thanks to Bill Ginsler and the town of Big Spring, WI for site access. Helen Sarakinos of the Wisconsin River Alliance and Marty Melchior and Andy Selle of Inter-fluve, Inc. were also instrumental in research logistics.

I am grateful for the assistance provided by numerous faculty, staff, and students from the Departments of Geography, Environmental Science & Engineering, and Ecology at the University of North Carolina, and from the Center for Limnology at the University of Wisconsin. I am especially appreciative to those that helped with lab and fieldwork: Derek Anderson, Richelle Baroudi, Zack Feiner, Victoria Julian, Ryan Kroiss, Mark Lochner, Noah Lottig, Steve Neary, Nick Pollite, Hollis Rhinelander, Matt Smith, Leah Vandenbusch, Sally Whisler, Sarah Zahn, and anybody else I forgot. To my fellow rivergeeks, Adam Riggsbee, Steve Powers, Daisy Small, Rebecca Manners, Erich Hester, and Scott Ensign, thank you for sharing many good times with me outdoors and some not so good times indoors. May you all be blessed with beautiful field sites that are free of poison ivy and poisonous snakes.

To my guiding light and smashing hammer, Martin Doyle, I am forever grateful for your advisement and professional development. Emily Stanley, your wisdom, guidance, and generosity will never be forgotten. I am truly fortunate to have two extraordinary mentors. I am also appreciative of my other three committee members, Larry Band, Peter Robinson, and Steve Whalen, who provided the knowledge and direction that helped shape this research. A special thanks to Steve Whalen and Bob Wetzel for allowing me to use their resources for lab analyses.

PREFACE

Let there be light.

God
Genesis 1:3

You cannot step twice into the same river; for other waters are continually flowing in.

Heraclitus

I keep the subject of my inquiry constantly before me, and wait till the first dawning opens gradually, by little and little, into a full and clear light.

Isaac Newton

TABLE OF CONTENTS

LIST OF TABLES

LIST OF FIGURES

LIST OF SYMBOLS AND ABBREVIATIONS

α	Empirical coefficient for relating y to Q
a	Total absorption coefficient (m^{-1})
a_d	Absorption coefficient of dissolved constituents (m^{-1})
a_p	Absorption coefficient of particulates (m^{-1})
a_w	Absorption coefficient of pure water (m^{-1})
a_{440}	Absorption coefficient at 440 nm (m^{-1})
AMSL	Above Mean Sea Level
ANOVA	ANalysis Of VAriance model
β	Empirical coefficient for relating K_d to Q
b	Total scattering coefficient (m^{-1})
b_d	Scattering coefficient of dissolved constituents (m^{-1})
b_p	Scattering coefficient of particulates (m^{-1})
b_w	Scattering coefficient of pure water (m^{-1})
b_{POM}	Scattering coefficient of particulate organic matter (m^{-1})
BLAM	Benthic Light Availability Model
BSC	Big Spring Creek
BR	Baraboo River
c	Total light (beam) attenuation coefficient (m^{-1})
c_d	Light attenuation coefficient of dissolved constituents (m^{-1})
c_p	Light attenuation coefficient of particulates (m^{-1})
c_w	Light attenuation coefficient of pure water (m^{-1})
chl-a	Chlorophyll-a (µg/L)

CDOM	Chromophoric dissolved organic matter
D	Absorbance ($\log_{10} \Phi_0/\Phi$)
D	Kolmogorov-Smirnov test statistic for a normal distribution
DEM	Digital Elevation Model
DOC	Dissolved organic carbon (mg/L)
DR	Deep River
E_0	Below-water surface PAR (mol/m^2/day)
E_{bed}	Benthic PAR (mol/m^2/day)
E_{can}	Above-canopy PAR (mol/m^2/day)
E_s	Above-water surface PAR (mol/m^2/day)
F	Filtered water sample
GLA	Gap Light Analyzer software
IR	Infrared solar radiation
K	b_{POM}/a_{POM}
K_d	Diffuse attenuation coefficient for downward PAR (m^{-1})
LAI	Leaf Area Index
LCM	Land-cover Classification Map
NTU	Nephelometric turbidity units
OWQ	Optical water quality
Φ_0	Incident radiant flux (mol/s)
Φ	Transmitted radiant flux (mol/s)
PAR	Photosynthetically active radiation, 400-700 nm
PHYTO	Phytoplankton (µg/L)

POM	Particulate organic matter (mg/L)
PPFD	Photosynthetic photon flux density (µmol/m^2/s)
Q	Discharge or volume of water per time (m^3/s)
Q_{peak}	Maximum discharge during a flood
Q_{ds}	Discharge of river just downstream of a tributary (m^3/s)
Q_{trib}	Discharge of tributary just before confluence with mainstem (m^3/s)
Q_{us}	Discharge of river just upwnstream of a tributary (m^3/s)
r	Reflection coefficient
r^2	Coefficient of determination
RCC	River Continuum Concept
s	Shading coefficient
s_t	Topographic shading coefficient
s_v	Vegetation shading coefficient
SCH	Standard cell holder; used to obtain a
SS	Suspended Sediment (mg/L)
T_n	Turbidity (NTU)
TCH	Turbidity cell holder; used to obtain c
TSS	Total suspended solids (mg/L)
UF	Unfiltered water sample
UV	Ultraviolet solar radiation
υ	Empirical exponent for relating y to Q
VIS	Visible solar radiation
ω	Empirical exponent for relating K_d to Q

WR	Wisconsin River
X	Apparent absorption coefficient (m^{-1})
y	Water depth (m)
y_{BD}	Black disk visibility distance (m)
z_{SD}	Secchi disk visibility depth (m)

CHAPTER I. INTRODUCTION

> "Meeting human water needs and sustaining the services that aquatic ecosystems provide remain one of the greatest challenges of the 21st century."
> - Palmer & Bernhardt 2006

FLUVIAL ECOSYSTEMS AND HYDROGEOMORPHIC CONTROLS

Fluvial ecosystems are shaped by the hydrologic and geomorphic template (Hynes 1970, Poff and Ward 1990). This hydrogeomorphic template includes basin topography, land cover, channel geometry, sediment size, and the quantity and quality of water. The variability of these controls, together with their interdependent relationships, create fluvial ecosystems that are dynamic over both space and time. Some researchers have gone so far to say that the multiplicity and variability of hydrogeomorphic controls prevent generalizations on ecosystem dynamics (Phillips 2007). Yet, scientists are expected to decipher these general trends and develop predictive models that can be used to preserve and rehabilitate anthropogenic damaged aquatic ecosystems (Palmer and Bernhardt 2006).

An emerging theme in fluvial ecology is to predict spatiotemporal trends of ecosystem variables using empirical correlations to hydrogeomorphic controls. Examples include correlating organic matter and nutrient transport to discharge (Doyle et al. 2005), fish distribution to suspended sediment concentration (Burcher et al. 2007), macroinvertebrate distribution to channel geometry and substrate (Burcher et al. 2007), and mussel distribution to channel gradient (Gangloff and Feminella 2007). While this

coupling of hydrogeomorphology and fluvial ecology has led to several key contributions in the field (e.g., nutrient spiraling concept; Newbold et al. 1982), we have only begun to understand how spatiotemporal variations in hydrogeomorphic controls structure fluvial ecosystems.

ROLE OF LIGHT

The influence of hydrology and geomorphology on ecosystem-limiting factors has been well studied, particularly habitat availability and nutrient cycling (e.g., Doyle and Stanley 2006, Strayer et al. 2006); however, the more fundamental limitation of light availability has received much less attention. Light is the primary energy source of rivers, driving photosynthesis and photochemical reactions, dictating thermal fluctuations, and influencing the behavior of aquatic biota (Wetzel 2001, p. 49). Davies-Colley et al. (2003) argues that the neglect of riverine light studies can be attributed to (i) light not being widely accepted as a limiting resource in riverine ecosystems, (ii) boundary conditions (banks, riparian vegetation) making ambient light measurements challenging, and (iii) the optical water quality of rivers being highly variable and difficult to characterize. The little information that is available on light in rivers is derived mostly from New Zealand rivers under predominantly baseflow conditions, leaving substantial limitations in our understanding of the temporal and spatial availability of light in rivers.

PURPOSES AND METHODS

The objectives of this research were to investigate the hydrologic and geomorphic controls of benthic light availability for a wide range of rivers, characterize their spatial

and temporal variability, and develop a model for predicting benthic light availability using readily available or easily collected data. The fundamental questions addressed within this thesis were:

1. What are the dominant controls of benthic light availability in rivers?
2. Do spatial and temporal variations in benthic light availability follow general trends?
3. How is benthic light availability affected by anthropogenic disturbances?

The above questions were answered using a combination of meta-analyses, field studies, laboratory studies, and model simulations. Field studies were conducted on four rivers: Big Spring Creek – a 2nd-order spring-fed stream in central Wisconsin; Deep River – a 6th-order river in central North Carolina; Baraboo River – a 6th-order river in central Wisconsin , and Wisconsin River – a 7th-order river that empties into the Mississippi River. Laboratory studies were performed on water samples collected from these four rivers.

STRUCTURE OF DISSERTATION

Papers Presented in Chapters

This thesis is written in the form of 3 chapters, all of which are independent manuscripts for journal submission, followed by a conclusion. There is some repetition of introductory material, but this was done so that the manuscripts could stand alone.

Chapter 2 is a comprehensive treatment on the optical water quality of rivers. First, this chapter reviews all the constituents in rivers that influence optical water quality, focusing on the spatiotemporal trends of each constituent. Second, it presents a

new method for partitioning the light attenuation coefficient into its constituent fractions. Third, it compares the baseflow optical water quality of four rivers with vastly different physical characteristics. Fourth, it analyzes spatial and temporal distributions of optical water quality for the four rivers. Fifth, it calculates an optical water quality budget for one of the rivers based on tributary inputs. Finally, this chapter compares spatial trends (i.e., along the river continuum from headwaters to mouth) of optical water quality between American and New Zealand rivers, paying particular attention to the magnitude and shape of the longitudinal distributions.

Chapter 3 introduces the reach-scale Benthic Light Availability Model (BLAM), which calculates the amount of daily photosynthetically active radiation (PAR) that reaches the riverbed (E_{bed}; in mol/m^2/day). First, it describes model development, detailing how each hydrogeomorphic control influences benthic light availability. Second, it presents model output for two rivers with vastly different physical characteristics: Big Spring Creek and Deep River. Third, it assesses model accuracy by comparing modeled E_{bed} to in situ measurements of E_{bed}. Finally, it identifies the dominant controls on benthic light availability in rivers by comparing correlations between the hydrogeomorphic controls and E_{bed}.

Chapter 4 demonstrates how BLAM can be applied to the basin-scale by using a GIS framework. This GIS-based model was used to calculate E_{bed} along the 187-km mainstem of the Baraboo River, Wisconsin . This chapter also uses three model simulations to demonstrate how various levels of agricultural land conversion affect E_{bed} along the river continuum. Additionally, this chapter discusses some of the ecological implications of altered light regimes in rivers.

Manuscript Details

CHAPTER 2: Julian, J.P., M.W. Doyle, S.M. Powers, E.H. Stanley, and J.A. Riggsbee. Optical water quality in rivers. Water Resources Research.

CHAPTER 3: Julian, J.P., M.W. Doyle, and E.H. Stanley. Empirical modeling of light availability in rivers. Journal of Geophysical Research - Biogeosciences.

CHAPTER 4: Julian, J.P., M.W. Doyle, and E.H. Stanley. Light along the river continuum. Ecological Applications.

REFERENCES

Burcher, C. L., H. M. Valett, and E. F. Benfield. 2007. The land-cover cascade: Relationships coupling land and water. Ecology **88**:228-242.

Davies-Colley, R. J., W. N. Vant, and D. G. Smith. 2003. Colour and Clarity of Natural Waters. Ellis Horwood, New York.

Doyle, M. W., and E. H. Stanley. 2006. Exploring potential spatial-temporal links between fluvial geomorphology and nutrient-periphyton dynamics in streams using simulation models. Annals of the Association of American Geographers **96**:687-698.

Doyle, M. W., E. H. Stanley, D. L. Strayer, R. B. Jacobson, and J. C. Schmidt. 2005. Effective discharge analysis of ecological processes in streams. Water Resources Research **41**:1-16.

Gangloff, M. M., and J. W. Feminella. 2007. Stream channel geomorphology influences mussel abundance in southern Appalachian streams, USA. Freshwater Biology **52**:64-74.

Hynes, H. B. N. 1970. The Ecology of Running Waters. University of Toronto Press, Toronto.

Newbold, J. D., P. J. Mulholland, J. W. Elwood, and R. V. O'Neill. 1982. Organic carbon spiralling in stream ecosystems. Oikos **38**:266-272.

Palmer, M. A., and E. S. Bernhardt. 2006. Hydroecology and river restoration: Ripe for research and synthesis. Water Resources Research **42**:W03S07, doi:10.1029/2005WR004354.

Phillips, J. D. 2007. The perfect landscape. Geomorphology **84**:159-169.

Poff, N. L., and J. V. Ward. 1990. Physical habitat template of lotic systems: Recovery in the context of historical pattern of spatiotemporal heterogeneity. Environmental Management **14**:629-645.

Strayer, D. L., H. M. Malcolm, R. E. Bell, S. M. Carbotte, and F. O. Nitsche. 2006. Using geophysical information to define benthic habitats in a large river. Freshwater Biology **51**:25-38.

Wetzel, R. G. 2001. Limnology: Lake and River Ecosystems. Academic Press, San Diego.

CHAPTER II. OPTICAL WATER QUALITY IN RIVERS

1. INTRODUCTION

Optical water quality (OWQ) is "the extent to which the suitability of water for its functional role in the biosphere or the human environment is determined by its optical properties" (Kirk 1988). Accordingly, OWQ governs the behavior of photons in aquatic ecosystems and determines underwater light quantity (number of photons) and quality (wavelength). It therefore influences primary productivity, water temperature, faunal movements, photo-degradation of organic matter, and numerous other photo-assisted biogeochemical reactions (Wetzel 2001). Changes in OWQ can indicate important environmental trends such as eutrophication, sedimentation, or general water quality degradation. Additionally, OWQ is a key component of aesthetics, recreation, and management of water resources. Thus, OWQ is a master variable that both reflects prevailing environmental conditions and dictates multiple aspects of structure and function in these ecosystems.

The significance of light has long been recognized in oceans, estuaries, and lakes, but has mostly been dealt with in a descriptive, qualitative fashion in rivers. Of the body of work that exists on rivers, most address only individual influences such as light attenuation by sediments. Further, its high variability and difficulty of characterization in rivers (Davies-Colley et al. 2003) has prevented a comprehensive understanding of

riverine OWQ. The lack of data persists despite the central role ascribed to light availability in fluvial ecology models such as the River Continuum Concept (RCC; Vannote et al. 1980). Nonetheless, the eclectic nature of OWQ and the ease of field measurement has resulted in its adoption as a water quality standard in some countries (Davies-Colley et al. 2003).

The goal of this paper is to provide a comprehensive overview of the controls and the spatial and temporal dynamics of riverine OWQ, and place this understanding in the context of prevailing fluvial ecosystem theory. First, the constituents influencing OWQ are reviewed, focusing on the spatiotemporal trends in rivers. Second, a new method is developed for partitioning the light attenuation coefficient into its constituent fractions. Third, we compare baseflow OWQ between four rivers with vastly different physical characteristics to illustrate its inter-site variability. Fourth, we analyze the spatial and temporal distributions of OWQ for the four rivers. Fifth, we quantify an OWQ budget for one of the rivers, including tributary inputs. Finally, available data are synthesized to identify general spatial trends robust across broad geographic areas.

2. COMPONENTS AND CONTROLS OF OPTICAL WATER QUALITY

When light enters water, it has one of two fates: absorption or scattering. Scattering is the predominant influence on the quantity of light, while absorption is the predominant influence on the quality of light, with the caveat that increased scattering increases the probability of absorption (Kirk 1994). The relative quantities of scattering and absorption are expressed by an absorption coefficient (a) and a scattering coefficient (b), which respectively are the fraction of radiant flux (light per time) that is absorbed and

scattered by an infinitesimally thin layer of aquatic medium. Together, *a* and *b* establish the light (beam) attenuation coefficient (*c*), the fraction of radiant flux that is lost over the infinitesimally thin layer of aquatic medium, in m^{-1}:

$$c = a + b \tag{2.1}$$

Accordingly, *c* is low for rivers that are optically clear, and high for turbid rivers. The amount of radiant flux at depth (Φ) in the aquatic medium is derived using *c* in the Beer-Lambert law:

$$\Phi = \Phi_0 * e^{-cr} \tag{2.2}$$

where Φ_0 is incident radiant flux in mol/s (1 mol = 6.02 x 10^{23} photons), and *r* is the pathlength in m. In rivers, the amount of light at depth is ultimately dictated by the diffuse attenuation coefficient (K_d), which accounts for solar zenith angle, the ratio of diffuse to direct solar radiation, and diffuse light within the water column. K_d and *c* are directly proportional (Kirk 1994), and thus trends in K_d follow those of *c*. In examining the OWQ of rivers, however, only the values of *a*, *b*, and *c* are of interest because they are the inherent optical properties (i.e., not dependent on the solar radiation field) of the aquatic medium.

Any component of the water column can absorb and scatter light, but there are only five that significantly attenuate light in rivers: water (w), chromophoric dissolved organic matter (CDOM), suspended sediment (SS), particulate organic matter (POM), and phytoplankton (PHYTO) (Davies-Colley et al. 2003). Because light attenuation is an additive process (Kirk 1994), the sum of light attenuation by each one of these components sets the OWQ of a river such that:

$$c = c_w + c_{CDOM} + c_{SS} + c_{POM} + c_{PHYTO} \tag{2.3}$$

$$c = c_w + c_d + c_p \quad (2.4)$$

where c_d is the attenuation coefficient of the dissolved constituents (c_{CDOM}) and c_p is the attenuation coefficient of the particulate constituents ($c_{SS} + c_{POM} + c_{PHYTO}$). We now briefly review the drivers of spatial and temporal variability in each of these attenuation coefficients based on previous literature.

2.1. Pure Water

Water molecules scatter and absorb light; however, the amount of scattering by water in rivers is negligible relative to the total light attenuation by all five components (Davies-Colley et al. 2003). The spectral absorption by water follows a parabolic trend where absorption is high for short (ultraviolet, UV) and long wavelengths (infrared, IR), and low for medium wavelengths (visible, VIS). The light attenuation coefficient of pure water (c_w) for photosynthetically active radiation (PAR: 400 – 700 nm) is 0.150 m^{-1}, with 0.148 and 0.002 m^{-1} being attributed to the absorption coefficient of pure water (a_w) and the scattering coefficient of pure water (b_w), respectively (Buiteveld et al. 1994). Because of their very low light attenuation coefficient, water molecules are only a significant contributor to total light attenuation in the clearest rivers (e.g., undisturbed, spring-fed headwater streams), where there is very little CDOM, SS, POM, or PHYTO.

2.2. Chromophoric Dissolved Organic Matter (CDOM)

Chromophoric dissolved organic matter is the only dissolved constituent of rivers that is effective at attenuating light. The spectral absorption by CDOM is highest at short wavelengths (UV) and decreases exponentially with increasing wavelength. Like water

molecules, scattering by CDOM in rivers is negligible. CDOM originates mainly from the decomposition of plant tissue into dissolved humic substances that contain chromophores, the molecular components that absorb light. CDOM is not a commonly analyzed constituent in river studies, but given that CDOM concentrations correlate well with dissolved organic carbon (DOC) concentrations (Wetzel 2001), we rely on the spatial and temporal trends of DOC to illustrate the spatiotemporal trends of CDOM. Most of the DOC present in rivers is delivered by terrestrial groundwater inputs, but can also be derived from canopy throughfall, exudates of aquatic vegetation, in-channel detritus leaching, and animal excretions (Webster et al. 1995). Terrestrially derived DOM has higher concentrations of CDOM compared to in-stream sources (Wetzel 2001). High DOC concentrations are predominantly found in rivers surrounded by wet, sandy soils (Wetzel 2001) and rivers that drain wetland dominated basins (Aitkenhead and McDowell 2000). Conversely, rivers fed by lakes/reservoirs tend to have low DOC concentrations due to the long water residence times allowing greater processing (i.e., removal) of DOC (Larson et al. 2007).

Temporally, DOC concentrations tend to be higher during warmer and wetter periods, and especially high following storms that flush out CDOM from the drainage basin (Walling and Webb 1992, Webster et al. 1995); however, there are exceptions (e.g., Meyer 1986). Rivers that drain wetlands usually experience elevated DOC concentrations following drought conditions due to the increased availability of DOC from aerated wetland soils (Walling and Webb 1992). Overall, the spatial and temporal variation of DOC in rivers is largely dictated by the hydrologic regime (Sedell and Dahm 1990).

The absorption coefficient at 440 nm (a_{440}) is a widely-used index for the concentration of CDOM (Kirk 1994). Values of a_{440} for rivers have been observed to be as low as 0.16 (Ybbs River, Austria) and as high as 12.44 (Carrao River, Venezuela) (Kirk 1994). During baseflow conditions, CDOM is usually the main contributor to light absorption in rivers (Davies-Colley et al. 2003).

2.3. Suspended Sediment

Suspended sediment (SS), also referred to as non-volatile suspended solids (NVSS), is the mineral portion of the total suspended solids (TSS) in rivers. These mineral particulates scatter light strongly, with the magnitude of scattering being dependent on particle size, shape, and composition (Davies-Colley and Smith 2001). Absorbance by mineral particulates is minimal, but there are exceptions when certain compounds are present (e.g., iron oxides; Babin and Stramski 2004). The SS in a river originates from a range of sources within its drainage basin, most from in-channel erosion, surface runoff, and tributary inputs (Walling and Webb 1992). Because fluvial sediment is usually source-limited, SS concentrations largely depend on the drainage basin's geology, climate regime, topographic relief, level of glaciation, vegetative cover, impoundment distribution, and land-use (Milliman and Meade 1983, Syvitski et al. 2000).

Temporal trends of SS are governed by the river's hydrologic regime (Walling and Webb 1992). SS increases with increasing discharge (Q), and thus is highest during storm flows. The rate at which SS decreases following storm flows depends on the particles' settling velocity in conjunction with the river's hydraulic conditions (Brush et

al. 1952). Seasonal trends in SS occur in drainage basins with large ice/snow accumulations, but for most rivers, temporal distributions of SS are largely dictated by *Q* (Syvitski et al. 2000). Spatially, SS should decrease in the downstream direction because overland sediment runoff decreases and the contribution of sediment-free groundwater to total *Q* increases (Leopold and Maddock 1953). However, land-use disturbances such as deforestation, cultivation, and urbanization have caused SS to increase in the downstream direction for most rivers due to increased source inputs (Walling and Webb 1992). Because of their low settling velocity, high attenuation cross-sections (attenuation per unit mass), and prevalence in most rivers, clays and fine silts (0.2 – 8 µm) tend to dominate the overall light attenuation in rivers (Davies-Colley et al. 2003).

2.4. Particulate Organic Matter

Particulate organic matter (POM), also referred to as volatile suspended solids (VSS), is the organic portion of TSS in rivers. POM is effective at both absorbing and scattering light. Its spectral signature is similar to CDOM, where absorption decreases with increasing wavelength. Like SS, the magnitude of scattering by POM is dependent on particle size, shape, and composition (Davies-Colley and Smith 2001). POM originates from either the breakdown of larger organic particles or by flocculation of DOM (Webster et al. 1995). POM enters the water column mainly from lateral surface runoff and in-channel processes. Like SS, temporal trends of POM are mostly governed by the river's hydrologic regime. POM concentrations are directly proportional to *Q*, with highest concentrations occurring concomitantly with storm flows due to increased surface runoff and suspension of benthic OM (Webster et al. 1995). Compared to SS,

POM has greater seasonality; however, seasonal trends are extremely diverse due to variations in catchment vegetation and hydrologic regime (Webster et al. 1995, Golladay 1997).

Spatial trends in POM are largely controlled by the type and areal coverage of surrounding terrestrial vegetation. Rivers located in forested catchments have relatively high POM concentrations, and those with dense riparian vegetation have particularly high POM concentrations (Golladay 1997). Lower-gradient rivers usually have higher POM concentrations because of their greater connectivity with a broader floodplain that is inundated more frequently (Golladay 1997, Wetzel 2001). Webster, et al. (1995) found that POM concentrations increased slightly in the downstream direction; however, most studies have not found significant longitudinal trends of POM, most likely due to local variations in sources and sinks, dependency on hydrologic regime, and improper sampling strategies (Walling and Webb 1992, Golladay 1997). Next to SS, POM is usually the second most effective OWQ constituent at attenuating light in rivers (Davies-Colley et al. 2003).

2.5. Phytoplankton

Phytoplankton (PHYTO) is technically a constituent of POM, but because of its unique relationship with light through photosynthesis, it is considered as a separate component of OWQ. Phytoplankton absorb and scatter light strongly, and thus when and where present in high concentrations, can be the dominant control on riverine OWQ. Like SS and POM, the amount of light attenuated by PHYTO is not only dictated by its concentration in the water column, but also by the size and shape of algal cells and

colonies (Kirk 1994). The spectral signature of PHYTO is similar to that of POM, but with two distinct absorption peaks at approximately 440 and 675 nm. Potamoplankton (i.e., river phytoplankton) originate from detached benthic populations and inflows from lake/wetland surface waters (Wetzel 2001). While studies have shown the abundance of potamoplankton to be correlated to light (Koch et al. 2004), nutrients (Basu and Pick 1996), temperature (Stevenson and White 1995), and grazing pressure (Caraco et al. 1997), the ubiquitous control on potamoplankton is hydraulic residence time (Soballe and Kimmel 1987, Reynolds 2000, Ameziane et al. 2003, Hilton et al. 2006). Due to the rapid mixing that occurs in rivers, the generation rate of potamoplankton must be faster than their downstream displacement rate for large populations to develop (Reynolds 2000). Higher concentrations of PHYTO therefore tend to occur in areas of longer hydraulic residence time such as impounded reaches and lower reaches of large rivers. For example, Vahatalo, et al. (2005) found that the average concentration of chlorophyll-a (*chl-a*), which is a common metric for calculating the concentration of PHYTO, in the Neuse River system in North Carolina, USA was 2.8 $\pm$ 3.2 µg/L for free-flowing reaches versus 21.7 $\pm$ 18.7 µg/L for impounded reaches. Because of the competing limitations of light availability and hydraulic residence time, most rivers have few, if any, suitable reaches to sustain large enough concentrations of PHYTO to significantly influence OWQ.

While the spatial variability of potamoplankton is high, its temporal variability is even greater (e.g., Ameziane et al. 2003) due to both seasonal and diurnal responses. Generally, PHYTO is highest during the Summer and mid-day; however, potamoplankton is usually composed of numerous diverse species that reproduce at

various rates and times (Wetzel 2001). Additionally, PHYTO in rivers is greatly affected by discharge variability (Marker and Collett 1997, Reynolds 2000). Its high spatiotemporal variability, together with the consequence of influencing and being affected by changes in OWQ (via photosynthesis), cause PHYTO to be the most complex component of riverine OWQ to predict. Fortunately, rarely are PHYTO concentrations high enough to significantly affect OWQ in rivers, except when lentic-fed or impounded (Davies-Colley et al. 2003).

2.6. Synopsis

Based on these five components, the first-order controls on riverine OWQ are the drainage basin's climate and geology, with topography, land-use, and ecosystem composition being second-order controls. While every river possesses a unique OWQ regime, the spatial and temporal trends of the above five components allow for a few generalizations. Temporally, rivers have the highest OWQ (i.e., lowest c) during baseflow (low Q) and the lowest OWQ during and immediately following floods (high Q). Spatially, many headwater streams have high OWQ due to very low CDOM, SS, POM, and PHYTO concentrations. As a river increases in size downstream, and source areas of SS and POM are accessed, the river becomes more turbid and OWQ decreases. In the lowest reaches of a river, the mainstem channel becomes more hydrologically connected to its floodplain, thereby increasing supply of CDOM to the river. The longer residence time of the lower reaches also allows for a greater abundance of PHYTO. This trend of decreasing OWQ along the river continuum (headwaters to mouth) is an underlying tenet of the RCC (Vannote et al. 1980), but has not been empirically verified.

This review highlights a basic understanding of the components of OWQ and their control, but also highlights the fact that comprehensive quantitative studies of OWQ are rare and that much of our current understanding of light-driven processes in rivers is based on assumed knowledge about spatial and temporal patterns in OWQ. To test some of these prevailing assumptions, we analyze OWQ along the river continuum in two Midwestern rivers (Baraboo River and Wisconsin River, Wisconsin, USA), and compare published synoptic datasets. We also analyze temporal OWQ in a small Midwestern stream (Big Spring Creek, Wisconsin, USA) and a large Southeastern river (Deep River, North Carolina, USA).

3. STUDY SITES

Four non-tidal, freshwater U.S. rivers were selected for our study (Figure 1). We assessed temporal trends in OWQ on two of the rivers: Deep River (DR) and Big Spring Creek (BSC). The dissimilarities between these two rivers allowed us to investigate OWQ over a large range of physical characteristics: from a small, relatively clear stream whose hydrology is driven by groundwater (BSC) to a large, relatively turbid river whose hydrology is predominantly driven by surface runoff (DR). We assessed spatial trends in OWQ on the Wisconsin River (WR) and Baraboo River (BR). The dissimilarity in flow regulation between these two rivers allowed us to investigate OWQ along the river continuum for a heavily regulated river (WR) and an unregulated river (BR).

3.1. Deep River (DR)

Deep River is a 6th-order stream located in the Central Piedmont of North Carolina (Figure 1). DR drops in elevation from 283 to 48 m above mean sea level (AMSL) over a length of 202 km. The 2,770-km^2 watershed of the DR study site is predominantly forest (72%), followed by agriculture (25%), and urban (3%) (*NCDWQ* 2000). The pre-settlement landcover was dominated by oak-hardwood forest (Schafale and Weakley 1990), which still comprises most of the river's riparian corridor. Its basin receives 110 cm/yr of precipitation with no distinct seasonality (*NOAA* 2007). Most of the urbanization in the basin is located in the headwaters, which together with its heavily entrenched channels leads to high, flashy flood flows during storms. The DR study site (35^{o}29'20"N, 79^{o}25'12"W) near Glendon, NC was located 18 km upstream of the former Carbonton Dam and 3 km above the upstream extent of the former reservoir.

3.2. Big Spring Creek (BSC)

Big Spring Creek is a 2nd-order stream located in the Central Plain of Wisconsin (Figure 1). BSC drops in elevation from 275 to 245 m AMSL over a length of 5.06 km. Its 21.1-km^2 drainage basin is mostly agriculture (46%), followed by forest (31%), grassland (21%), and wetland (2%) (*WISCLAND* 1993). The pre-settlement landcover was dominated by oak savanna (bur oak, white oak, bluestem) (Curtis 1959). The riparian corridor of BSC is composed of a mixture of reed canary grass (*Phalaris arundinacea*) and mixed-hardwood forest. Its basin receives 84 cm/yr of precipitation with a seasonal peak in monthly precipitation during the summer (*NOAA* 2007). BSC is a spring-fed stream with relatively constant *Q*. The BSC study site (43^{o}40'15"N,

89°39'14"W) was located 1.6 km upstream of the Big Spring Dam and 0.4 km above the upstream extent of the drawn-down reservoir.

3.3. Baraboo River (BR)

Baraboo River is a 6th-order stream that begins in the Western Uplands of Wisconsin and meanders through the Driftless Area of central Wisconsin before it empties into the Wisconsin River (Figure 1). BR drops in elevation from 420 to 235 m AMSL over a length of 187 km. The 1,690-km^2 Baraboo River Basin is mostly agriculture (47%), followed by forest (31%), grassland (15%), wetland (5%), urban (1%), and barren (1%) (*WISCLAND* 1993). The pre-settlement landcover was dominated by southern oak forest (white, black, and red oaks) in the uplands and oak savanna (bur oak, white oak, bluestem) in the lowlands (Curtis 1959). The riparian corridor of BR is composed mostly of mixed-hardwood forest and various grasses. Its basin receives 86 cm/yr of precipitation with a seasonal peak in monthly precipitation during the summer (*NOAA* 2007). BR historically had nine dams on its mainstem (*WDNR* 2006). All nine dams have been removed, the last one in 2001, and now its entire 187-km mainstem is free-flowing.

3.4. Wisconsin River (WR)

Wisconsin River is a 7th-order stream that begins at Lac Vieux Desert in the Northern Highlands of Wisconsin and empties into the Mississippi River (Figure 1). It drops in elevation from 515 to 185 m AMSL over a length of 684 km. The 31,400-km^2 Wisconsin River Basin is mostly forest (41%), followed by agriculture (27%), wetland

(15%), grassland (11%), open water (3%), urban (1%), shrubland (1%), and barren (1%) (*WISCLAND* 1993). The pre-settlement landcover was dominated by northern mesic forest (maple, hemlock, yellow birch) in the northern half of the basin and oak savanna (bur oak, white oak, bluestem) in the southern half of the basin (Curtis 1959). The riparian corridor of WR is composed of a mosaic of wetlands, prairie, oak savanna, and floodplain forest. Its basin receives 84 cm/yr of precipitation with a seasonal peak in monthly precipitation during the summer (*NOAA* 2007). There are currently 26 mainstem dams on the Wisconsin River (*WDNR* 2006).

4. METHODS

4.1. Sample Collection

4.1.1. Spatial Sampling

We assessed longitudinal trends in OWQ by performing synoptic surveys along the continuum of BR and WR. Water samples were collected during baseflow from 23 mainstem locations and 7 tributaries along BR on Aug 13, 2006 and from 20 mainstem locations along WR on Sep 16, 2006. All samples were collected in acid-washed amber polyethylene bottles except DOC samples, which were collected in pre-combusted glass vials treated with 600 µL of 2M HCl. All filtered water samples, including DOC, were obtained using *Whatman* GF/F (0.7 µm) glass fiber filters. All water samples were kept dark and refrigerated at ~4^{o}C until analysis. Water chemistry and OWQ analyses were performed within 72 hours of sample collection.

4.1.2. Temporal Sampling

We compared short-term (3-10 days) and long-term (Apr-Sep) changes in OWQ during baseflow and flood conditions at DR and BSC to assess temporal trends (Table 1). Automated samples were collected in acid-washed bottles using *Teledyne-ISCO* 6712 autosamplers. Manual samples were collected following the same protocol as *section 4.1.1*. All samples were kept dark and refrigerated at ~4^{o}C until analysis. Water chemistry and OWQ analyses were performed within 72 h of sample collection, with only two exceptions (2 flood samples for BSC).

4.2. Hydrology

We obtained 15-minute discharge records from the USGS gages #05405000 and #05407000 for BR and WR, respectively (Figure 1). Discharge records for BSC and DR were obtained from stage-*Q* rating curves we developed using 15-min water-level readings from stage recorders (*Intech WT-HR 2000* for BSC and *HOBO 9 m* for DR) and in-situ *Q* measurements taken with a *Marsh-McBirney* current meter at the sampling sites.

4.3. Water Chemistry

We measured TSS, NVSS (or SS), and VSS (or POM) on all water samples according to APHA Standard Methods procedure 2540D/E (*APHA* 1998) using 1.5 µm glass fiber filters (*ProWeigh, Environmental Express*). We measured DOC as non-purgeable organic carbon (NPOC) with a *Shimadzu* TOC-Vcsh Analyzer according to APHA Standard Methods procedure 5310B (*APHA* 1998). We used *chl-a* concentration as a proxy for PHYTO concentration. For DR, BSC, and BR, we measured *chl-a* with a

Turner Designs TD-700 fluorometer according to APHA Standard Methods procedure 10200H (*APHA* 1998) using *Whatman* GF/F glass fiber filters. For WR, we measured *chl-a* with a *Beckman DU Series 600* UV/VIS spectrophotometer according to Hauer and Lamberti (1996).

4.4. Optical Measurements

4.4.1. Turbidity

We measured turbidity (T_n) with a *Hach* 2100P turbidimeter in nephelometric turbidity units (NTU), which is a relative measure of *b* (Kirk 1994). We used the average value of three T_n measurements for each sample, thoroughly mixing the sample prior to each measurement.

4.4.2. Inherent Optical Properties (*a*, *b*, and *c*)

We used a *Beckman DU Series 600* UV/VIS spectrophotometer to determine the inherent optical properties of the water samples. The spectrophotometer measured the amount of incident radiant flux (Φ_0) that was received by a light detector (Φ) after being transmitted through a water sample pathlength (r). All water samples were contained in the same quartz cuvette (r = 0.01 m). Adopting the method of Bricaud, et al. (1983), we derived the light attenuation coefficient (c) by using a *Beckman* turbidity cell holder (TCH), which prevented scattered light from reaching the light detector by reducing the collection angle to 0.94^{o} (collimated light beam) and moving the water sample to 52 mm from the light detector. With this configuration, the light detector only captured the

incident light that was left after absorption and scattering by the water sample. By transforming Equation 2 and using the TCH, *c* was calculated as follows:

$$c = -\ln(\Phi/\Phi_0)_{TCH}/r \quad (2.5)$$

We derived the absorption coefficient (*a*) by using a *Beckman* standard cell holder (SCH), which placed the water sample 10 mm from the light detector and increased the collection angle to 14^o. This large collection angle and close proximity of the water sample to the detector ensured that almost all scattered light was detected, thus quantifying only the absorption by the water sample (Davies-Colley et al. 2003). Residual scattering not captured by the light detector was corrected for by subtracting out the apparent absorption coefficient at 740 nm (X_{740}) because essentially all measured absorption at 740 nm is due to scattering (Davies-Colley et al. 2003). Using the SCH, *a* was calculated as follows:

$$X = -\ln(\Phi/\Phi_0)_{SCH}/r \quad (2.6)$$

$$a = X - X_{740} \quad (2.7)$$

where X is the apparent absorption coefficient for the measured wavelength. Equation 7 assumes that the angular range of scattering for the desired wavelength is the same as that at 740 nm. Using equation 1, we calculated the scattering coefficient (*b*) by subtracting *a* from *c*, as recommended by Davies-Colley, et al. (2003).

4.4.3. Spectrophotometer Scans

We scanned each water sample in 1-nm intervals between 340-740 nm at 1200 nm/min. Each scan took approximately 20 seconds, thus we assumed that particulate settling was minimal. Each sample was thoroughly mixed prior to each scan. In order to

derive the variables in equations 5 – 7 and partition *c* (described below), we performed four configurations of scans on each water sample (Figure 2): TCH-UF (turbidity cell holder, unfiltered sample), TCH-F (turbidity cell holder, filtered sample), SCH-UF (standard cell holder, unfiltered sample), SCH-F (standard cell holder, filtered sample). We performed 3 scans for each configuration and used mean values for subsequent analyses. From the spectrophotometer scans, we used readings at 440 nm (index of CDOM), 740 nm (residual scattering), and the average of 400 -700 nm (PAR). Unless denoted by a subscript identifier (e.g., a_{440}), all reported attenuation coefficients are average values for PAR.

We also used the spectrophotometer scans to compare OWQ between the four study sites and to previous studies. The spectrophotometer scans (Figure 2) illustrate the change in absorbance (D) with wavelength (λ), where:

$$D = \log_{10} (\Phi_0/\Phi) \qquad (2.8)$$

The magnitude of the absorbance at 740 nm illustrates the degree of scattering in the water column (Figure 2), which indicates the concentration of particulates since scattering by dissolved constituents is negligible. The magnitude of the absorbance at 340 nm illustrates the degree of absorption in the water column (Figure 2), which indicates the CDOM concentration since absorption of light by CDOM increases exponentially with decreasing wavelength. The proportional spacing between the top two absorbance curves (TCH-UF and SCH-UF) illustrates the scattering to absorption ratio (b/a), which indicates the dominant process of light attenuation in the water column. The magnitude of light attenuation by PHYTO is indicated by the height of the shoulder in the

SCH-UF absorbance curve at 675 nm (Gallegos and Neale 2002), which is an absorption peak of *chl-a* (Figure 2).

4.5. Partitioning the Light Attenuation Coefficient

We partitioned the light attenuation coefficient into its constituent fractions (Equation 4) by using combinations of TCH vs. SCH and UF vs. F (Table 2). Using the TCH on an unfiltered sample quantifies the collective light attenuation coefficient by the dissolved (c_d) and particulate (c_p) constituents. Because the spectrophotometer was blanked with Milli-Q water prior to measurements, we added the attenuation coefficient of pure water (c_w) to the TCH-UF reading to obtain the total light attenuation coefficient (c). Values for c_w, a_w, and b_w were obtained from the data of Buiteveld, et al. (1994). Using the SCH on an unfiltered sample quantifies the collective light absorption coefficient by the dissolved (a_d) and particulate (a_p) constituents. We added the absorption coefficient of pure water (a_w) to the SCH-UF reading to obtain the total light absorption coefficient (a). Using the TCH on a filtered sample quantifies c_d. Using the SCH on a filtered sample quantifies a_d. We derived particulate attenuation coefficients by subtracting the dissolved and water attenuation coefficients from the total attenuation coefficients (Equation 4). For example, $c_p = c - c_d - c_w$ (TCH-UF – TCH-F, Table 2). We derived scattering coefficients by subtracting the absorption coefficients from the attenuation coefficients (Equation 1).

We partitioned c_p into c_{SS} and c_{POM} by using the a_p and b_p of water samples where TSS was 100% POM. When the particulates in a water sample are composed entirely of POM, b_p can be attributed entirely to POM ($b_p = b_{POM}$). Because absorption by SS is

usually negligible, a_p for any water sample can be attributed entirely to POM ($a_p = a_{POM}$). Given that $b_{POM} = Ka_p$, where K is b_{POM}/a_{POM} , the light attenuation coefficient of POM (c_{POM}) can be approximated with:

$$c_{POM} = a_{POM} + b_{POM} = a_p + Ka_p \quad (2.9)$$

This equation assumes that K is a constant for all POM in the water column. It also assumes that c_{PHYTO} is negligible or either incorporated into c_{POM}.

4.6. Optical Water Quality Budget

We quantified the effect of tributaries on spatial trends in OWQ by creating an OWQ budget for the Baraboo River using the additive principle suggested by Davies-Colley, et al. (2003):

$$c_{ds}Q_{ds} = c_{us}Q_{us} + c_{trib}Q_{trib} \quad (2.10)$$

where c is the light attenuation coefficient in m^{-1}, Q is discharge in m^3/s, and the subscripts *ds*, *us*, and *trib* denote downstream, upstream, and tributary, respectively. This method assumes that OWQ is volume conservative, where constituents do not experience physical or chemical changes (e.g., sedimentation of SS) between the upstream and downstream sites. To obtain c, we used Equation 5 on water samples collected from seven confluences. At each confluence, we sampled immediately upstream of the confluence (c_{us}), at the tributary outlet before it entered the mainstem channel (c_{trib}), and below the confluence before any other tributaries entered the mainstem channel (c_{ds}). Q was derived with the weighted area method (Gordon et al. 2004), using the downstream USGS gage at river kilometer (RK) 160 (Figure 1). Watershed areas were calculated with the Arc Hydro extension (CRWR, Univ. of Texas) in ArcGIS 9.1 (*ESRI*). We used

hydrography data (1:24,000 scale) to characterize stream-link magnitudes (i.e., stream order via the Strahler method; (Gordon et al. 2004)). "Major" tributaries (sensu Benda et al. 2004) were identified on the basis of a stream order greater than or equal to n – 1, where n is the stream order of the mainstem channel before the confluence.

4.7. Synoptic Optical Water Quality Datasets

We assessed longitudinal trends in OWQ by comparing our two longitudinal OWQ profiles from BR and WR with published synoptic OWQ datasets that met two conditions: (i) OWQ was measured in at least five locations from near the headwaters to the river's mouth; and (ii) the mainstem channel was greater than 100 km. Three datasets fulfilled these criteria, all from New Zealand: Motueka River (110 km; Davies-Colley 1990), Pomahaka River (147 km; Harding et al. 1999), and Waikato River (330 km; Davies-Colley 1987). The Waikato R. study measured secchi disk depth (z_{SD}), which we converted to *c* using the method of Gordon and Wouters (1978; $c = 6/z_{SD}$). The Pomahaka R. and Motueka R. studies measured black disk visibility (y_{BD}), which we converted to *c* using the method of Davies-Colley (1988; $c = 4.6/y_{BD}$ for rivers). We used these five synoptic OWQ surveys to test the prediction of the RCC (Vannote et al. 1980) that optical water quality decreases (i.e., *c* increases) along the river continuum from headwaters to mouth.

5. RESULTS

5.1. Optical Water Quality Comparisons

Big Spring Creek (BSC) had the highest OWQ (i.e., most optically clear) because of its low SS, POM, DOC, and PHYTO (Table 3). These characteristics caused the water of BSC to be essentially colorless because of the lack of scattering or absorption of light. BSC had the lowest average baseflow c at 2.73 $\pm$ 0.89 m^{-1} (mean $\pm$ std. dev.) and the lowest average baseflow T_n at 3.99 $\pm$ 1.32 NTU of the four study sites (Table 4). Deep River (DR) had a yellowish hue due to preferential blue-light absorption by its high DOC concentration. The average baseflow c and T_n for DR was 5.78 $\pm$ 1.57 m^{-1} and 5.02 $\pm$ 1.86 NTU, respectively. Wisconsin River (WR) at Muscoda also had a yellowish hue due its high DOC concentration (Table 3). The c and T_n for WR at Muscoda were 15.71 m^{-1} and 13.6 NTU, respectively. Baraboo River (BR) at La Valle had the lowest OWQ predominantly because of high SS and POM (Table 3) which imparted a dark-brownish hue on the water. This site had the highest c and T_n of the four study sites at 29.26 m^{-1} and 27.40 NTU, respectively.

Spectrophotometer scans of baseflow samples illustrated the relative differences in OWQ among the four study sites (Figure 3). BR had the highest TCH-UF absorbance curve at 740 nm and thus had the highest total scattering coefficient (b) at 25.41 m^{-1}, followed by WR at 13.13, DR at 4.39, and BSC at 2.53. We found a strong correlation between TSS (SS + POM; Table 3) and b (r^2 = 0.98, p = 0.027), which supports the relationship of increased scattering with increased concentration of particulates. DR had the highest SCH-F absorbance curve at 340 nm and thus had the highest CDOM absorption coefficient (a_{440}) at 4.44 m^{-1}, followed by WR at 2.36, BR at 1.60, and BSC at 0.41. DOC explained 82% of the variance in a_{440}, although the regression was not statistically significant (p = 0.135), likely due to the small sample size (n = 4; Table 3).

At all four sites, scattering was the dominant process of light attenuation (b/a > 1), with BR having the highest b/a at 6.60, followed by WR at 5.08, BSC at 4.10, and DR at 1.64. The magnitude of light attenuation by PHYTO was negligible at DR and BSC because of the lack of a shoulder at 675 nm in the SCH-UF absorbance curves (Figure 3). Their low *chl-a* concentrations (Table 3) support this result. BR and WR had small shoulders at 675 nm due to higher *chl-a* (Table 3). However, the height of the shoulders relative to the magnitude of the absorbance curves for these sites was small, which results in minimal contribution of PHYTO to light attenuation.

Turbidity was a highly significant ($p < 0.001$) predictor of c at all four sites (Figure 4). The plots for DR and BSC (Figure 4A, B) represent changes in c and T_n in response to changes in Q at-a-station; whereas, the plots for BR and WR (Figure 4C, D) represent longitudinal changes in c and T_n throughout the basin.

5.2. Temporal Trends: Deep River and Big Spring Creek

5.2.1. Turbidity and Discharge

Turbidity generally increased with increasing Q for DR and BSC (Figure 5). Q explained 77% of the variance in T_n at DR (Figure 5B; $p < 0.001$). We attribute the variance to hysteresis, inter-storm, and seasonal effects. For example, T_n values for the storm on June 14, 2006 were lower, despite being a larger flood, than the storm on Aug. 30, 2006 (Figure 5A). The two likely causes for this scenario are: (1) There was a separate flood on June 13, 2006 that depleted the accumulated source of fine sediment and POM for the June 14th flood, and/or (2) More sediment and POM were available for the Aug. 30th storm due to crop harvesting during this time. The relationship between c

and Q at DR ($r^2 = 0.71$; $c = 1.43Q^{1.04}$) was similar to the relationship between T_n and Q (Figure 5B).

Discharge explained only 27% of the variance in T_n at BSC (Figure 5D; $p < 0.001$). We attribute most of the variance to seasonal effects. The reduced vegetative ground coverage of BSC basin during the winter allowed greater surface sediment runoff, especially during the numerous snowmelt runoff events that occurred in central Wisconsin during the 2005-2006 winter. This scenario is the likely cause of the two high T_n measurements in March 2006 (Figure 5C). The other considerable seasonal effect on T_n in BSC was the die-off of in-channel vegetation during the late-summer. BSC had a dense benthic coverage of aquatic macrophytes, which began to senesce in late-July (Zahn 2007). This senescence not only added plant fragments to the water column, but also fine sediment that was previously trapped by the vegetation. This scenario is the likely cause of the increasing T_n values starting in August of both years (Figure 5C). Another contributing factor to increased T_n at BSC was bioturbation, with the greatest turbidity pulses being caused by cows and geese. The extremely high T_n in Feb. 2006 (64 NTU, Figure 5C) was most likely caused by one of these two animals. The relationship between c and Q at BSC ($r^2 = 0.43$; $c = 1370.9Q^{4.85}$) was similar to the relationship between T_n and Q (Figure 5D).

5.2.2. Baseflow OWQ of Big Spring Creek

The OWQ of Big Spring Creek varied relatively little during the 10-day baseflow period from June 15 – 24, 2006 (Figure 6A). Particulates (c_p: 81%) accounted for most of the light attenuation, followed by CDOM (c_d: 13%) and water (c_w: 6%) (Figure 6A).

The particulates consisted of 47% POM (2.2 mg/L) and 53% mineral sediment (2.7 mg/L). The concentration of *chl-a* was relatively low and constant over the 10 days (6.3 $\pm$ 1.0 µg/L). The baseflow period of BSC was characterized by small and brief pulses of SS, POM, and CDOM. Overall, CDOM (a_{440}) remained fairly constant at 0.67 m^{-1} and TSS decreased from 5.4 to 3.4 mg/L. The decrease in TSS was therefore the cause for the decrease in *c* over the 10-day period, from 3.3 to 2.0 m^{-1} (Figure 6A).

5.2.3. Baseflow OWQ of Deep River

The OWQ of Deep River increased (i.e., *c* decreased) slightly during the 10-day baseflow period from May 21 – 30, 2006 (Figure 6B). During this baseflow period, c_p accounted for most (64%) of the light attenuation, followed by c_d (33%) and c_w (3%; Figure 6B). The particulates consisted of 34% POM (2.1 mg/L) and 66% mineral sediment (4.1 mg/L). The concentration of *chl-a* was minimal and relatively constant over the 10 days (1.2 $\pm$ 0.1 µg/L). The baseflow period of DR was characterized by decreases in SS (5.6 to 2.9 mg/L) and CDOM (4.4 to 2.2 m^{-1}), resulting in a decrease of *c* from 6.7 to 3.6 m^{-1} (Figure 6B). During this time, POM % increased at an average rate of 3.0% per day (20 to 50%). TSS, however, remained fairly constant at 6.3 mg/L, suggesting that sediment was settling out while additional sources of POM were being added to the water column. During the other baseflow sampling period (July 11 – 17, 2006; data not illustrated), POM % increased at an average rate of 4.5% per day (20 to 47%) while TSS remained fairly constant at 7.6 mg/L.

5.2.4. Flood OWQ of Deep River

In contrast to the limited change in OWQ during baseflow, the magnitude and composition of *c* varied greatly through a flood at DR on Aug 30, 2006 (Figure 6C; Q_{peak} = 60 m^3/s, recurrence interval (RI) of ~2 months). This flood occurred following a prolonged (~1 month) low-flow period (Figure 5A) and thus pre-flood water column concentrations of TSS (3.0 mg/L) and CDOM (2.7 m^{-1}) were relatively low. Before the flood, *c* was 3.5 m^{-1}, with c_p accounting for most light attenuation (60%), followed by c_d (35%) and c_w (5%). Pre-flood POM averaged 87% of TSS. The value of *c* increased rapidly during the rising limb of the flood due mostly to a pulse of TSS, and *c* reached a maximum of 137.3 m^{-1} at 12 hours after Q_{peak}. This lag was caused by an additional TSS pulse, which was most likely from a tributary with a slower travel time. As particulates settled out of the water column following Q_{peak}, *c* decreased exponentially until it reached its average baseflow value of 5.8 m^{-1} at 8 days following Q_{peak}. CDOM also increased in response to the flood and maintained elevated concentrations during the entire sampling period, which is characteristic of subsurface flow following a dry period (Walling and Webb 1992). Consequently, the relative proportion of light attenuation by CDOM increased following the flood, reaching a maximum of 53% (Figure 6C).

5.2.5. Components of Optical Water Quality

Partitioning the total light attenuation coefficient (*c*) by means of Equation 4 and Table 2 revealed that scattering by particulates (b_p) was the dominant process of mid-summer baseflow light attenuation at DR and BSC (Table 5). Absorption by CDOM (a_d) and particulates (a_p) were the two other main contributors to baseflow light attenuation at both sites (Table 5). For all combined baseflow sampling at BSC, *c* averaged 2.73 $\pm$ 0.89

m^{-1}, of which 82% was from TSS (c_p), 12% from CDOM (c_d), and 6% from water (c_w). For all combined baseflow sampling at DR, c averaged 5.78 $\pm$ 1.57 m^{-1}, of which 60% was from TSS (c_p), 37% from CDOM (c_d), and 3% from water (c_w).

Using water samples where TSS was 100% POM, we found that b_{POM}/a_{POM} (or K; see Section 4.5.) for DR was ~3 (3.06 $\pm$ 0.65, n = 5). There were no water samples from BSC where TSS was 100% POM, and therefore we used K from DR for BSC. Assuming that K equals 3, the light attenuation coefficient of POM (c_{POM}) is approximately $4a_p$ (Equation 9). Using Equation 9 and Table 5, we calculated the amount of baseflow light attenuation by water, CDOM, SS, and POM at each site (Figure 7). Light attenuation by PHYTO was included in POM, but given its low concentrations at both sites (Table 3), its contribution to light attenuation was probably minimal. Vahatalo, et al. (2005) found that a_{PHYTO} for the Neuse River basin, which is adjacent to the Deep River basin and had slightly higher *chl-a* concentrations than DR, contributed 2.3 $\pm$ 2.9% to a. During baseflow at DR, POM (43%) was the greatest contributor to light attenuation, followed by CDOM (37%), SS (17%), and water (3%; Figure 7). During baseflow at BSC, POM and SS both contributed 41% to total light attenuation, followed by CDOM (12%) and water (6%; Figure 7).

5.3. Spatial Trends: Baraboo River and Wisconsin River

5.3.1. Wisconsin River Continuum

Particulate and dissolved concentrations in the water column fluctuated greatly along the 684-km WR for the first 550 km, with sporadic increases and decreases in all four components (Figure 8A). The large fluctuations in water chemistry were likely

associated with major tributary inputs and impoundments along this section of river (Figure 8B). Downstream of the last mainstem dam (RK 538), SS, POM, and PHYTO steadily increased, while CDOM remained fairly constant (Figure 8A). SS, POM, and PHYTO all reached their maximum values at the last sampling site (RK 674). The scattering to absorption ratio (*b/a*) along WR was highly irregular, ranging from 1.8 (RK 205) to 5.3 (RK 674), indicating large changes in SS and POM relative to CDOM (Appendix 1).

The light attenuation coefficient (*c*) along WR followed a similar trend as SS and POM by fluctuating between 0.2 and 13.8 m^{-1} for the first 548 km and then steadily increasing after the last mainstem dam, reaching a maximum of 22.8 m^{-1} (Figure 8B, Appendix 1). There were two local peaks in *c* along WR, both of which occurred immediately downstream of confluences with turbid major tributaries. Between RK 250 and 292 (Big Rib River confluence at RK 256), *c* increased from 8.9 to 13.8 m^{-1}. Between RK 488 and 524 (Baraboo River confluence at RK 506), *c* also increased from 8.9 to 13.8 m^{-1} (Figure 8B). The *c* of BR before it entered WR was 25.2 m^{-1} (Figure 9B).

5.3.2. Baraboo River Continuum

Water chemistry along the 187-km BR (Figure 9A) fluctuated less than along WR (Figure 9B). CDOM remained fairly constant along the entire length of BR (Figure 9A). SS and POM increased slightly over the first 28 km, and then rapidly over the next 46 km. After RK 74, SS decreased gradually and POM decreased rapidly. The increase in SS and POM at RK 28 was immediately downstream of the confluence of a turbid major tributary (Cleaver Creek, RK 25). PHYTO along BR was not measured directly, and

therefore we relied on the shoulder height at 675 nm in the SCH-UF absorbance curve (index for PHYTO, Figure 2) to make inferences on its longitudinal distribution. PHYTO was minimal in the headwaters (i.e., no shoulder), increased gradually to RK 40, and then decreased gradually toward the mouth of BR. This decrease in PHYTO at RK 40 coincided with a sharp increase in *c* (Figure 9B). The scattering to absorption ratio (*b/a*) increased along BR from 0.8 (RK 3) to 7.8 (RK 142), before decreasing to 5.9 at the mouth (RK 181) (Appendix 2). The increase in *b/a* was associated with increased concentrations of SS and POM while CDOM remained relatively constant (Figure 9A). The decrease in *b/a* over the last 39 km of BR was associated with decreased concentrations of SS and POM (Figure 9A) and lower channel gradient (Figure 9B), which indicates that the particulates were likely settling out of the water column over this reach.

The trend of *c* along the BR continuum was similar to that of SS and POM: (i) increasing gradually over the first 38 km; (ii) increasing rapidly over the next 34 km; (iii) increasing gradually over the next 70 km; and (iv) decreasing rapidly over the last 39 km (Figure 9B, Appendix 2). These trends in *c* matched the pattern of major confluences along BR, where *c* increased rapidly after three major confluences and began to decrease 40 km downstream of the last major confluence (Figure 9B). Also of note is that the local trough in *c* at RK 115 occurred immediately downstream of the confluence with the much clearer Narrows Creek (c = 16.63 m^{-1}; Figure 10).

5.4. Optical Water Quality Budget of Baraboo River

We used the synoptic OWQ and *Q* data through the BR watershed to develop an OWQ budget in which we quantified the relative influence of tributary OWQ (c_{trib}) on mainstem OWQ (c_{us}; Equation 10, Figure 10). All but two of the tributaries sampled were major tributaries (Kratche Creek and Narrows Creek) and two of the major tributaries from Figure 9B were not sampled (Cleaver Creek at RK 25 and Seymour Creek at RK 34). Generally, c_{trib} and Q_{trib} increased in the downstream direction, which is characteristic of greater drainage areas contributing greater amounts of SS and POM. The value of c_{us} increased in the downstream direction for the first 73 km, but then leveled off or decreased. The rate of increase in c_{us} (0.38 m^{-1}/km) over the first 73 km was more than two times the rate of increase in c_{trib} (0.17 m^{-1}/km), which resulted in an OWQ inversion in which c_{trib} was greater than c_{us} in the upper basin, but lower than the c_{us} in lower basin. Accordingly, the largest increase in *c* (+3.22 m^{-1}) occurred in the upper basin at the W. Branch Baraboo R. confluence, while the largest decrease in *c* (-4.82 m^{-1}) occurred in the lower basin at the Narrows Cr. confluence (Figure 10).

The predicted product of $c_{ds}Q_{ds}$* (via Equation 10) and the actual product of $c_{ds}Q_{ds}$ (via Figure 10) agreed fairly well (Table 6). All predicted products were within 20% of the actual product, except the two uppermost confluences (Table 6). These two exceptions may have been caused by the greater variability in mixing/sedimentation processes in headwater streams, and/or the greater uncertainty of *Q* for small watersheds. The other five confluences suggest that OWQ in BR is generally volume conservative.

6. DISCUSSION

6.1. Riverine Optical Water Quality

6.1.1. The Five Components

Optical water quality in rivers is dictated by the trends of five components: pure water, suspended sediment, particulate organic matter, chromophoric dissolved organic matter, and phytoplankton. The optical properties of pure water remain constant, and therefore its contribution to light attenuation decreases with increases in any of the other four components. Using a wide variety of rivers, we found that riverine OWQ is primarily dictated by the particulates in the water column rather than by dissolved constituents (Table 5, Appendix 1, 2). Our results are similar to Davies-Colley and Close (1990), who analyzed 96 New Zealand rivers during baseflow and found that 87% of the total light attenuation was attributed to particulates.

Our study also showed that during and immediately following floods, the dominance of c_p increases (Figure 6C) as SS and POM increase. The relative dominance of SS vs. POM is likely to vary between (Figure 7) and within rivers (Figure 8A) due to source limitations. For example, the OWQ of rivers in the Midwest USA, such as BR, that drain areas with organic-rich soils and abundant vegetation is likely to be dominated by POM; whereas, the OWQ of rivers in the Southwest USA, such as the Colorado River, that drain areas of organic-poor soils and sparse vegetation is likely to be dominated by SS.

The contribution of CDOM to OWQ is also likely to vary between rivers (Figure 7) due to source limitations. However, along the river continuum, CDOM typically remains fairly constant (Figure 9A; (Smith et al. 1997)), except in rivers with large water contributions from wetlands (e.g., Gallegos 2005), heavily regulated rivers such as WR (Figure 8A), and heavily disturbed rivers (e.g., Davies-Colley 1987). The temporal

trends in CDOM are mostly influenced by the hydrologic regime of the river (Figure 6). Because most of the CDOM present in rivers is derived from terrestrial groundwater inputs (Webster et al. 1995, Wetzel 2001), the contribution of CDOM to light attenuation is usually greater following storms (via watershed flushing) and increases as particulates settle out of the water column (Figure 6C).

We did not quantify c_{PHYTO}, but other riverine OWQ studies (Davies-Colley and Close 1990, Duarte et al. 2000, Vahatalo et al. 2005) found that the contribution of PHYTO to light attenuation was either minimal or negligible over a wide range of rivers due to unfavorable conditions to phytoplankton growth. While particulates dominate OWQ for most rivers, there are exceptions, most notably in tidal and blackwater rivers (e.g., Gallegos 2005). In these rivers, PHYTO and CDOM have a much greater influence on OWQ. Future OWQ research opportunities can be directed towards determining if trends observed here hold for diverse types of rivers worldwide.

6.1.2. Optical Water Quality Measurements and Proxies

Riverine optical water quality has been measured using a variety of instruments, including a beam transmissometer (Davies-Colley and Smith 1992), secchi disk (Davies-Colley 1987), black disk (Davies-Colley 1990), and spectrophotometer (Vahatalo et al. 2005). While each method has its advantages and disadvantages (see Davies-Colley et al. 2003), we used a spectrophotometer because of its versatility. By using the four-configuration spectrophotometer scan (Figure 2), we were able to distinguish between absorption and scattering of both particulate and dissolved constituents (Table 2). Most studies that have investigated riverine OWQ using a spectrophotometer have only

analyzed absorption (e.g., Vahatalo et al. 2005). However, this study (Table 5, Appendices 1 and 2) and others (Davies-Colley 1987) have shown the dominance of scattering on OWQ in rivers. Future spectrophotometric studies of riverine OWQ should use a method similar to ours (Figure 2, Table 2) in order to derive the total light attenuation coefficient (c).

Despite the utility of the four-configuration spectrophotometer scan, the time, detail, and cost involved in such analyses may not make it a practical tool for water resource managers to assess riverine OWQ. We therefore recommend the use of turbidity (T_n) as a proxy for c. Comparisons of T_n and c showed that T_n is a strong predictor of c (Figure 4), and data from studies of New Zealand rivers (Davies-Colley 1987, Davies-Colley and Smith 1992, Smith et al. 1997) produced similar relationships. While T_n cannot be used to predict the exact value of c in unmeasured rivers, the strong correlation between c and T_n demonstrate that turbidity can be used to assess spatial and temporal trends in OWQ for most rivers. The use of T_n as a proxy for c is advantageous because: (i) there is a longer and more extensive record of T_n in rivers than c; (ii) T_n is easier and less expensive to measure than c; and (iii) T_n is increasingly becoming a popular metric in fluvial ecology studies. The use of T_n as a proxy for c is probably only valid for non-tidal, non-blackwater rivers where scattering is the dominant process of light attenuation. In tidal and blackwater rivers, where absorption is likely to be the dominant process of light attenuation, other proxies such as CDOM or *chl-a* will need to be used.

6.2. OWQ across the Hydrograph

Every study that has compared OWQ to *Q*, including this study, has found that water clarity decreases (i.e., *c* increases) exponentially with increasing *Q* ($c = \alpha Q^{\beta}$) due primarily to increased TSS (e.g., Davies-Colley 1987, 1990, Smith et al. 1997). The rating coefficient (α) and exponent (β) are river-dependent, but in general, β is highest for rivers with large sources of readily available sediment or organic matter (e.g., Davies-Colley 1990, Davies-Colley et al. 1992). The source of readily available sediment is influenced by basin geology, topography, land-use, and storm frequency (Syvitski et al. 2000). Our results suggest that storm frequency is the dominant control on β. For example, even though the DR basin has more readily available sediment due to greater relief and more intensive anthropogenic land-use, β is higher for BSC (4.85) than DR (1.04), which we attribute to the BSC basin's much lower storm frequency (Figure 5A, C). The low storm frequency of its basin allows BSC to remain clear for most of the year due to infrequent surface runoff. This infrequent surface runoff also allows more time for sources of SS and POM to accumulate, which together results in a high stormflow *c* to baseflow *c* ratio (c_{sf}/c_{bf}). The higher storm frequency of the DR basin sustains elevated turbidity at baseflow and also prevents large source accumulations of SS and POM, which together results in a lower c_{sf}/c_{bf}, hence a lower β.

The regularity of storms may also influence the variance of *c* with *Q*, with highly irregular storm frequency (e.g., BSC) producing greater variance in the attenuation-discharge relationships (Figure 5). The variance in *c* vs. *Q* is further influenced by seasonal effects such as exposed soil surface in winter, crop-harvesting, and vegetation senescence (basin-wide and in-channel). An additional consequence of inter-storm and seasonal effects is that the variance in *c* with *Q* increases with increasing *Q*, as we found

for both DR and BSC (Figure 5B, D). Thus, our ability to predict *c* decreases with increasing *Q*.

In addition to inter-storm and seasonal effects, the change of *c* with *Q* is also influenced by the composition of OWQ. Our results from baseflow and storm sampling at DR showed that POM remained in the water column longer than SS, and thus its relative role in light attenuation increased with time following floods. We attribute this temporal trend to POM having a lower settling velocity than SS. The size of sediment transported by a river, thus, also influences change of *c* with *Q*. For example, the DR basin, which is located in the clay-rich Piedmont of North Carolina, delivers large concentrations of clay to DR, which can remain in suspension for more than a week due to its low settling velocity (Brush et al. 1952). With an average storm frequency of approximately one per week in 2006 (Figure 5A), turbidity in DR remains relatively high for long periods. If the Deep River basin was instead located in the sand-rich Coastal Plain of North Carolina, turbidity would decrease at a faster rate following floods due to the higher settling velocity of sand.

Our study also showed that the contribution of CDOM to *c* increases following floods as particulates settle out of suspension and groundwater contributions increase (Figure 6). Rivers in which PHYTO significantly influences OWQ will most likely experience diurnal and seasonal changes in *c* with *Q* due to the response of PHYTO to sunlight and temperature (Ameziane et al. 2003). Therefore, the relative proportions of CDOM, SS, POM, and PHYTO in a river greatly influences its change in *c* with *Q*.

6.3. OWQ along the River Continuum

We now address the prediction proposed by Vannote, et al. (1980) that optical water quality decreases (i.e., *c* increases) along the river continuum. Of the five case-studies, Motueka R. had the least developed basin, with most of its area being forest and conservation lands (Basher 2003). Accordingly, Motueka R. had the highest OWQ (lowest *c*) along its entire length (Figure 11). The Pomahaka basin was also relatively undeveloped with most of its land being grasslands (Harding et al. 1999). Accordingly, Pomahaka R. had the second highest OWQ along its entire length (Figure 11). The Waikato R. began at the outlet of Lake Taupo and thus was very clear at its headwaters. Urbanization and intensive agriculture increased with distance along the Waikato R., causing it to become increasingly turbid (Davies-Colley 1987).

The average *c*-values along the river continuum for the two US rivers were an order of magnitude higher than the NZ rivers (Figure 11), which we attribute to greater availability of organic-rich fine sediments, more aggressive agricultural practices, and poorer water quality management. Two of the five rivers had mainstem dams: Waikato R. (8) and Wisconsin R. (26). Reservoirs tend to reduce SS, POM (Grant et al. 2003), and CDOM (Larson et al. 2007), and increase PHYTO (Vahatalo et al. 2005), and thus are likely to disrupt spatial trends in *c* (Figure 8). Therefore, the three unregulated rivers, Baraboo R., Pomahaka R., and Motueka R., provided the best case-studies to analyze OWQ along the river continuum.

The OWQ of the three unregulated rivers followed a similar trend, where *c* increased over the first 70% of the river continuum and then began to decrease (Figure 11). We suggest that this asymptotic trend, as well as the longitudinal distribution of riverine OWQ, is dictated by the channel network configuration (i.e., density and location

of tributaries; (Benda et al. 2004)). Tributaries are point sources for all five OWQ components, and therefore confluences should be sites where changes in OWQ are most likely to occur. Baraboo R. (Figures 9B and 10) provided an excellent example of confluence effects on OWQ. Between RK 20 and 40, three major tributaries entered Baraboo R., which coincided with the greatest increase in *c*; whereas 40 km after the last major tributary, *c* began to decrease. For the Pomahaka R., Harding, et al. (1999) attributed the increase in *c* to turbid inflows from tributaries draining agriculturally-dominated regions. Like Baraboo R., the decrease in *c* over the last 30% of Pomahaka and Motueka Rivers coincided with the absence of major tributaries. This lack of major tributaries near the outlet of large rivers is consistent with the Network Dynamics Hypothesis (Benda et al. 2004), which states that the distance between "geomorphically significant tributaries" increases with distance downstream due to the continually reduced drainage area available in dendritic, pear-shaped basins. The decrease in *c* along the last 30% of the three unregulated rivers was most likely the result of a decreased supply of TSS from large tributaries. We expect the longitudinal distribution of *c* to be asymptotic for dendritic, pear-shaped basins, similar to the Motueka, Pomahaka, and Baraboo Rivers (Figure 11).

Wisconsin R. provided a counterexample to the above pattern, as five major tributaries enter the channel over its last 38% and *c* increased (Figure 8B). These tributary locations were a consequence of a rectangular-shaped basin providing a relatively constant available drainage area along the river's continuum (Figure 1). Major tributaries are point sources of SS and POM, which likely caused the increase in *c* over

the last 30% of Wisconsin R. (Figure 11). We therefore expect the trend of *c* along the river continuum to vary for different basin configurations.

Because land use is a dominant influence on the magnitude of *c* in a river (Figure 11), we propose that channel network configuration can also influence the magnitude of *c* by either augmenting or mitigating the effects of land use. While land use influences the availability of the five OWQ components, it is the channels that actually deliver these components to the mainstem river. To illustrate this concept, we use the DR and BSC basins (Figure 1) as an example. If we assume that both basins are the same geomorphically (size, relief, geology) and both are dominated by intensive agriculture land-use, but retain the drainage density depicted in Figure 1, then DR would likely be more turbid, at least for periods following storms, because of its greater access to the readily available SS and POM. BSC would be clearer due to a greater proportion of its *Q* being supplied by particulate-free groundwater. Drainage density and *c* should therefore be directly proportional.

Additionally, channel network configuration can affect temporal OWQ. For DR during a flood, we found that the peak in *c* lagged the peak in *Q* by 12 hours (Figure 6C), which we attributed to TSS inputs from tributaries with a longer travel time. Wider basins such as DR (Figure 1) typically have longer tributaries (Benda et al. 2004), and since it is the headwaters of tributaries that supply most of the TSS to the river (Gomi et al. 2002), these wider basins will typically have longer durations of increased turbidity due to longer travel times from source to river. The drainage density of the basin can also affect these travel times through network routing. A caveat to the effect of basin size and

configuration on OWQ is that the larger the basin, the less predictable temporal OWQ will be due to greater variability in precipitation distribution.

Our hypothesis of channel network configuration dictating OWQ shares some of the principles of the Link Discontinuity Concept (LDC; Rice et al. 2001). The LDC states that tributaries are not just disruptions to the river continuum that temporarily reset downstream changes in physical conditions as proposed by the RCC; but rather, "by defining patterns of water and sediment flux, they are entirely responsible for moderate- and large-scale variations in physical habitat along all river channels" (Rice et al. 2001). Spatial patterns in OWQ are consistent with the LDC that rivers may be more appropriately viewed as a series of links, where two separate fluxes of water and sediment meet to form a new channel (Equation 10). In order to apply the LDC to OWQ, we need to include CDOM, POM, and PHYTO fluxes as well. Applying this links concept to OWQ assumes some degree of volume conservation, which we found for Baraboo River (Figure 10, Table 6). Volume conservation will not always apply due to mixing/sedimentation processes, especially at headwater links (Gomi et al. 2002); but for larger rivers, we expect the additive principle to predict downstream OWQ within 20% (Table 6). There are also biochemical transformations that could affect volume conservation (e.g., Moreira-Turcq et al. 2003), but their effect is probably negligible due to the dominance of particulates on riverine OWQ.

The major limitation of the links concept for OWQ is that changes in OWQ occur in the absence of tributaries as well (Figure 9B). Due to the increasing contribution of particulate-free groundwater to total *Q* and the increasing potential of sedimentation in the downstream direction (Leopold and Maddock 1953), the absence of major tributaries

typically leads to downstream decreases in *c*. So even though riverine OWQ is strongly influenced by tributary inputs (Figure 10), the entire basin configuration must be assessed in order to develop accurate OWQ budgets for rivers.

7. CONCLUSIONS

While light is recognized as a primary limiting variable in rivers, it has received comparatively limited empirical study. Water resource managers should be aware of spatial and temporal variability of OWQ as it is an important indicator of water quality change and dictates aesthetics of water resources of interest to the general public. Ecologically, light availability is likely to become an increasingly important regulatory of primary production and species composition in rivers subject to greater human land use and nutrient enrichment (Hilton et al. 2006). By knowing the controls and spatiotemporal trends of riverine OWQ, fluvial ecologists will be more able to quantify the amount of light throughout riverine habitats and understand consequences of light variability on multiple ecological processes. Additionally, remote sensing applications will benefit from OWQ studies as the optical characteristics of the water column must be known to derive its depth and composition from radiance measurements.

Most of the referenced literature in this treatise is derived from studies in New Zealand. The reason most riverine OWQ studies have been performed in New Zealand is that they have and regulate OWQ standards (see Davies-Colley et al. 2003). We advocate broad adoption of similar OWQ standards to foster ecosystem health. Designating and regulating OWQ standards will require considerable monitoring. From an OWQ management perspective, our study suggests that tributaries should be

monitored with greater frequency and extent since they are the point sources for the components that set OWQ. Because the biogeochemistry of small streams is more sensitive to local changes than larger rivers (Gomi et al. 2002), we recommend that OWQ management strategies be directed toward the 1st- and 2nd-order streams. Further, we suggest that the abovementioned trends and concepts, particularly the role of channel network configuration, can also be used to understand the spatio-temporal trends of other water quality variables. The OWQ of rivers has greater significance because it affects receiving waters such as estuaries and coastal environments, whose biota greatly depend on aquatic light availability (e.g., coral (Fabricius 2005), birds (Henkel 2006), submersed aquatic vegetation (Dennison et al. 1993). This study has highlighted the high spatiotemporal variability of riverine OWQ, and in doing so has opened up a number of promising research avenues including the need to understand the effects of land use and climate change on OWQ as critical steps toward a broader awareness of the fundamental role of light as a driver of multiple processes in fluvial ecosystems.

REFERENCES

American Public Health Association (APHA), American Water Works Association, and Water Environment Federation (1998), Standard Methods for the Examination of Water and Wastewater. American Public Health Association.

Aitkenhead, J. A., and W. H. McDowell (2000), Soil C : N ratio as a predictor of annual riverine DOC flux at local and global scales, *Global Biogeochemical Cycles, 14*, 127-138.

Ameziane, T., et al. (2003), Origin and transport of phytoplankton in a large river: the Garonne, France, *Archiv Fur Hydrobiologie, 156*, 385-404.

Babin, M., and D. Stramski (2004), Variations in the mass-specific absorption coefficient of mineral particles suspended in water, *Limnology and Oceanography*, *49*, 756-767.

Basher, L. R. (2003), The Motueka and Riwaka catchments: a technical report summarising the present state of knowledge of the catchments, management issues and research needs for integrated catchment management, 122 pp, Manaaki Whenua Landcare Research, Lincoln.

Basu, B. K., and F. R. Pick (1996), Factors regulating phytoplankton and zooplankton biomass in temperate rivers, *Limnology and Oceanography*, *41*, 1572-1577.

Benda, L., et al. (2004), The network dynamics hypothesis: how channel networks structure riverine habitats, *BioScience, 54*, 413-427.

Bricaud, A., et al. (1983), Optical efficiency factors of some phytoplankters, *Limnology and Oceanography*, *28*, 816-832.

Brush, L. M., Jr., et al. (1952), A study of sediment in suspension, *IASH Commission on Land Erosion, 59*, 293-310.

Buiteveld, H., et al. (1994), The optical properties of pure water, paper presented at SPIE Proceedings on Ocean Optics XII.

Caraco, N. F., et al. (1997), Zebra mussel invasion in a large, turbid river: Phytoplankton response to increased grazing, *Ecology, 78*, 588-602.

Curtis, J. T. (1959), *The Vegetation of Wisconsin*, 657 pp., The University of Wisconsin Press, Madison.

Davies-Colley, R. J. (1987), Optical properties of the Waikato River, New Zealand, *Mitteilungen aus dem Geologisch-Palaontologischen Institut der Universitat Hamburg, SCOPE/UNEP Sonderband, 64*, 443-460.

Davies-Colley, R. J. (1988), Measuring water clarity with a black disk, *Limnology and Oceanography*, *33*, 616-623.

Davies-Colley, R. J. (1990), Frequency distributions of visual water clarity in 12 New Zealand rivers, *New Zealand Journal of Marine and Freshwater Research*, *24*, 453-460.

Davies-Colley, R. J., and M. E. Close (1990), Water colour and clarity of New Zealand rivers under baseflow conditions, *New Zealand Journal of Marine and Freshwater Research*, *24*, 357-365.

Davies-Colley, R. J., et al. (1992), Effects of clay discharges on streams: 1. Optical properties and epilithon, *Hydrobiologia*, *248*, 215-234.

Davies-Colley, R. J., and D. G. Smith (1992), Offsite measurement of the visual clarity of waters, *Water Resources Bulletin*, *28*, 951-957.

Davies-Colley, R. J., and D. G. Smith (2001), Turbidity, suspended sediment, and water clarity: A review, *Journal of the American Water Resources Association*, *37*, 1085-1101.

Davies-Colley, R. J., et al. (2003), *Colour and Clarity of Natural Waters*, 310 pp., Ellis Horwood, New York.

Dennison, W. C., et al. (1993), Assessing water-quality with submersed aquatic vegetation, *Bioscience*, *43*, 86-94.

Duarte, C. M., et al. (2000), Particulate light absorption and the prediction of phytoplankton biomass and planktonic metabolism in northeastern Spanish aquatic ecosystems, *Canadian Journal of Fisheries and Aquatic Sciences*, *57*, 25-33.

Fabricius, K. E. (2005), Effects of terrestrial runoff on the ecology of corals and coral reefs: review and synthesis, *Marine Pollution Bulletin*, *50*, 125-146.

Gallegos, C. L. (2005), Optical water quality of a blackwater river estuary: the Lower St. Johns River, Florida, USA, *Estuarine Coastal and Shelf Science*, *63*, 57-72.

Gallegos, C. L., and P. J. Neale (2002), Partitioning spectral absorption in case 2 waters: discrimination of dissolved and particulate components, *Applied Optics*, *41*, 4220-4233.

Golladay, S. W. (1997), Suspended particulate organic matter concentration and export in streams, *Journal of the North American Benthological Society*, *16*, 122-131.

Gomi, T., et al. (2002), Understanding processes and downstream linkages of headwater systems, *BioScience*, *52*, 905-916.

Gordon, H. R., and A. W. Wouters (1978), Some relationships between Secchi depth and inherent optical properties of natural waters, *Applied Optics*, *17*, 3341-3343.

Gordon, N. D., et al. (2004), *Stream Hydrology: An Introduction for Ecologists*, 429 pp., John Wiley & Sons, Chichester.

Grant, G. E., et al. (2003), A geological framework for interpreting downstream effects of dams on rivers, in *A Peculiar River: Geology, Geomorphology, and Hydrology of the Deschutes River, Oregon* edited by J. E. O'Connor and G. E. Grant, pp. 209-225, AGU.

Harding, J. S., et al. (1999), Changes in agricultural intensity and river health along a river continuum, *Freshwater Biology*, *42*, 345-357.

Hauer, F. R., and G. A. Lamberti (1996), *Methods in Stream Ecology*, 674 pp., Academic Press, San Diego.

Henkel, L. A. (2006), Effect of water clarity on the distribution of marine birds in nearshore waters of Monterey Bay, California, *Journal of Field Ornithology*, *77*, 151-156.

Hilton, J., et al. (2006), How green is my river? A new paradigm of eutrophication in rivers, *Science of the Total Environment*, *365*, 66-83.

Kirk, J. T. O. (1988), Optical water quality - What does it mean and how should we measure it?, *Journal of the Water Pollution Control Federation*, *60*, 194-197.

Kirk, J. T. O. (1994), *Light and Photosynthesis in Aquatic Ecosystems*, 509 pp., Cambridge University Press, New York.

Koch, R. W., et al. (2004), Phytoplankton growth in the Ohio, Cumberland and Tennessee Rivers, USA: inter-site differences in light and nutrient limitation, *Aquatic Ecology*, *38*, 17-26.

Larson, J. H., et al. (2007), Effects of upstream lakes on dissolved organic matter in streams, *Limnology and Oceanography*, *52*, 60-69.

Leopold, L. B., and T. Maddock, Jr. (1953), The hydraulic geometry of stream channels and some physiographic implications, *USGS Professional Paper*, *252*, 1-57.

Marker, A. F. H., and G. D. Collett (1997), Spatial and temporal characteristics of algae in the River Great Ouse. I. Phytoplankton, *Regulated Rivers-Research & Management*, *13*, 219-233.

Meyer, J. L. (1986), Dissolved organic carbon dynamics in two subtropical blackwater rivers, *Archiv fur Hydrobiologie 108*, 119-134.

Milliman, J. D., and R. H. Meade (1983), World-wide delivery of river sediment to the oceans, *The Journal of Geology*, *91*, 1-21.

Moreira-Turcq, P. F., et al. (2003), Characteristics of organic matter in the mixing zone of the Rio Negro and Rio Solimoes of the Amazon River, *Hydrological Processes*, *17*, 1393-1404.

National Oceanic and Atmospheric Administration (NOAA) (2007), National Climate Data. http://www.noaa.gov/climate.html.

North Carolina Division of Water Quality (NCDWQ) (2000), Cape Fear River Basinwide Water Quality. NC Department of Environment and Natural Resources, http://h2o.enr.state.nc.us/basinwide/Capefear/capefearindex.htm.

Popp, A. S. (2005), Longitudinal patterns of carbon, chlorophyll, and nutrients in the Wisconsin River, University of Wisconsin, Madison.

Reynolds, C. S. (2000), Hydroecology of river plankton: The role of variability in channel flow, *Hydrological Processes*, *14*, 3119-3132.

Rice, S. P., et al. (2001), Tributaries, sediment sources, and the longitudinal organisation of macroinvertebrate fauna along river systems, *Canadian Journal of Fisheries and Aquatic Sciences*, *58*, 824-840.

Schafale, M. P., and A. S. Weakley (1990), *Classification of the Natural Communities of North Carolina: Third Approximation*, 325 pp., NC Natural Heritage Foundation, Inc., Raleigh.

Sedell, J. R., and C. N. Dahm (1990), Spatial and temporal scales of dissolved organic carbon in streams and rivers, in *Organic Acids in Aquatic Ecosystems*, edited by E. M. Perdue and E. T. Gjessing, pp. 261-279, John Wiley & Sons, Berlin.

Smith, D. G., et al. (1997), Optical characteristics of New Zealand rivers in relation to flow, *Journal of the American Water Resources Association*, *33*, 301-312.

Soballe, D. M., and B. L. Kimmel (1987), A large-scale comparison of factors influencing phytoplankton abundance in rivers, lakes, and impoundments, *Ecology*, *68*, 1943-1954.

Stevenson, R. J., and K. D. White (1995), A comparison of natural and human determinants of phytoplankton communities in the Kentucky River basin, USA, *Hydrobiologia*, *297*, 201-216.

Syvitski, J. P., et al. (2000), Estimating fluvial sediment transport: The rating parameters, *Water Resources Research, 36*, 2747-2760.

Vahatalo, A. V., et al. (2005), Light absorption by phytoplankton and chromophoric dissolved organic matter in the drainage basin and estuary of the Neuse River, North Carolina (USA), *Freshwater Biology*, *50*, 477-493.

Vannote, R. L., et al. (1980), The river continuum concept, *Can. J. Fish. Aquat. Sci.*, *37*, 130-137.

Walling, D. E., and B. W. Webb (1992), Water quality: I. Physical characteristics, in *The Rivers Handbook: Hydrological and Ecological Principles*, edited by P. Calow and G. E. Petts, pp. 48-72, Blackwell Scientific, Oxford.

Webster, J. R., et al. (1995), Organic processes in streams of the eastern United States, in *River and Stream Ecosystems*, edited by C. E. Cushing, et al., pp. 117-187, Elsevier, Amsterdam.

Wetzel, R. G. (2001), *Limnology: Lake and River Ecosystems*, 1006 pp., Academic Press, San Diego.

Wisconsin Department of Natural Resources (WDNR). (2006), Wisconsin Dam Database. http://dnr.wi.gov/org/water/wm/dsfm/dams/datacentral.html.

Wisconsin Initiative for Statewide Cooperation on Landscape Analysis and Data (WISCLAND) (1993), Land Cover of Wisconsin. Wisconsin Department of Natural Resources, http://dnr.wi.gov/maps/gis/datalandcover.html#data.

Zahn, S. E. (2007), Submerged macrophytes in Big Spring Creek, WI: Distribution and influence on phosphorous dynamics, 29 pp, University of Wisconsin, Madison.

Table 2.1. Temporal sampling of OWQ at Big Spring Creek (BSC) and Deep River (DR).

	May 21-30, 2006	Jun 14-16, 2006	Jul 11-17, 2006	Aug 29 – Sep 11, 2006	Apr 24-26, 2006	Jun 15-24, 2006	Jun 24, 2005 - Sep 18, 2006
Location	DR	DR	DR	DR	BSC	BSC	BSC
Method	Automated	Manual	Automated	Automated	Automated	Automated	Manual
Flow	Baseflow	Flood	Baseflow	Flood	Baseflow	Baseflow	Baseflow / Flood[1]
Sample interval (h)	12	~24	6	6	4	6	discrete
Sample number	20	3	25	50	12	36	22 / 2

[1] The 2 flood samples for BSC were collected at a station ~2 km downstream of the study site. A paired *t*-test (n = 44) revealed that *c* was not statistically different between these two sites (t = -1.36, p = 0.18).

Table 2.2. Partitioning of the light attenuation coefficient.

	TCH		**SCH**		**(TCH – SCH)**
UF	c	=	a	+	b
	=		=		=
F	c_d	=	a_d	+	b_d
	+		+		+
(UF – F)	c_p	=	a_p	+	b_p
	+		+		+
Pure water	c_w	=	a_w	+	b_w

TCH = Turbidity Cell Holder; SCH = Standard Cell Holder
UF = Unfiltered water sample; F = Filtered water sample

Table 2.3. Discharge and water chemistry of study sites. Values are mean ± std. dev. (number of observations). *Q* data for all four sites is from water year 2006.

	Deep River at Glendon[1]	Big Spring Creek at Big Spring[1]	Baraboo River at La Valle[1,2]	Wisconsin River at Muscoda[3]
Q (m^3/s)	9.67 ± 14.36	0.29 ± 0.02	9.57 ± 5.96	193.1 ± 77.7
DOC (mg/L)	6.8 ± 1.4 (65)	1.2 ± 0.3 (94)	2.7 ± 0.2 (43)	6.9 ± 0.6 (8)
SS (mg/L)	20.1 ± 55.9 (124)	4.3 ± 3.0 (64)	60.7 ± 24.3 (50)	28.1 ± 39.2 (32)
POM (mg/L)	5.2 ± 8.4 (124)	2.5 ± 1.0 (64)	8.9 ± 2.3 (50)	16.6 ± 5.1 (32)
chl-a (µg/L)	1.5 ± 1.1 (21)	6.3 ± 1.0 (10)	28.0 ± 11.3 (10)	45.4 ± 23.3 (7)

Source: 1 – this study; 2 – *Q* from USGS gage (#05405000); 3 – Popp (2005) and USGS gage (#05407000).

Table 2.4. Baseflow OWQ of study sites: Deep River (n = 74), Big Spring Creek (n = 49), Baraboo River (n = 1), and Wisconsin River (n = 1). Values are mean ± SD.

	Deep River at Glendon	Big Spring Creek at Big Spring	Baraboo River at La Valle	Wisconsin River at Muscoda
T_n (NTU)	5.02 ± 1.86	3.99 ± 1.32	27.40	13.60
c (m^{-1})	5.78 ± 1.57	2.73 ± 0.89	29.26	15.71
b/a	1.25 ± 0.29	2.63 ± 0.87	6.60	5.08
a_{440} (m^{-1})	4.10 ± 1.09	0.61 ± 0.20	1.60	2.36

Table 2.5. Partitioned OWQ for Deep River (DR) and Big Spring Creek (BC). Values in parentheses are percentage of the total light attenuation coefficient.

	c	c_w	c_d	c_p	a	a_w	a_d	a_p	b	b_w	b_d	b_p
DR	5.78 ± 1.57 (100)	0.150 (3)	2.15 ± 0.64 (37)	3.48 ± 1.13 (60)	2.57 ± 0.67 (45)	0.148 (3)	1.80 ± 0.49 (31)	0.63 ± 0.25 (11)	3.20 ± 1.03 (55)	0.002 (0)	0.35 ± 0.20 (6)	2.85 ± 0.95 (49)
BSC	2.73 ± 0.89 (100)	0.150 (6)	0.34 ± 0.11 (12)	2.25 ± 0.88 (82)	0.76 ± 0.19 (28)	0.148 (6)	0.33 ± 0.13 (12)	0.28 ± 0.17 (10)	1.97 ± 0.77 (72)	0.002 (0)	0.00 ± 0.14 (0)	1.97 ± 0.77 (72)

Table 2.6. Predicted vs. actual tributary effects on OWQ in Baraboo River. $c_{ds}Q_{ds}$* is the predicted product according to Equation 10, and $c_{ds}Q_{ds}$ is the actual product according to Figure 10.

RK	$c_{trib}Q_{trib}$	$c_{us}Q_{us}$	$c_{ds}Q_{ds}$	$c_{ds}Q_{ds}$*	$c_{ds}Q_{ds}$* / $c_{ds}Q_{ds}$
4	0.014	0.034	0.035	0.048	1.38
8	0.032	0.097	0.230	0.129	0.56
9	0.334	0.233	0.487	0.567	1.16
28	0.151	2.345	2.277	2.495	1.10
40	8.901	3.867	11.433	12.768	1.12
73	3.857	64.178	81.852	68.034	0.83
115	10.588	132.445	132.592	143.034	1.08

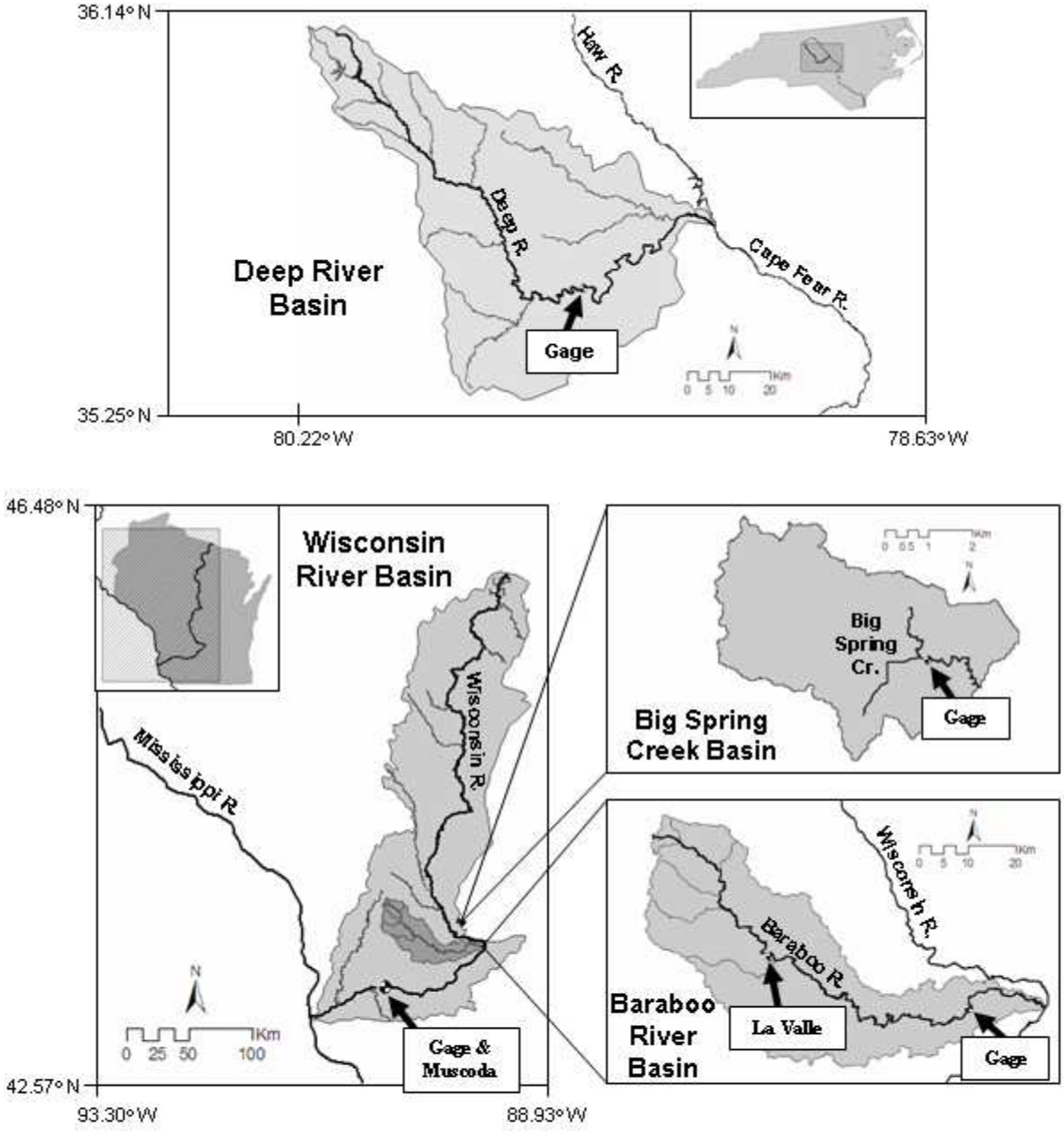

Figure 2.1. Optical water quality study sites. Major tributaries are depicted for all four basins. Gage identifies where Q was measured and water samples were collected. Big Spring Creek Basin is adjacent to but not located in the Wisconsin River Basin.

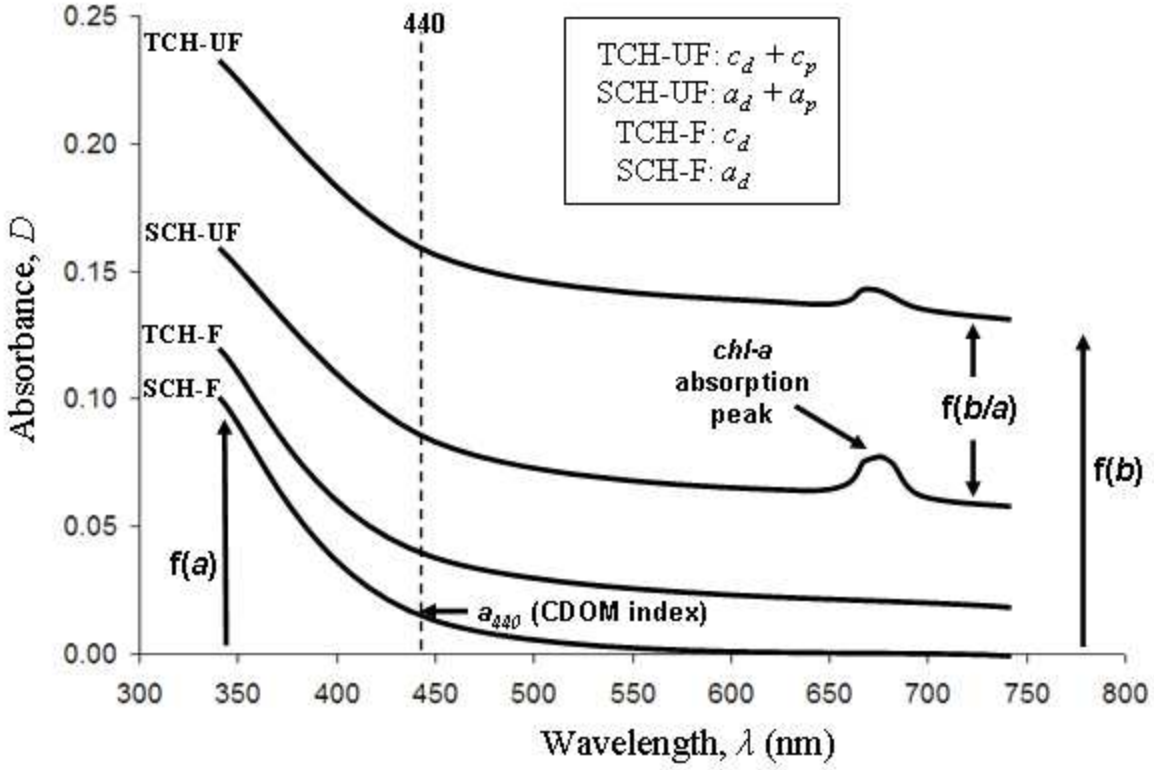

Figure 2.2. Heuristic diagram of the four-configuration spectrophotometer scan.

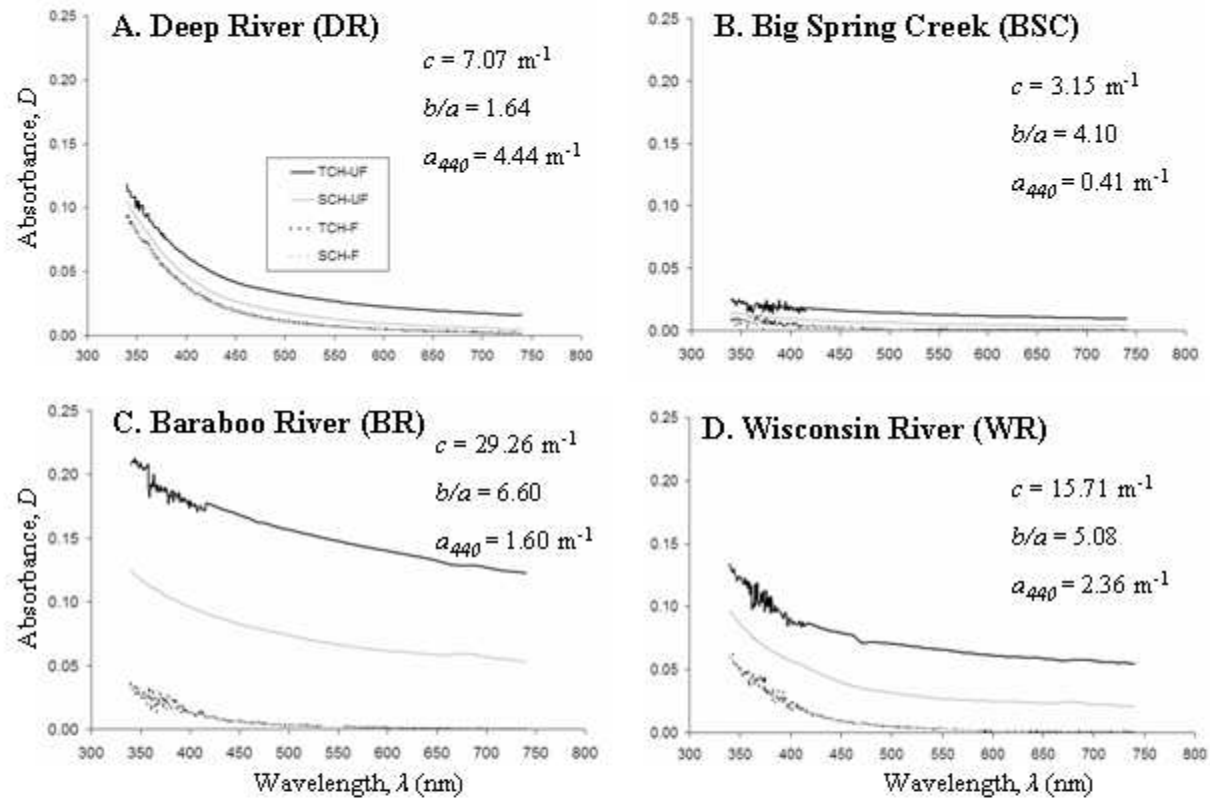

Figure 2.3. Representative spectrophotometer scans of the four study sites during baseflow.

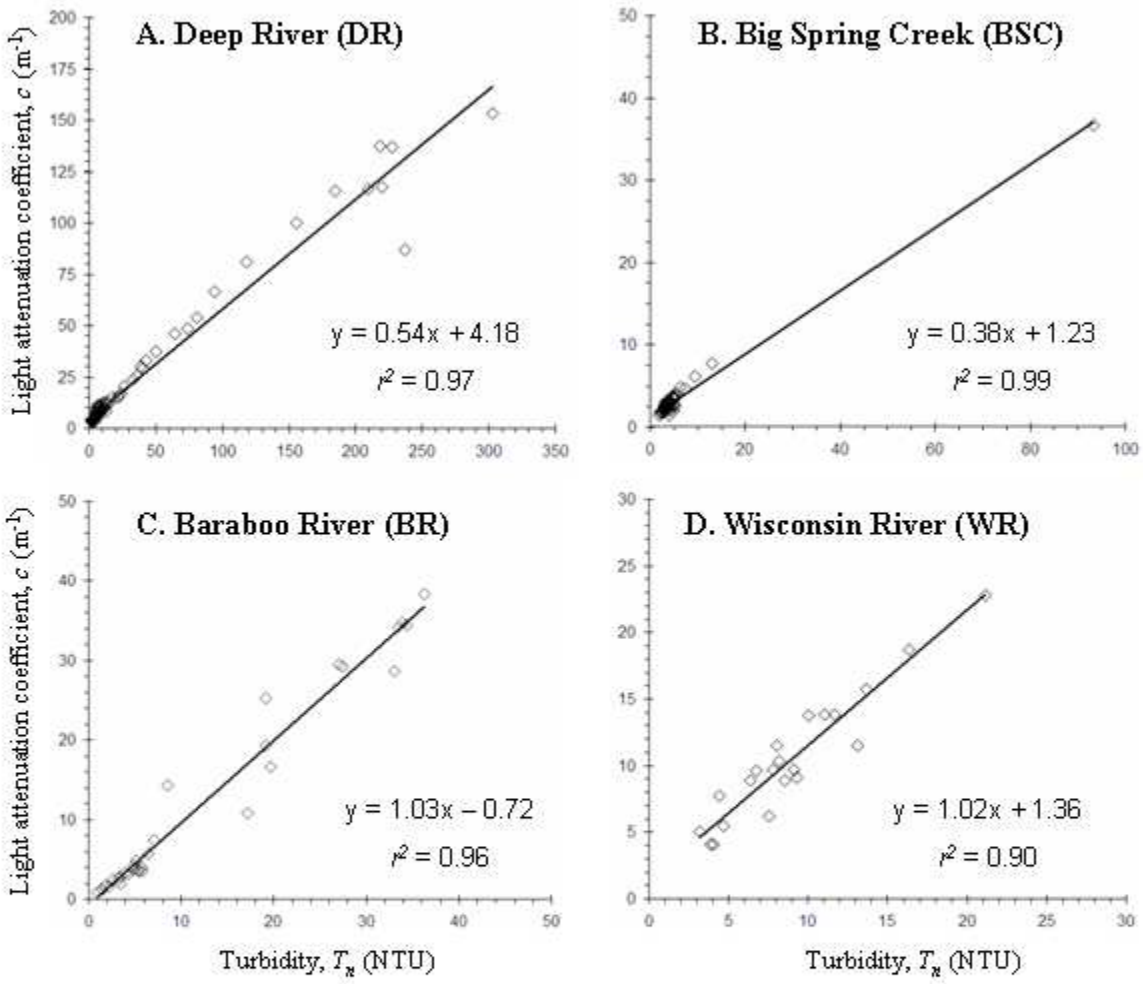

Figure 2.4. Light attenuation coefficient (c) vs. turbidity (T_n) for the four study sites. DR and BSC illustrate changes in c and T_n in response to changes in Q at-a-station. BR and WR illustrate longitudinal changes in c and T_n throughout the basin. Note the different x- and y-axes between the plots.

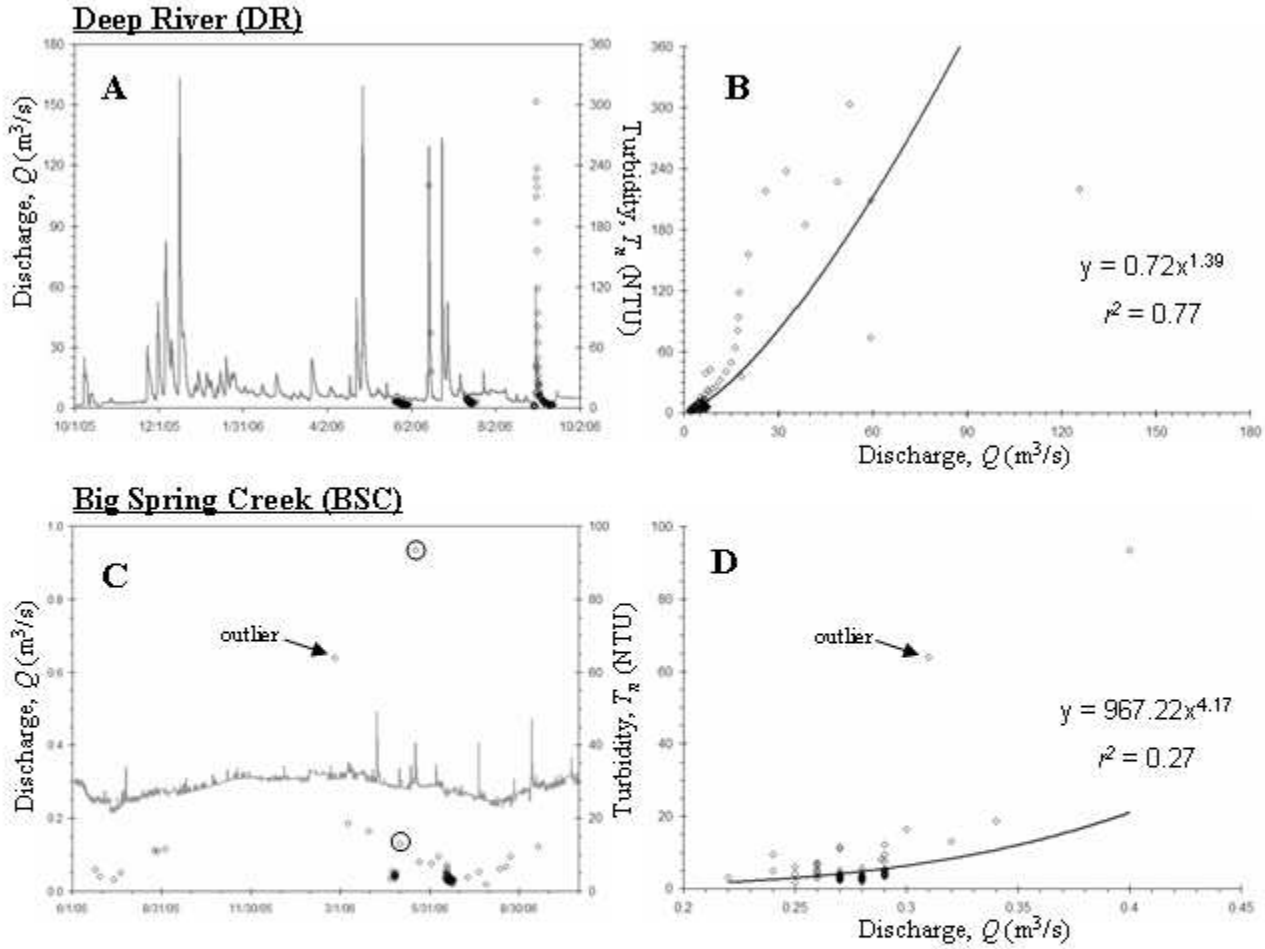

Figure 2.5. Discharge (Q) and turbidity (T_n) record for Deep River (A,B) and Big Spring Creek (C,D). The four tightly grouped sample intervals in A are the four sampling periods for DR. The two tightly grouped sample intervals in C are the two sampling periods for BSC. Circled values in C are the two flood samples of BSC. The outlier (from bioturbation) was not factored into the regression analysis in D. Note the different x- and y-axes between DR and BSC.

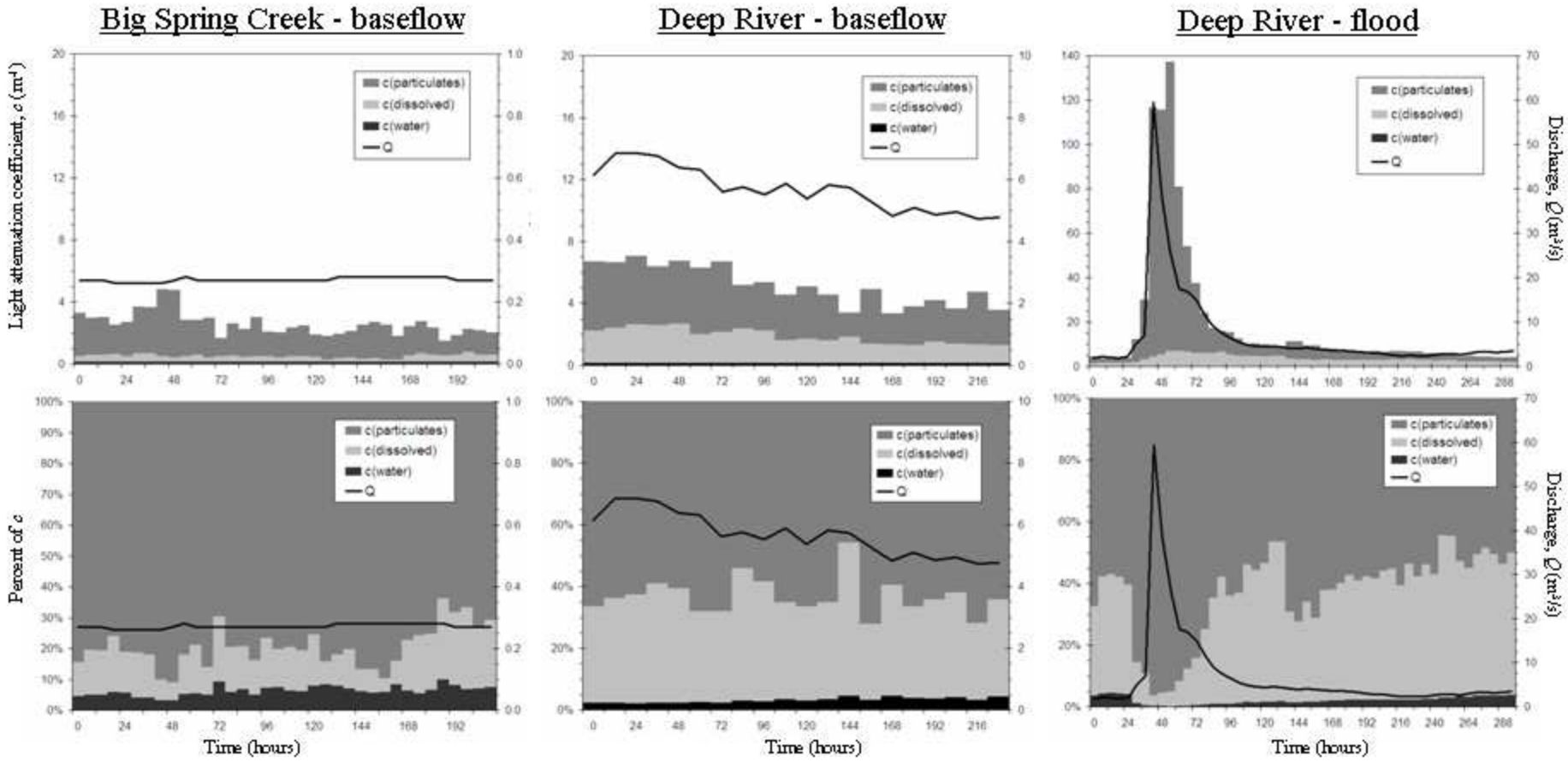

Figure 2.6. (A) OWQ of Big Spring Creek during baseflow (6/15/06 – 6/24/06). Sampling interval was 6 hours. (B) OWQ of Deep River during baseflow (5/21/06 – 5/30/06). Sampling interval was 12 hours. (C) OWQ of Deep River during a flood (8/29/06 – 9/11/06). Sampling interval was 6 hours. Note the different y-axes.

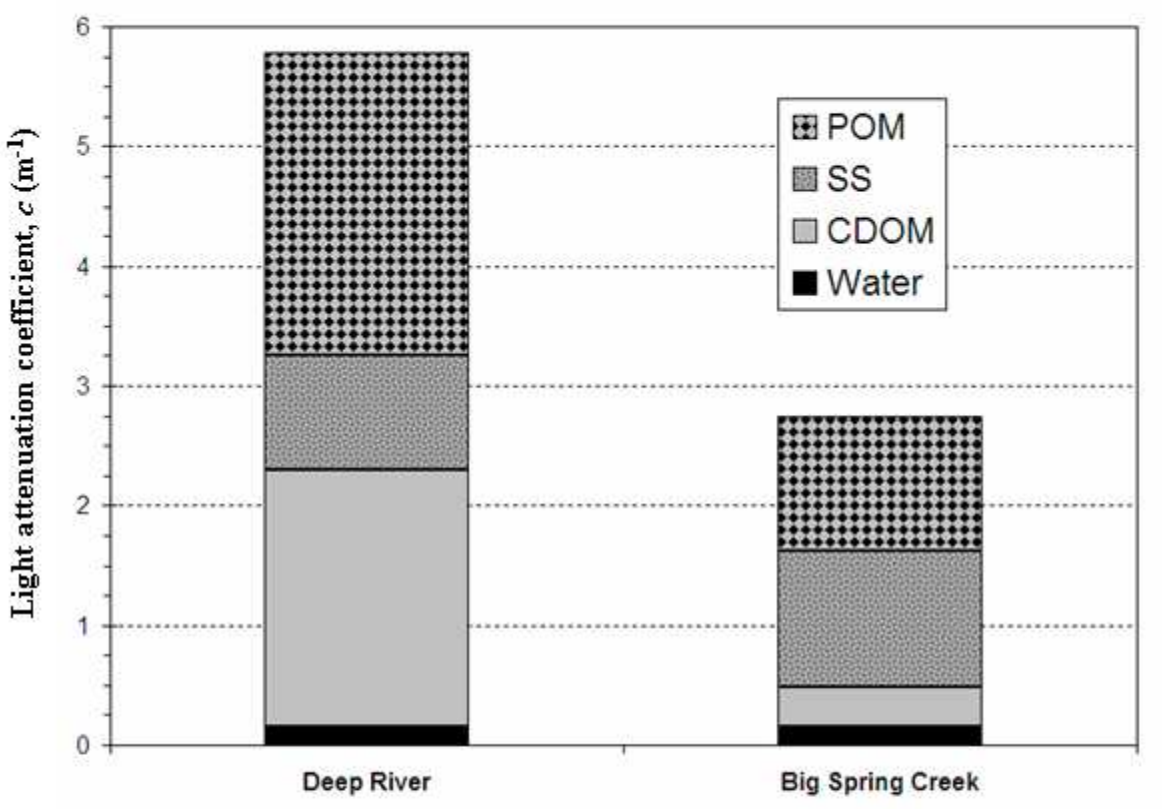

Figure 2.7. Contributions of OWQ components to the total light attenuation coefficient at Deep River and Big Spring Creek during baseflow.

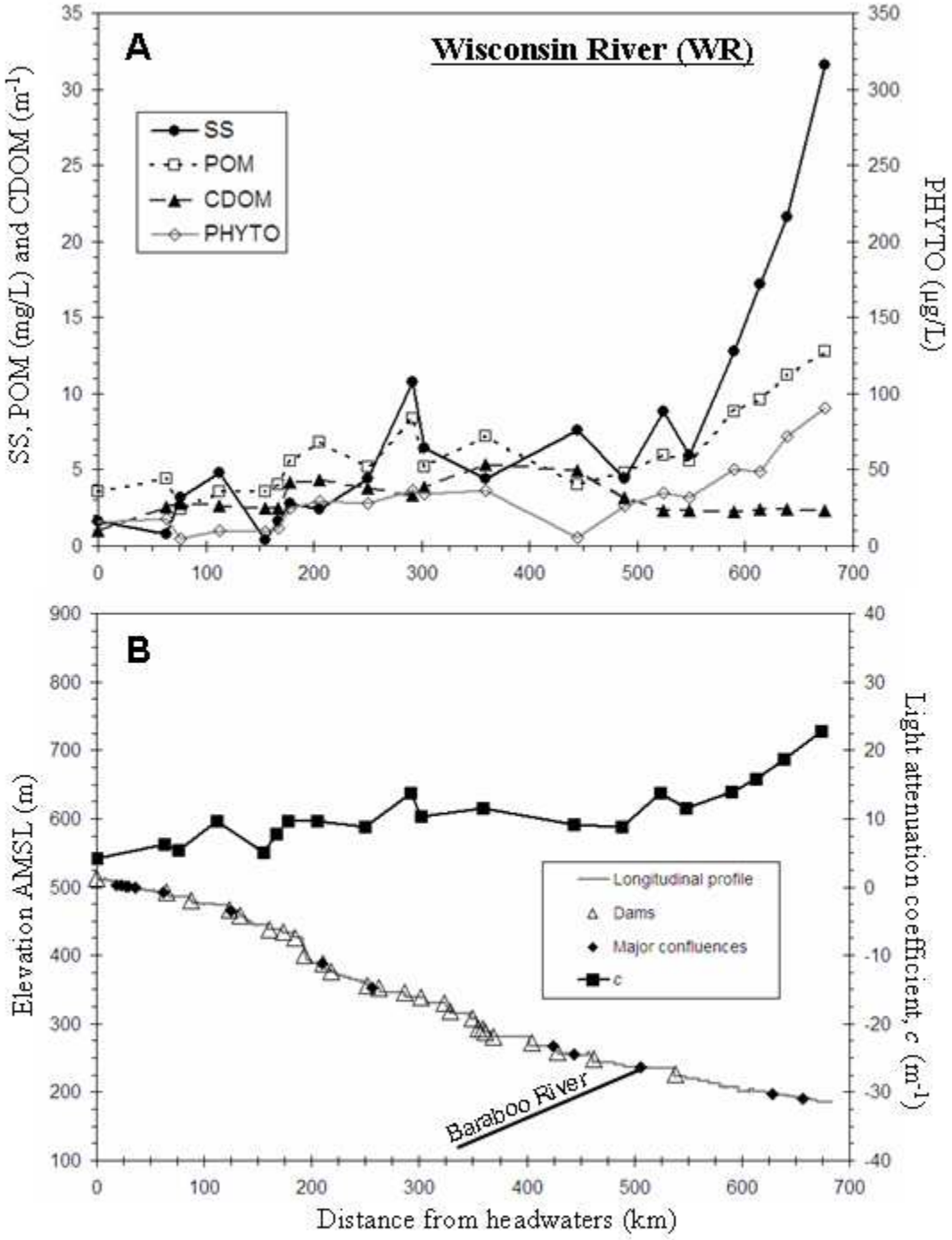

Figure 2.8. (A) Water chemistry along Wisconsin River on Sep. 16, 2006. (B) Longitudinal profile and optical water quality along Wisconsin River on Sep. 16, 2006. A major confluence is where a tributary with a stream order ≥ n-1 enters WR (n = stream order of WR before confluence).

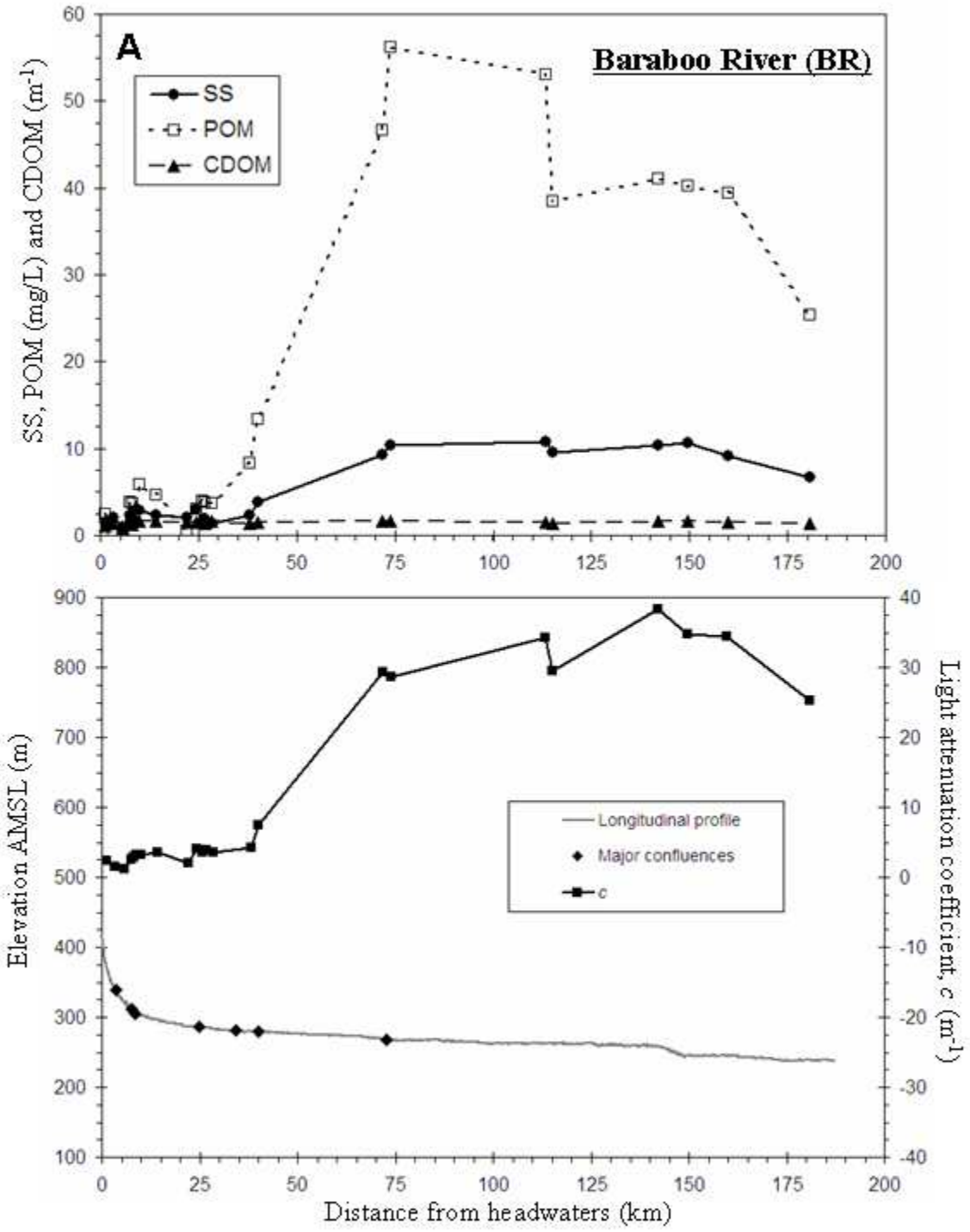

Figure 2.9. (A) Water chemistry along Baraboo River on Aug. 13, 2006. (B) Longitudinal profile and optical water quality along Baraboo River on Aug. 13, 2006. A major confluence is where a tributary with a stream order $\geq$ n-1 enters BR (n = stream order of BR before confluence). There were no dams along BR.

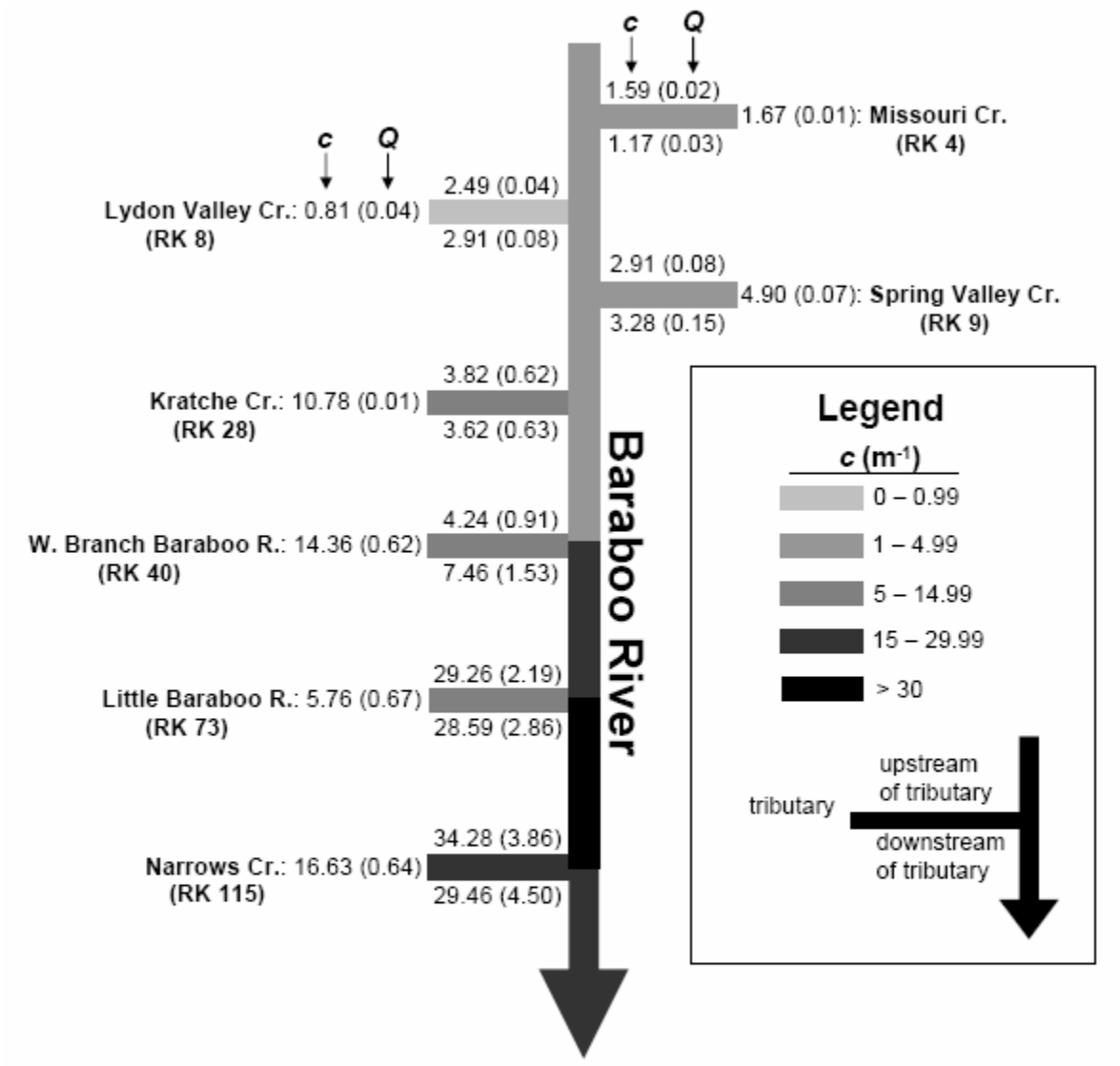

Figure 2.10. Optical water quality budget for Baraboo River. All but two of the tributaries are major tributaries (Kratche Creek and Narrows Creek). The distance of the confluence from the headwaters in km (RK) is given below its name. Schematic is not drawn to scale.

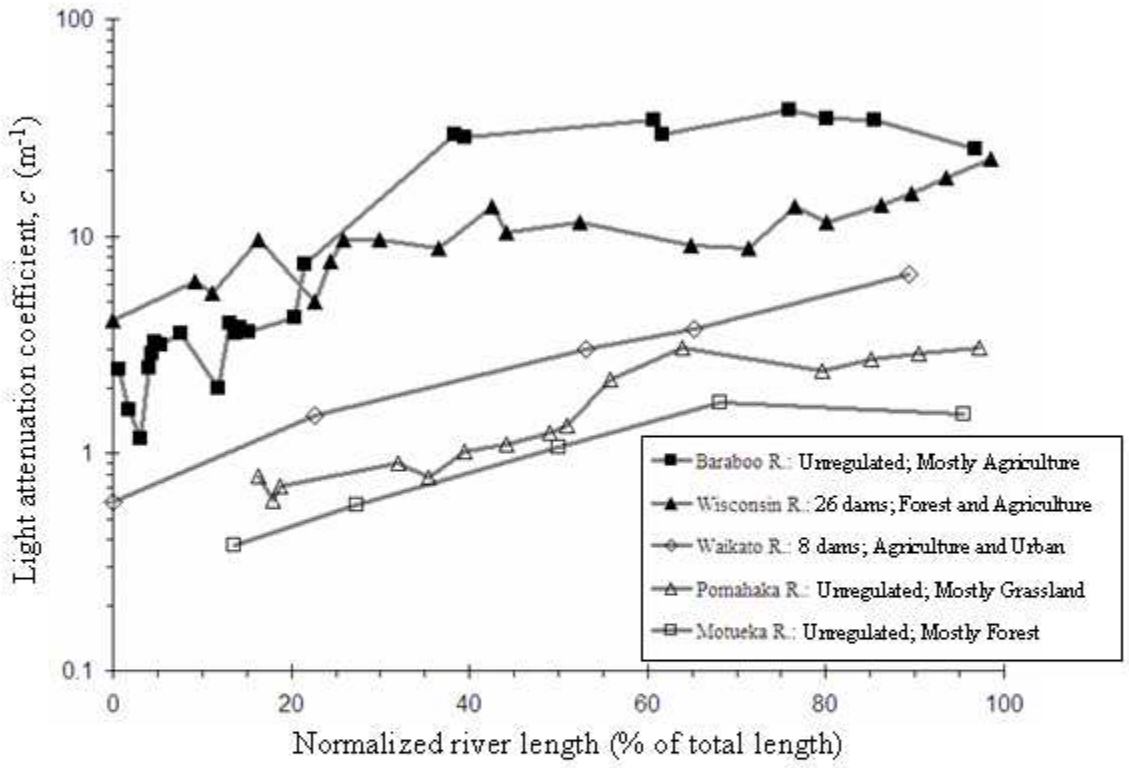

Figure 2.11. OWQ along the river continuum. Degree of flow regulation and dominant land-use is provided next to the name of each case-study.

CHAPTER III. EMPIRICAL MODELING OF LIGHT AVAILABILITY IN RIVERS

1. INTRODUCTION

Many fundamental processes of aquatic ecosystems are driven by light availability, including photosynthesis, photochemical reactions, thermal fluctuations, and various animal behaviors (Wetzel 2001). While the influence of hydrology and geomorphology on other ecosystem-limiting factors are increasingly studied (e.g., nutrient cycling, habitat; Doyle and Stanley 2006, Strayer et al. 2006), the more fundamental limitation of light availability has received considerably less attention. Light studies in rivers have been largely neglected because (i) of greater attention to nutrients in controlling primary production, (ii) boundary conditions (banks, riparian vegetation) make ambient light measurements challenging, and (iii) the optical water quality of rivers is highly variable and difficult to characterize (Davies-Colley et al. 2003). The little information that is available on riverine light regimes is derived mostly from New Zealand rivers under predominantly baseflow conditions, limiting current understanding of the temporal and spatial availability of light in rivers.

Most of our knowledge on aquatic optics is derived from studies in oceans (Jerlov 1976, Mobley 1994) and lakes (Kirk 1994, Wetzel 2001). These studies have shown that once light enters the aquatic environment, it is attenuated exponentially with depth. The

rate of light attenuation with depth is dependent on the type and quantity of water constituents, but generally follows predictable trends (Kirk 1994). Light availability in rivers is optically more complex (Westlake 1966, Davies-Colley et al. 2003), requiring consideration of channel hydrology and geomorphology among other factors.

Characterizing the light environment in rivers requires information on the surrounding topography, riparian vegetation, channel geometry, optical water quality, and hydrologic regime (Figure 1). These components, hereafter referred to as hydrogeomorphic controls, are primarily shaped by the river basin's climate and geology. Topography affects light availability as an opaque barrier between solar irradiance and the river, and includes mountains, canyon walls, and riverbanks. Riparian vegetation also shades the water surface, but is not opaque. The percentage of light that riparian vegetation attenuates depends on the direction and intensity of above-canopy irradiance and the canopy structure including its type, height, density, and spatial distribution (Song and Band 2004). Channel geometry refers to the three spatial dimensions of planform, width, and depth. Planform and width augment or mitigate terrestrial shading by influencing the size of the canopy opening relative to the sunpath. Because light intensity decreases exponentially with increasing water column thickness (Kirk 1994), the depth of the channel affects how much light reaches the riverbed.

Once light enters the water column, the amount reaching the riverbed (i.e., benthic light) is influenced by optical water quality and hydrologic regime. Optical water quality is the biogeochemical property that dictates the rate of light attenuation with depth and is set by the relative proportions of pure water, chromophoric dissolved organic matter, suspended sediment, particulate organic matter, and phytoplankton in the water column

(Kirk 1994). Optical water quality can vary widely spatially along a river (Davies-Colley 1987, Julian et al. In review-a) and temporally between flow discharges (Smith et al. 1997, Julian et al. In review-a). Hydrologic regime – the frequency, magnitude, timing, duration, and variability of streamflow (Poff et al. 1997) – directly influences optical water quality and water depth, which in turn dictate the amount of light available at depth in a river (Smith et al. 1997, Julian et al. In review-a).

Most previous studies that have characterized light availability in rivers have only assessed the control of optical water quality (Davies-Colley 1987, Davies-Colley and Close 1990, Davies-Colley et al. 1992, Phlips et al. 2000, Koch et al. 2004). The aquatic controls of optical water quality and hydrologic regime have been concomitantly addressed by only a few studies (Davies-Colley 1990, Smith et al. 1997). The terrestrial controls of topography, riparian vegetation, and channel geometry have been concomitantly addressed by only a few studies as well (Davies-Colley and Payne 1998, Davies-Colley and Quinn 1998). The most comprehensive riverine light studies have assessed topography, riparian vegetation, channel geometry, and optical water quality (DeNicola et al. 1992, Taylor et al. 2004), with hydrologic regime omitted. Further, all of the above studies have been site-specific. A comprehensive, explicit, and adaptable framework for characterizing light regimes in rivers has yet to be developed.

The overarching goal of this study was to generate such a framework via development of an empirically-based benthic light availability model (BLAM). Specific objectives were to quantify the amount of light attenuation by each hydrogeomorphic control, derive a comprehensive expression that incorporates both the spatial and temporal variability of these controls, and apply this model to rivers with a wide range of

physical characteristics. First, we outline the analytical framework of BLAM for predicting the amount of photosynthetically active radiation (PAR: 400 – 700 nm) at the riverbed. Second, we apply BLAM to two dissimilar rivers: a large, turbid river in central North Carolina, and a small, optically clear stream in central Wisconsin. Third, we compare model results of these two rivers to assess the dominant controls on both temporal and spatial light availability for rivers in general. Fourth, we assess the accuracy of BLAM by comparing modeled PAR values to measured PAR values at a transect in one of our study reaches. Finally, we provide some examples of applications for BLAM and how readily available or commonly collected data can be used to construct light availability models at other sites.

2. METHODS

2.1. Model Development

To quantify benthic light availability and its various controls, we combined previously developed and verified optical and hydrological methods. The first-order control on light availability is above-canopy PAR (E_{can}; in mol m^{-2} d^{-1}), where one mol equals 6.02 x 10^{23} photons. E_{can} is the total amount of PAR that is available to the river before any shading from topography or riparian vegetation (Figure 1). E_{can} is therefore independent of the river basin's characteristics, with no required site-specific assumptions. E_{can} can be obtained directly from a local weather station, measured directly with a PAR sensor, or modeled using solar simulation software.

Topography and riparian shading decrease the amount of PAR that reaches the water surface, reducing E_{can} to E_s (Figure 1). We refer to the ratio of E_s:E_{can} as the

shading coefficient (*s*). The shading coefficient can be derived from numerous methods (see Davies-Colley and Payne 1998), but we prefer the "canopy photo method," where a hemispherical canopy photograph is overlaid by the sunpath to calculate the amount of solar radiation transmitted through openings in the canopy (Figure 2). After review of all the methods to quantify stream shade and several pilot studies, we found that this method provided the best combination of precision, simplicity, time-efficiency, versatility, and affordability. Most other methods used to quantify stream shade (e.g., clinometer, densiometer, solar pathfinder) assume an opaque canopy, which can underestimate the amount of transmitted PAR by as much as 85% due to canopy gap light transmission (Chazdon and Pearcy 1991). The canopy photo method was designed for forestry applications (Evans and Coombe 1959), but has been successfully used to quantify stream shade (Taylor et al. 2004).

Reflection at the air-water interface decreases the amount of PAR that enters the water column, reducing E_s to E_0, where E_0 is PAR available immediately below the water surface (Figure 1). We refer to the ratio of E_0:E_s as the reflection coefficient (*r*). The value of *r* can be found in situ by measuring PAR immediately above (E_s) and below (E_0) the water surface. Alternatively, *r* can be estimated using Fresnel's formula (Kirk 1994, Mobley 1994). The product of E_{can}, *s*, and *r* is the amount of PAR that enters the water column.

Once light enters the water column, it is attenuated exponentially with depth due to scattering and absorption by constituents in the water column (Kirk 1994). The proportion of PAR at depth in the river is derived using the Beer-Lambert law:

$$E_d(y) = E_0 \times e^{-K_d \times y} \qquad (3.1)$$

where $E_d(y)$ is downward PAR (in µmol m^{-2} s^{-1}) at depth y (in m), and K_d is the diffuse attenuation coefficient for downward PAR (in m^{-1}). K_d is predominantly set by the optical water quality, and to a lesser degree by the solar zenith angle and the ratio of diffuse to direct light. K_d can be normalized to remove the effects of solar zenith angle and ratio of diffuse to direct light (see Gordon 1989), but for most rivers dependence of K_d on these two variables is minimal (Baker and Smith 1979, Zheng et al. 2002).

Combining the Beer-Lambert law (Equation 1) with the quantifications of shading and reflection allows calculation of the amount of E_{can} that reaches the stream bed (E_{bed}) at one location in time:

$$E_{bed} = (E_{can} \times s \times r) * e^{-K_d \times y} \tag{3.2}$$

Spatial variability of E_{bed} (i.e., longitudinally along the river) can be derived by adjusting the shading and depth (s and y). The other parameters of E_{can}, r, and K_d do not vary considerably along a river reach, defined here as a length of river with no major confluences and longitudinally consistent optical water quality.

In addition to spatial distributions, these contributing equations can be used to quantify temporal variability of E_{bed} (i.e., at-a-station over time). We do this by relating y and K_d to water discharge (Q):

$$y = \alpha Q^{\upsilon} \tag{3.3}$$

$$K_d = \beta Q^{\omega} \tag{3.4}$$

where α, β, υ, and ω are rating parameters for y and K_d. We used the power function to relate both variables to Q based on previously developed empirical evidence from Leopold and Maddock (1953) for y and Davies-Colley (1990) for K_d. The combination of these two relations modifies Equation 2 into a temporally variable form:

$$E_{bed} = (E_{can} \times s \times r) \times e^{-\alpha\beta Q^{(\upsilon+\omega)}}. \quad (3.5)$$

Equation 5 therefore predicts the temporal variations in benthic light availability as a function of discharge variability, while Equation 2 predicts spatial variations in benthic light availability through a river reach. We focus here on light availability at the channel bed (E_{bed}) because it provides a relatively fixed datum and it is the minimum value of underwater irradiance. This approach, however, can be used to predict light availability at any depth in the water column by simply adjusting *y* in Equation 2.

2.2. Study Sites

We applied BLAM to two river reaches: Big Spring Creek (BSC) – a small, relatively clear stream in Wisconsin, USA whose hydrology is driven by groundwater; and Deep River (DR) – a large, relatively turbid river in North Carolina, USA whose hydrology is predominantly influenced by surface runoff. The dissimilarities between these two systems allowed us to (i) investigate light regimes over a large range of physical characteristics and (ii) display quantitative outputs for a stream influenced more by terrestrial controls (BSC) versus one influenced more by aquatic controls (DR).

Big Spring Creek is a 2nd-order stream located in the Central Plain of Wisconsin near Big Spring, WI (43^{o}39’40”N, 89^{o}38’30”W; 250 m AMSL; Figure 3). The BSC study reach was a 1.3 km section downstream of Big Spring Dam, a small run-of-river dam. Being a run-of-river dam, it did not alter the hydrology of BSC and comparisons between an upstream (of the dam) and downstream station revealed that downstream optical water quality was not significantly affected by the dam (Julian et al. In review-a). There were no major tributaries and optical water quality was longitudinally consistent

along the entire study reach [Julian, unpublished data]. Land cover in the 21.1-km^2 watershed of BSC was mostly agriculture (46%), followed by forest (31%), grassland (21%), and wetland (2%) (*WISCLAND* 1993). The discontinuous riparian corridor of BSC was composed of a mixture of reed canary grass (*Phalaris arundinacea*) and mixed-hardwood forest. Aquatic vegetation in the study reach consisted of epiphytic filamentous algae and an abundance of benthic macrophytes, with the dominant species being leafy pondweed *(Potamogeton foliosus* Raf.), curly-leaved pondweed *(Potamogeton crispus* L.), water stargrass (*Zosterella dubia* (Jacq.) Small), American waterweed (*Elodea canadensis*), and stoneworts (*Nitella* spp.). The basin receives 84 cm/yr of precipitation with a seasonal peak in monthly precipitation during the summer (*NOAA* 2007). However, BSC is a spring-fed stream with relatively constant *Q*.

Deep River is a 6th-order stream located in the Central Piedmont of North Carolina near Carbonton, NC (35^{o}31'00"N, 79^{o}21'00"W; 76 m AMSL; Figure 3). The DR study reach was the 5.8 km section downstream of the former Carbonton Dam, which was removed in December 2005. There were no major tributaries and optical water quality was longitudinally consistent along the entire study reach [Julian, unpublished data]. The 2,770-km^2 watershed was dominated by forest (72%), followed by agriculture (25%), and urban (3%) land cover (*NCDWQ* 2000). The nearly continuous riparian corridor of DR was composed of oak-hardwood forest. Aquatic vegetation in the study reach consisted of patches of hornleaf riverweed (*Podostemum ceratophyllum* Michx.), water moss (*Fontinalis sullivantii* Lindb.), epiphytic filamentous algae, and algal biofilms. The basin receives 110 cm/yr of precipitation with no distinct seasonality in monthly precipitation (*NOAA* 2007). Most of the urbanization in the basin was located in

the headwaters, which together with its heavily entrenched channels, lead to high, flashy flood flows during storms.

2.3. Data Collection and Model Inputs

2.3.1. Above-Canopy PAR (E_{can})

We modeled E_{can} with Gap Light Analyzer (GLA) software (Frazer et al. 1999), using the parameters in Table 1 and the respective locations and elevations of BSC and DR. From GLA, we derived an average daily E_{can} value for BSC during May 15 – Sep 15 and an average daily E_{can} value for DR during May 1 – Sep 30. We also obtained actual daily E_{can} values from the UV-B Monitoring and Research Program (*USDA* 2007), which reported 3-min averages of 20-sec readings from a *LI-COR* quantum sensor. Sites NC02 (Raleigh, NC) and WI02 (Dancy, WI) were used for DR and BSC, respectively.

2.3.2. Reflection Coefficient (r) and Diffuse Attenuation Coefficient (K_d)

We measured r and K_d at various locations and discharges along the study reaches using a *LI-COR* LI-192 underwater quantum irradiance (PAR) sensor, which measures photosynthetic photon flux density (PPFD) in $\mu mol\ m^{-2}\ s^{-1}$. All measurements were taken at unshaded locations during full sun conditions between May 15 – Sep 15, 2006, between 0900 – 1500 local standard time, and using 15-second averages. We calculated r by taking PAR measurements directly above the water surface (E_s) and directly below the water surface (E_0; $r = E_0/E_s$). A total of 27 and 25 r measurements were taken at BSC and DR, respectively. In addition to E_0, we measured PAR at the riverbed (E_{bed}) and at 10-cm intervals between these two depths. We derived K_d from the linear regression

coefficient of ln $E_d(y)$ with respect to y (Equation 1). A total of 34 and 21 K_d measurements were taken at BSC and DR, respectively.

2.3.3. Shading Coefficient (s) and Water Depth (y)

We used synoptic sampling to quantify the within-reach variability of s and y. We used a *Nikon Coolpix 4500* camera with fisheye lens to collect digital hemispherical canopy photos along the study reaches, which we processed and analyzed with GLA software to obtain E_s and s. The details of the canopy photo method using GLA software are documented by Frazer, et al. (1999) and the parameters used for canopy photo analyses are listed in Table 1. We took 39 canopy photos along BSC on June 27, 2006, with an average distance of 33 m between photos. We took 22 canopy photos along DR on Aug. 27, 2006, with an average distance of 264 m between photos. Photo locations were selected based on changes in channel width, canopy structure, and channel orientation (azimuth).

We quantified y along the two study reaches using longitudinal profiles surveyed with a total station (*Trimble* 3350DR) and graded prism rod. We measured 129 locations along BSC on Jun 15, 2005 with an average interval of 10 m, and 67 DR locations on Sep 12, 2005 with an average interval of 86 m. Survey locations were selected based on changes in channel slope and water depth. Both longitudinal profiles were surveyed during baseflow.

2.3.4. Temporal Sampling

At each river, we established a fixed sampling station where we quantified depth, discharge, and turbidity. Temporal trends in these variables were assessed at a station 0.75 km downstream of the dam on BSC and 0.25 km downstream of the former dam on DR (Figure 3). Water depth (y) was measured every 15 minutes by stage recorders (*Intech WT-HR 2000* for BSC and *HOBO 9-m* for DR). We calculated discharge (Q) using stage-Q rating curves developed with in-situ Q measurements taken with a *Marsh-McBirney* current meter. We estimated flood discharges at DR with the weighted area method (Gordon et al. 2004), using a downstream USGS gage (#02102000) for a reference Q. All reported Q and y are daily average values.

The rating parameters α and υ were derived from the regression of y vs. Q (Equation 3), and β and ω were derived from the regression of K_d vs. Q (Equation 4). We used turbidity (T_n) as an intermediate regressor (i.e., K_d was first regressed with respect to T_n, then T_n was regressed with respect to Q) due to the impracticality of measuring K_d during high flows. Because of the dominant effect of particulates on light attenuation in rivers, riverine optical water quality can be characterized fairly accurately using T_n measured in nephelometric turbidity units (NTU) with a turbidimeter (Kirk 1994, Julian et al. In review-a). We measured T_n with a HACH 2100P turbidimeter from water samples collected during various flow periods (Table 2).

2.4. Data Analysis

2.4.1. Statistical Methods

To assess the dominant controls on benthic light availability, we compared correlations between E_{bed} and the parameters of BLAM (Equations 2 and 5). One-way

analysis of variance (ANOVA; $p < 0.05$) was used to test for differences in *s* among various riparian communities and channel orientations. We classified riparian community as forest, grass, or mixed, and channel orientation by the four azimuthal axes: 0-180^o, 45-225^o, 90-270^o, and 135-315^o. We used JMP IN 5.1 (*SAS Institute*, Cary, NC) to perform all statistical tests.

We also used JMP IN 5.1 to perform Monte Carlo simulations that quantified the probabilistic frequency of daily E_{bed} for an independent randomly selected E_{can} and an independent randomly selected *Q*, which are the two temporally variable parameters in Equation 5. We used 10,000 iterations (paired random samples) for each site, selecting from measured values of E_{can} (via the weather station) and *Q* (via the stage recorder). Probability distributions were tested for normality using the Kolmogorov-Smirnov test statistic (D), where D < 0.05 indicated a normal distribution.

2.4.2. Effect of Channel Orientation on the Shading Coefficient

While the effects of channel width and canopy structure on *s* are intuitive (i.e., increased width increases s, increased canopy area and density decreases *s*), the effect of channel orientation on *s* is more complicated and has rarely been considered in light availability studies (e.g., Yard et al. 2005). We quantified the variation in *s* as a function of channel orientation by keeping width and canopy structure constant, which we accomplished by rotating the canopy photos. For example, by rotating the canopy photo 90^o in Figure 2B, we changed its orientation from South-North to West-East without altering its width or canopy structure. We used GLA to examine the effect of channel orientation on *s* by using 45° incremental rotations (8 analyses for each photo) and

quantifying the change in E_{bed} at these successive channel orientations. This technique was performed for four scenarios: closed canopy (forested banks, narrow channel), open canopy (forested banks, wide channel), half canopy (one grassed bank, one forested bank), and no canopy (grassed banks).

2.4.3. Model Accuracy Assessment

In order to assess the accuracy of BLAM, we compared modeled daily E_{bed} (Equation 5) to actual daily E_{bed} (measured with a PAR sensor at the channel bed). We measured E_{can}, E_s, E_0, and E_{bed} continuously at BSC with four PAR sensors during the period Jun 16 – 25, 2006. E_{can} was monitored with a PAR sensor (HOBO, *Onset*) placed in a nearby open field, which measured photosynthetic photon flux density (PPFD) in 1-min intervals. The other three PAR sensors (LI-192, *LI-COR*) were set in an array in BSC at a transect 175 m downstream of the sampling station. We attached these three sensors to a metal rod driven into the bed of the channel, with one sensor located just above the water surface, one immediately below the water surface, and one on the riverbed to measure E_s, E_0, and E_{bed}, respectively. The three sensors were connected to a *LI-COR* LI-1400 data logger, which recorded PPFD in 15-min intervals. PPFD measurements were integrated and summed to obtain daily PAR values. We leveled all four sensors with a bubble level and placed a mesh barrier upstream of the in-channel array to prevent debris from collecting around the sensors. The E_{bed} sensor was disturbed on Jun 21, leaving us with 9 daily E_{bed} values. The E_0 sensor malfunctioned Jun 18 – 22, leaving only 5 daily E_0 values. We also monitored daily E_s with PAR sensors (HOBO,

Onset) placed at two other transects in BSC: one located at the sampling station (Jun 14 – 23, 2006) and the other 520 m upstream of the sampling station (Jun 25 – 26, 2006).

2.5. Model Assumptions and Limitations

BLAM (i.e., Equations 2 and 5) is a one-dimensional model that assumes the river is well-mixed with no lateral variation in optical water quality. This assumption is not valid for river sections with large dead-water zones and sections directly below confluences. Kenworthy and Rhoads (1995) found that full mixing downstream of tributaries occurs at an approximate distance of four downstream channel widths. BLAM also does not take into account shading by aquatic biota, such as aquatic macrophytes. While we only assessed daily benthic PAR in the center of the channel, our approach can be used to assess light availability at any wavelength, depth, lateral distance, and time-step.

We performed all of our measurements and analyses when Leaf Area Index (LAI) was greater than 90% of annual maximum. This period of > 90% LAI was conservatively estimated from previous studies on seasonal leaf dynamics in the study site's region: central North Carolina (May 1 – Sep 30; Palmroth et al. 2005) and central Wisconsin [May 15 – Sep 15; *Stanley*, unpublished data]. By confining our model results to these periods of > 90% LAI, we effectively removed seasonal variations in E_{can} and E_s, and minimized seasonal variations in r and K_d. BLAM can be used to investigate seasonal variability in E_{bed} with additional measurements, but this analysis was beyond the scope of the present study.

3. RESULTS

3.1. Controlling Parameters

3.1.1. Overview of Site Conditions

BSC had a baseflow water surface width of 7.48 ± 1.75 m (mean ± standard deviation) and depth of 0.60 ± 0.22 m over the 1.3-km study reach (Figures 3A and 4A). Its flow was relatively constant and clear (Figure 5A, Table 3). The channel of BSC was heavily shaded, except in deforested sections (Table 3). DR had a baseflow water surface width of 35.0 ± 4.7 m and depth of 1.2 ± 0.6 m (Figures 3B and 4B). Its flow was highly variable and more turbid (Figure 5B, Table 3). The channel of DR was moderately shaded (Table 3). The temporal trend and average of above-canopy PAR was similar for both sites (Figure 5, Table 3).

Discharge remained relatively constant at BSC (Figure 5A, Table 3). Average Q was 0.37 ± 0.04 m^3/s and only 4 stormflows with peaks greater than 0.40 m^3/s (75^{th} percentile) occurred during the study period. Discharge at DR was greater and considerably more variable (Figure 5B, Table 3), as average Q was 9.56 ± 10.70 m^3/s. During the study period, DR experienced 11 stormflows with peaks greater than 8.62 m^3/s (75^{th} percentile).

Water depth at the BSC sampling station ranged 0.91 – 1.18 m and averaged 1.01 ± 0.05 m. Spatially, y was variable along the sand-bed channel of BSC, fluctuating between 0.23 and 1.26 m (Figure 4A). At the DR sampling station, y ranged 0.33 – 2.86 m and averaged 0.65 ± 0.38 m. Spatially, y was highly variable along the gravel-bed channel of DR, ranging 0.34 – 3.55 m (Figure 4B).

3.1.2. Terrestrial Shading

Daily above-canopy PAR (E_{can}) at both sites fluctuated considerably in response to varying degrees of cloudiness (Figure 5, Table 3). Between May 15 and Sep. 15, 2006, E_{can} at BSC averaged 41.98 $\pm$ 13.88 mol m^{-2} d^{-1}. GLA-modeled E_{can} for this same period was 39.83 mol m^{-2} d^{-1} at BSC, only a 5% difference than the measured average. Between May 1 and Sep. 30, 2006, E_{can} at DR averaged 41.17 $\pm$ 12.35 mol m^{-2} d^{-1}. GLA-modeled E_{can} for this same period was 39.68 mol m^{-2} d^{-1} at DR, only a 4% difference than the measured average.

The proportion of E_{can} remaining after terrestrial shading (s) varied widely along the 1.3-km BSC study reach due to changes in the riparian community (Table 3). Spatially averaged s was 0.51 $\pm$ 0.25, i.e., approximately 51% of the available daily PAR passed through the canopy and reached the water surface over the entire reach. The fixed sampling station at BSC had an s of 0.17. s was more consistent along the 5.8-km reach of DR due to a continuous and relatively uniform riparian corridor (Table 3) and averaged 0.68 $\pm$ 0.08. The fixed sampling station at DR had an s of 0.78.

3.1.3. Aquatic Light Attenuation

The proportion of E_s remaining after reflection at the air-water interface (r) was relatively constant at both sites, averaging 0.92 $\pm$ 0.03 at BSC and 0.93 $\pm$ 0.03 at DR. Mean baseflow K_d was 0.60 $\pm$ 0.09 m^{-1} and 1.84 $\pm$ 0.39 m^{-1} for BSC and DR, respectively. The relationship between K_d and T_n for both rivers was: $K_d = 0.17T_n$ (r^2 = 0.88; Figure 6). The relationship between T_n and Q was: $T_n = 190.57Q^{3.69}$ (r^2 = 0.54) for

BSC, and $T_n = 1.04Q^{1.31}$ ($r^2 = 0.85$) for DR. Together these relationships produced the rating parameters between K_d and Q (Equation 4, Table 3).

3.2. Temporal Light Availability

3.2.1. Temporal BLAM Output

Benthic PAR (E_{bed}) at the BSC sampling station varied between 0.10 and 5.94 mol m^{-2} d^{-1} during May 15 – Sep. 15, 2006 (Figure 5A) and average E_{bed} during this period was 2.83 $\pm$ 1.30 mol m^{-2} d^{-1}. Generally, E_{bed} at BSC was highest when E_{can} was high and Q was low (Figures 5A and 7A, B). Benthic PAR at the DR sampling station varied from 0.00 to 22.31 mol m^{-2} d^{-1} during May 1 – Sep. 30, 2006 (Figure 5B). The average E_{bed} during this period was 8.24 $\pm$ 6.00 mol m^{-2} d^{-1} and E_{bed} was typically highest when Q was low (Figures 5B and 7D). Although the correlation was statistically significant, E_{can} could account for only 11% of the observed variance in E_{bed} at DR (Figure 7C).

3.2.2. Magnitude-Frequency Distribution of Benthic Light Availability

The two temporally variable parameters in BLAM, assuming only summer conditions, are E_{can} and Q (Table 3). There was no dependence of Q on E_{can} (i.e., no multicollinearity) for BSC ($p = 0.57$) or DR ($p = 0.15$). This independence of parameters validated the use of Monte Carlo simulations at both sites. From these simulations and using Equation 5, the possible range of E_{bed} was 0 – 7 mol m^{-2} d^{-1} for BSC and 0 – 33 mol m^{-2} d^{-1} for DR (Figure 8). The probability of E_{bed} for BSC was approximately normally distributed (D = 0.04) with a peak at 3-4 mol m^{-2} d^{-1} (Figure 8A). In contrast, the

probability of E_{bed} for DR was non-normally (D = 0.10), broadly distributed with two modes, one at 0-1 and the other at 3-4 mol m^{-2} d^{-1} (Figure 8B). Most importantly, for DR there were many E_{bed} values with similar probabilities, whereas for BSC, probabilities were dissimilar for the relatively few E_{bed} values.

3.3. Spatial Light Availability

3.3.1. Spatial BLAM Output

Benthic PAR along the 1.3-km reach of BSC varied between 3.23 and 25.12 mol m^{-2} d^{-1} during baseflow (Figure 9A) with a reach average of 12.66 $\pm$ 6.69 mol m^{-2} d^{-1}. Generally, E_{bed} was highest in unshaded sections where *s* was high (Figures 9A and 10A). There was not a strong correlation between E_{bed} and *y* along BSC (Figure 10B). However, when divided into riparian groups, correlations between E_{bed} and *y* at BSC were stronger, with r^2 values of 0.25, 0.79, and 0.65 for forest, mixed, and grass, respectively.

Benthic PAR along the 5.8-km DR study reach varied between 0.03 and 14.70 mol m^{-2} d^{-1} during baseflow (Figure 9B) with a mean of 4.42 $\pm$ 3.28 mol m^{-2} d^{-1}. High E_{bed} values usually occurred in shallow sections where *y* was low (Figures 4B, 9B, and 10D). The correlation between E_{bed} and *s* at DR was relatively weak (Figure 10C). In sum, E_{bed} along BSC was well-predicted by shading but not depth, whereas E_{bed} at DR was well-predicted by depth but not shading.

3.3.2. Channel Geometry and Canopy Structure

The two spatially variable parameters in BLAM are *s* and *y* (Table 3), both of which are influenced by channel geometry. Channel depth dictates *y*, while channel width and orientation, along with canopy structure, dictate *s*. Canopy structure was the major influence on *s* for BSC because of its wide variation in riparian community: forest ($s = 0.26 \pm 0.10$, n = 15), grass ($s = 0.80 \pm 0.07$, n = 13), and mixed (0.52 ± 0.07, n = 11). These three groups were significantly different with respect to *s* ($p < 0.01$). Width could only explain 21% of the variance in *s* along the entire BSC reach, and explained even less variance within riparian groups ($r^2 = 0.01$, 0.03, and 0.02 for forest, grass, and mixed, respectively). The difference in *s* among the four axes of channel orientation was only marginally significant ($p = 0.06$).

Although *y* was the dominant control on E_{bed} along DR, *s* also affected E_{bed} because of its control on E_0. Compared to BSC, DR had a relatively uniform forested riparian corridor. The correlation between *s* and channel width was very weak ($r^2 = 0.03$) at DR, and there was no significant difference in *s* among the four axes of orientation ($p = 0.79$), which suggests that variation in *s* at this site probably resulted from the sum of independent variations in all three factors.

The effect of channel orientation on *s* varied for different canopy structures. For a transect at BSC with a closed canopy (forested banks, narrow channel), channel orientation did not change *s* by more than 0.06 (Figure 11). Similarly, for a transect at BSC with no canopy (grassed banks), channel orientation did not change *s* by more than 0.02. The no canopy scenario would also be characteristic of very wide rivers with forested banks. For a transect at BSC with a half canopy (one grassed bank, one forested bank), channel orientation changed *s* by as much as 0.39. For a typical transect at DR

with an open canopy (forested banks, wide channel), channel orientation changed *s* by as much as 0.20, with peaks at 90^o and 270^o (Figure 11). In all four canopy scenarios, the maximum *s* occurred at an azimuth of 90^o (West-East). Thus, given the same canopy structure and channel width, channel orientation has the potential to alter *s* considerably.

3.4. Comparisons between Modeled and Actual Benthic PAR

BLAM (Equation 5) predicted E_{bed} within 38% on average for the period of Jun 16 – 25, 2006 (Figure 12, Table 4). BLAM predicted E_{bed} within 20% on four of the nine days, and the greatest error was 92% (Table 4). A considerable portion of the error resulted from the difference in *s* between the sensor and modeled values. GLA calculated an *s* of 0.67 at this site, while the sensors (E_s/E_{can}) measured an *s* of 0.56 $\pm$ 0.05. Substituting the actual *s* into Equation 5 reduced the average error of BLAM to 15%. A PAR sensor placed at the BSC sampling station showed similar error in *s*, where GLA calculated 0.17 and the sensors measured 0.08 $\pm$ 0.01 (n = 7). However, a PAR sensor placed at another transect (520 m upstream of sampling station) showed very little error in *s*, where GLA calculated 0.79 and the sensors measured 0.78 $\pm$ 0.01 (n = 2).

Differences in K_d between sensor and modeled values also added model error. Using β and ω from Table 3, BLAM predicted a K_d of 0.58 $\pm$ 0.05 m^{-1} for the 9-day period, whereas the sensors ($\ln E_0 \ \ln E_{bed}^{-1} \ y^{-1}$) measured 0.85 $\pm$ 0.12 m^{-1}. Substituting the actual K_d and *s* into Equation 5 reduced the average error of BLAM to 4%. There were relatively minor differences in the other parameters between modeled and measured values: E_{can} (BLAM: 42.95 $\pm$ 10.61 mol m^{-2} d^{-1}, Sensors: 40.71 $\pm$ 10.86 mol m^{-2} d^{-1}) and *r* (BLAM: 0.92 $\pm$ 0.03, Sensors: 0.88 $\pm$ 0.04).

4. DISCUSSION

4.1. Controls on Riverine Benthic Light Availability

4.1.1. Atmosphere

Atmospheric constituents (clouds, particulates, gases) are the first-order controls on light availability in rivers. The enormous variability and unpredictability in the spatiotemporal distribution of these atmospheric constituents (Kirk 1994) prevented us from modeling E_{can} as a dependent variable. We therefore used E_{can} as the independent variable in BLAM. While solar simulation software (GLA) proved to be accurate within 5% of the average daily E_{can}, the weather station data were needed to derive actual frequencies of benthic light availability (Figure 8).

The weather station data would also be beneficial when correlations between ecological variables and E_{can} are sought (e.g., Mulholland et al. 2001). Daily E_{can} is likely to vary considerably in response to cloud cover (Figure 5) and therefore correlations of this nature require accurate measurements which can only be acquired from a local weather station or user-installed PAR sensor. When using weather station data, we suggest using only weather stations that frequently calibrate their sensors (e.g., USDA UV-B Monitoring and Research Program), or verifying the accuracy of the data by comparing it to nearby weather stations and analyzing yearly trends (e.g., progressively decreasing PAR intensities due to sensor degradation were frequently observed in preliminary weather station data analyses).

4.1.2. Terrestrial Controls

Before solar irradiance enters the water column, its intensity is reduced by the terrestrial controls of topography, riparian vegetation, and channel geometry. Topography was not an effective control on light attenuation at either case-study due to their limited relief. Topography is however capable of being a dominant control on light availability in mountainous headwater streams, canyon rivers, and heavily-incised rivers (Yard et al. 2005).

Riparian vegetation was a dominant control on E_{bed} at BSC because of the relatively narrow channel at this site (Figures 9A and 10A). In forested sections of BSC, riparian vegetation shaded as much as 85% of the incoming PAR. In contrast, riparian vegetation accounted for only a ~32% reduction of E_{can} at the wider DR. This trend confirms the common expectation that terrestrial shading decreases with increasing channel width (Vannote et al. 1980, Davies-Colley and Quinn 1998).

Channel orientation can also mitigate or exaggerate the effect of terrestrial shading. The relative change in *s* caused by channel orientation was greatest at DR, which had an open canopy, and in sections of BSC with a half-canopy (Figure 11). In river sections with either a closed canopy or no canopy, the orientation of the channel does not significantly alter *s* because of the uniform distribution of canopy gaps relative to the sunpath. For river sections with an open canopy, riparian shading is the most exaggerated (lowest *s*) by North-South orientations because of the higher opacity of the channel margins and the smaller window for direct solar radiation transmission (see Figure 2B for context). Conversely, East-West orientations provide a larger window for direct solar radiation transmission and orient the sunpath over the upper canopy, which

has more gaps than the lower canopy. Our finding that maximum *s* occurred at an azimuth of 90° for all riparian vegetation scenarios confirmed this relation.

4.1.3. Aquatic Controls

While the boundary conditions of rivers (terrestrial controls) create spatial variation in light availability within a season, the aquatic controls of hydrologic regime and optical water quality create temporal variation in light availability. In small, spring-fed streams such as BSC, this temporal variation may not be large due to a relatively constant hydrologic regime and optical water quality (Figure 5A). Further, temporal variation of E_{bed} in small rivers is likely to be suppressed by the influence of terrestrial shading (Figures 5A and 7A). But for most rivers, the variation in benthic light availability is likely to be quite large due to the variability in Q (Figure 5B), which dictates the temporal variability in y (Leopold and Maddock 1953) and K_d (Davies-Colley 1990, Julian et al. In review-a). While the correlation between y and Q was strong, the correlation between K_d and Q was far more variable. This greater variance is largely the result of inter-storm and seasonal effects on optical water quality (Julian et al. In review-a). The use of T_n as an intermediate regressor also added variance to the correlation. However, we found a strong and similar correlation between K_d and T_n at both study sites (Figure 6), and therefore suggest T_n as a proxy for K_d. In all, temporal variation of benthic light availability within river reaches is likely to be substantially and predominantly driven by variability in river depth and optical water quality.

4.2. Small vs. Large Rivers

Overall, DR had less spatial variability (Figure 9) but greater temporal variabilty (Figures 5 and 8) in E_{bed} than BSC. The magnitude-frequency distribution of benthic light availability in rivers is affected by all the parameters in Equation 5, but it is mostly governed by the temporal distributions of E_{can} and Q. Because of the dominating influence of s on E_{bed} for small rivers such as BSC, their temporal variability in E_{bed} is likely to follow the trend of E_{can}. In basins with frontal weather patterns, this trend is characterized by an approximately normal distribution in which most days have an intermediate E_{can} and few days have very low or very high E_{can} (similar to the distribution in Figure 8A). For large rivers such as DR, Q is likely to be the dominant influence on E_{bed}; however, E_{can} also affects the temporal distribution of E_{bed} because it is the first-order control on light availability. Therefore, the magnitude-frequency distribution of benthic light in large rivers is likely to have a broad and more bimodal distribution in which one peak is set by E_{can} and the other by Q. For example, the left peak in Figure 8B was caused by the high frequency of floods in DR, which lead to elevated turbidity for long periods (Julian et al. In review-a). This elevated turbidity attenuates most of the underwater light before it reaches the bed. The right peak in Figure 8B was caused by the distribution of E_{can}, which is similar to that of BSC (Figure 8A). Overall, s sets the maximum potential E_{bed}, while Q sets the potential range and frequency of E_{bed}.

Along the river continuum (from headwaters to mouth), the influence of shading on E_{bed} decreases due to the mitigating effect of width on s (Figures 2 and 11; Vannote et al. 1980). Conversely, the effect of y and K_d on E_{bed} increases with increasing river size due to the increase in depth (Leopold and Maddock 1953) and turbidity (Julian et al. In review-a) in the downstream direction. Using Equation 2 and assuming a continuous

forested riparian corridor, the combined effect of terrestrial shading and aquatic attenuation produces a longitudinal distribution of E_{bed} where it is low in the headwaters, high in the middle reaches, and essentially zero in the higher-orders (Figure 13). In general, s is the dominant control on E_{bed} in small rivers and y is the dominant control on E_{bed} in large rivers (Figure 10). The influence of y on E_{bed} increases with increasing turbidity. These above relations were developed from reach-scale comparisons and expected longitudinal patterns. In order to verify the trends in Figure 13, basin-scale surveys of light availability are needed.

4.3. Applications of BLAM

4.3.1. Required Data and Accuracy

BLAM incorporates the six major controls on light availability in rivers, and allows for both temporal and spatial variation in these controls. Using our approach, the minimum information needed to characterize light availability at one location in a river is a canopy photo and some measure of optical water quality (e.g., T_n). Applying our method to an entire reach would require measures of depth and additional canopy photos. Temporal characterization of light availability would require knowledge of the hydrologic regime and its relationship with y and K_d. For any application of BLAM, the extent of data collection would be determined by the desired precision.

Overall, BLAM provided fairly accurate estimates of E_{bed} (Figure 12). Most of the model error was in s and K_d. We derived the model value of s from GLA using generalized and average configuration parameters. These parameters are highly variable in both space and time (Kirk 1994), and are the primary control on canopy light

transmission (Song and Band 2004). To better characterize *s*, one would therefore need more spatiotemporally explicit values of the configuration parameters used in GLA.

We derived the model value of K_d from measurements taken in unshaded locations during mid-day and full sun conditions. Variations in the ambient light field only minimally affect K_d in most rivers due to their high scattering to absorption ratios (Zheng et al. 2002); however in optically clear rivers such as BSC, increased zenith angles (early-morning and late-afternoon) and reduced direct irradiance (cloudy and shaded) are likely to decrease K_d (Gordon 1989). Our model value was therefore probably more characteristic of the minimum K_d than the daily average K_d. Obtaining a daily average K_d for varying levels of cloudiness and streamside shade would involve greater sampling and more sophisticated techniques (e.g., Davies-Colley et al. 1984) than we used, especially for optically clear rivers.

4.3.2 River Ecosystem Dynamics

BLAM can be used to characterize spatial and temporal trends in river light regimes, however its greater utility is as a tool to investigate river ecosystem dynamics. Light is a first-order control on both abiotic (via the hydrological cycle, temperature, and photochemical reactions) and biotic (via temperature, photosynthesis, and visual perception) processes in rivers (Wetzel 2001). Further, it is the only control that exhibits a strong correlation to net ecosystem production over a wide range of rivers (Mulholland et al. 2001). Yet light budgets are rarely developed for river ecosystem studies. BLAM provides a fairly simple, inexpensive (time and money), and precise tool for creating these budgets.

If we can quantify the amount of solar radiation entering a river, we have a first approximation of one of the major components of ecosystem energy, which can then be used to assess metabolism (see Brown et al. 2004). One of the major metabolic processes in rivers is photosynthesis (or primary production) by algae and submersed aquatic macrophytes. All aquatic plants have a compensation irradiance, which is the amount of PAR required for photosynthesis to exceed respiration (Kirk 1994). Thus, by knowing how much PAR reaches the plants, we can approximate net primary productivity (NPP). For example, assuming a compensation irradiance of 3 mol m^{-2} d^{-1} for freshwater aquatic macrophytes (Kirk 1994, p. 278), benthic NPP would occur 46% of the days during the summer at BSC and 77% of the days during the summer at DR (Figure 8). Relations such as these calculated with BLAM can be used to investigate spatiotemporal trends in riverine vegetation, and consequently NPP and metabolism. Other potential applications of BLAM include riparian zone management (Kiffney et al. 2004), nutrient budgets (Doyle and Stanley 2006), environmental maintenance flows (Baron et al. 2002), stream restoration (Scarsbrook and Halliday 1999), biotic behavioral adaptations (Kelly et al. 2003), and feedbacks between geomorphology and ecology (Bott et al. 2006). Although these references establish the ecological importance of light in rivers, the role of light in each of these areas has largely been underappreciated and not fully demonstrated.

5. CONCLUSIONS

Compared to other aquatic ecosystems, rivers arguably possess the greatest spatiotemporal variability and complexity. This complexity has up to now prevented the development of a general framework in which to assess light regimes in rivers. By

combining previously verified optical and hydrological methods, we were able to generate the benthic light availability model (BLAM) which calculates the amount of PAR that reaches the riverbed. BLAM links river hydrogeomorphology and benthic light availability by incorporating the light attenuation of topography, riparian vegetation, channel geometry, optical water quality, and hydrologic regime.

The accuracy of BLAM is largely dependent on the accuracy of the techniques used to obtain s and K_d. We recommend that future studies assess the validity of these techniques, especially for varying degrees of cloudiness and shading. Further, we hope that our approach is tested on a wide variety of rivers, thereby improving upon the accuracy and range of empirical coefficients used in BLAM.

We used BLAM to demonstrate how the spatiotemporal variations in hydrogeomorphic controls dictate benthic light availability in a small, optically-clear stream and a large, turbid river. In addition to assessing the dominant controls on riverine light regimes, BLAM is a tool that can be used to investigate the role of light in river ecosystem dynamics and establish light availability targets in water resource management. BLAM also provides a framework for future models that characterize spatiotemporal variations of ultraviolet (UV) and infrared radiation (IR) in rivers. Our ultimate objective in developing BLAM is that it will be a catalyst for more investigations and applications of the vital role of light in rivers.

REFERENCES

Baker, K. S., and R. C. Smith (1979), Quasi-inherent characteristics of the diffuse attenuation coefficient for irradiance, *Soc. Photo-opt. Instrum. Eng.*, *208*, 60-63.

Baron, J. S., et al. (2002), Meeting ecological and societal needs for freshwater, *Ecological Applications*, *12*, 1247-1260.

Bott, T. L., et al. (2006), Ecosystem metabolism in Piedmont streams: Reach geomorphology modulates the influence of riparian vegetation, *Ecosystems*, *9*, 398-421.

Brown, J. H., et al. (2004), Toward a metabolic theory of ecology, *Ecology*, *85*, 1771-1789.

Chazdon, R. L., and R. W. Pearcy (1991), The importance of sunflecks for forest understory plants, *BioScience*, *41*, 760-766.

Davies-Colley, R. J. (1987), Optical properties of the Waikato River, New Zealand, *Mitteilungen aus dem Geologisch-Palaontologischen Institut der Universitat Hamburg, SCOPE/UNEP Sonderband*, *64*, 443-460.

Davies-Colley, R. J. (1990), Frequency distributions of visual water clarity in 12 New Zealand rivers, *New Zealand Journal of Marine and Freshwater Research*, *24*, 453-460.

Davies-Colley, R. J., and M. E. Close (1990), Water colour and clarity of New Zealand rivers under baseflow conditions, *New Zealand Journal of Marine and Freshwater Research*, *24*, 357-365.

Davies-Colley, R. J., et al. (1992), Effects of clay discharges on streams: 1. Optical properties and epilithon, *Hydrobiologia*, *248*, 215-234.

Davies-Colley, R. J., and G. W. Payne (1998), Measuring stream shade, *Journal of the North American Benthological Society*, *17*, 250-260.

Davies-Colley, R. J., and J. M. Quinn (1998), Stream lighting in five regions of North Island, New Zealand: control by channel size and riparian vegetation, *New Zealand Journal of Marine and Freshwater Research*, *32*, 591-605.

Davies-Colley, R. J., et al. (1984), Optical characterisation of natural waters by PAR measurement under changeable light conditions, *New Zealand Journal of Marine and Freshwater Research*, *18*, 455-460.

Davies-Colley, R. J., et al. (2003), *Colour and Clarity of Natural Waters*, 310 pp., Ellis Horwood, New York.

DeNicola, D. M., et al. (1992), Influences of canopy cover on spectral irradiance and periphyton assemblages in a praire stream, *Journal of the North American Benthological Society*, *11*, 391-404.

Doyle, M. W., and E. H. Stanley (2006), Exploring potential spatial-temporal links between fluvial geomorphology and nutrient-periphyton dynamics in streams using simulation models, *Annals of the Association of American Geographers*, *96*, 687-698.

Evans, G. C., and D. E. Coombe (1959), Hemispherical and woodland canopy photography and the light climate, *Journal of Ecology*, *47*, 103-113.

Frazer, G. W., et al. (1999), Gap Light Analyzer (GLA), version 2.0: Imaging software to extract canopy structure and gap light transmission indices from true-colour fisheye photographs, users manual and program documentation, 40 pp, Simon Fraser University and Institute of Ecosystem Studies, Burnaby, B.C. and Millbrook, NY.

Gordon, H. R. (1989), Can the Lambert-Beer law be applied to the diffuse attenuation coefficient of ocean water?, *Limnology and Oceanography*, *34*, 1389-1409.

Gordon, N. D., et al. (2004), *Stream Hydrology: An Introduction for Ecologists*, 429 pp., John Wiley & Sons, Chichester.

Jerlov, N. G. (1976), *Marine Optics*, 231 pp., Elsevier, Amsterdam.

Julian, J. P., et al. (In review), Optical water quality in rivers, *Water Resources Research*.

Kelly, D. J., et al. (2003), Effects of solar ultraviolet radiation on stream benthic communities: An intersite comparison, *Ecology*, *84*, 2724-2740.

Kenworthy, S. T., and B. L. Rhoads (1995), Hydrologic control of spatial patterns of suspended sediment concentration at a stream confluence, *Journal of Hydrology*, *168*, 251-263.

Kiffney, P. M., et al. (2004), Establishing light as a causal mechanism structuring stream communities in response to experimental manipulation of riparian buffer width, *Journal of the North American Benthological Society*, *23*, 542-555.

Kirk, J. T. O. (1994), *Light and Photosynthesis in Aquatic Ecosystems*, 509 pp., Cambridge University Press, New York.

Koch, R. W., et al. (2004), Phytoplankton growth in the Ohio, Cumberland and Tennessee Rivers, USA: inter-site differences in light and nutrient limitation, *Aquatic Ecology*, *38*, 17-26.

Leopold, L. B., and T. Maddock, Jr. (1953), The hydraulic geometry of stream channels and some physiographic implications, *USGS Professional Paper*, *252*, 1-57.

Mobley, C. D. (1994), *Light and Water: Radiative Transfer in Natural Waters*, 592 pp., Academic Press, San Diego.

Mulholland, P. J., et al. (2001), Inter-biome comparison of factors controlling stream metabolism, *Freshwater Biology*, *46*, 1503-1517.

National Oceanic and Atmospheric Administration (NOAA) (2007), National Climate Data. http://www.noaa.gov/climate.html.

North Carolina Division of Water Quality (NCDWQ) (2000), Cape Fear River Basinwide Water Quality. NC Department of Environment and Natural Resources, http://h2o.enr.state.nc.us/basinwide/Capefear/capefearindex.htm.

Palmroth, S., et al. (2005), Contrasting responses to drought of forest floor CO_2 efflux in a Loblolly pine plantation and a nearby Oak-Hickory forest, *Global Change Biology*, *11*, 421-434.

Phlips, E. J., et al. (2000), Light availability and variations in phytoplankton standing crops in a nutrient-rich blackwater river, *Limnology and Oceanography*, *45*, 916-929.

Poff, N. L., et al. (1997), The natural flow regime, *BioScience*, *47*, 769-784.

Scarsbrook, M. R., and J. Halliday (1999), Transition from pasture to native forest land-use along stream continua: effects on stream ecosystems and implications for restoration, *New Zealand Journal of Marine and Freshwater Research*, *33*, 293-310.

Smith, D. G., et al. (1997), Optical characteristics of New Zealand rivers in relation to flow, *Journal of the American Water Resources Association*, *33*, 301-312.

Song, C. H., and L. E. Band (2004), MVP: a model to simulate the spatial patterns of photosynthetically active radiation under discrete forest canopies, *Canadian Journal of Forest Research-Revue Canadienne De Recherche Forestiere*, *34*, 1192-1203.

Strayer, D. L., et al. (2006), Using geophysical information to define benthic habitats in a large river, *Freshwater Biology*, *51*, 25-38.

Taylor, S. L., et al. (2004), Catchment urbanisation and increased benthic algal biomass in streams: linking mechanisms to management, *Freshwater Biology*, *49*, 835-851.

U.S. Department of Agriculture (USDA). 2007. UV-B Monitoring and Research Program, http://uvb.nrel.colostate.edu/UVB/.

Vannote, R. L., et al. (1980), The river continuum concept, *Can. J. Fish. Aquat. Sci.*, *37*, 130-137.

Westlake, D. F. (1966), The light climate for plants in rivers, in *Light as an Ecological Factor*, edited by R. Bainbridge, et al., pp. 99-118, Blackwell Scientific, Oxford.

Wetzel, R. G. (2001), *Limnology: Lake and River Ecosystems*, 1006 pp., Academic Press, San Diego.

Wisconsin Initiative for Statewide Cooperation on Landscape Analysis and Data (WISCLAND) (1993), Land Cover of Wisconsin. Wisconsin Department of Natural Resources, http://dnr.wi.gov/maps/gis/datalandcover.html#data.

Yard, M. D., et al. (2005), Influence of topographic complexity on solar insolation estimates for the Colorado River, Grand Canyon, AZ, *Ecological Modelling*, *183*, 157-172.

Zheng, X., et al. (2002), Variability of the downwelling diffuse attenuation coefficient with consideration of inelastic scattering, *Applied Optics*, *41*, 6477-6488.

Table 3.1. GLA user-defined parameters

Parameter	Value
Projection	Polar
Orientation	Horizontal
Time step	1 minute
Azimuth regions	36
Zenith regions	9
Solar constant	1367 W/m^2
Cloudiness Index	0.50
Spectral fraction	0.45
Beam fraction	0.50
Sky-region brightness	UOC model
Clear-sky transmission coefficient	0.60

Table 3.2. Turbidity sampling at Big Spring Creek (BSC) and Deep River (DR).

	May 21-30, 2006	Jun 14-16, 2006	Jul 11-17, 2006	Aug 29 – Sep 11, 2006	Apr 24-26, 2006	Jun 15-24, 2006	Jun 24, 2005 - Sep 18, 2006
Location	DR	DR	DR	DR	BSC	BSC	BSC
Method[1]	Automated	Manual	Automated	Automated	Automated	Automated	Manual
Flow	Baseflow	Flood	Baseflow	Flood	Baseflow	Baseflow	Baseflow / Flood
Sample interval (h)	12	~24	6	6	4	6	discrete
Sample number	22	3	23	54	11	33	22 / 2

[1] Automated samples were collected with a *Teledyne-ISCO* 6712.

Table 3.3. BLAM input parameters for Big Spring Creek (BSC) and Deep River (DR). Temporal parameters apply to the sampling station only. Spatial parameters apply to baseflow only. Parentheses indicate the parameter is variable, inside of which is the range of values for the study period. Parameters that are not applicable to the calculation of E_{bed} are labeled "na."

	Temporal		Spatial	
Parameter	**BSC**	**DR**	**BSC**	**DR**
E_{can} (mol m^{-2} d^{-1})	(5.04 – 61.23)	(7.10 – 60.21)	39.83	39.68
s	0.17	0.78	(0.15 to 0.94)	(0.52 to 0.81)
r	0.92	0.93	0.92	0.93
y (m)	αQ^{υ}	αQ^{υ}	(0.23 – 1.26)	(0.34 – 3.55)
α	1.64	0.15	na	na
υ	0.49	0.67	na	na
K_d (m^{-1})	βQ^{ω}	βQ^{ω}	0.60	1.84
β	32.40	0.18	na	na
ω	3.69	1.31	na	na
Q	(0.30 – 0.51)	(3.17 – 77.79)	na	na

Table 3.4. Predicted vs. actual benthic PAR in Big Spring Creek, WI. Actual values were collected with PAR sensors at a transect 175 m downstream of the sampling station during Jun 16 – 25, 2006. Values for Jun 21 are not reported because the E_{bed} sensor was disturbed on that day. The shading coefficient (s) for this site as derived by GLA was 0.67. All other temporal parameters used in BLAM are listed in Table 3. Data not available due to equipment malfunction are labeled "na." E_{bed}* is the predicted benthic PAR according to Equation 5, and E_{bed} is the actual benthic PAR measured with a PAR sensor.

Source:	PAR Sensor	PAR Sensor	PAR Sensor	PAR Sensor	Stage Recorder	Weather Station	BLAM	
Date (M/D/Y)	E_{can} (mol/m^2/d)	E_s (mol/m^2/d)	E_0 (mol/m^2/d)	E_{bed} (mol/m^2/d)	Q (m^3/s)	E_{can} (mol/m^2/d)	E_{bed}* (mol/m^2/d)	E_{bed}* / E_{bed}
6/16/06	43.32	25.43	22.47	15.37	0.33	47.74	17.57	1.14
6/17/06	46.39	26.47	22.16	14.44	0.32	43.99	16.81	1.16
6/18/06	40.04	21.21	na	9.7	0.33	41.63	15.24	1.57
6/19/06	46.45	22.43	na	10.34	0.33	47.23	17.06	1.65
6/20/06	30.57	14.49	na	6.44	0.33	33.99	12.33	1.92
6/22/06	40.31	25.59	na	10.16	0.34	49.81	16.95	1.67
6/23/06	59.31	35.41	30.51	19.45	0.34	60.18	20.49	1.05
6/24/06	39.80	23.13	22.09	13.71	0.34	39.52	13.35	0.97
6/25/06	20.19	11.92	10.30	5.65	0.35	22.45	7.24	1.28

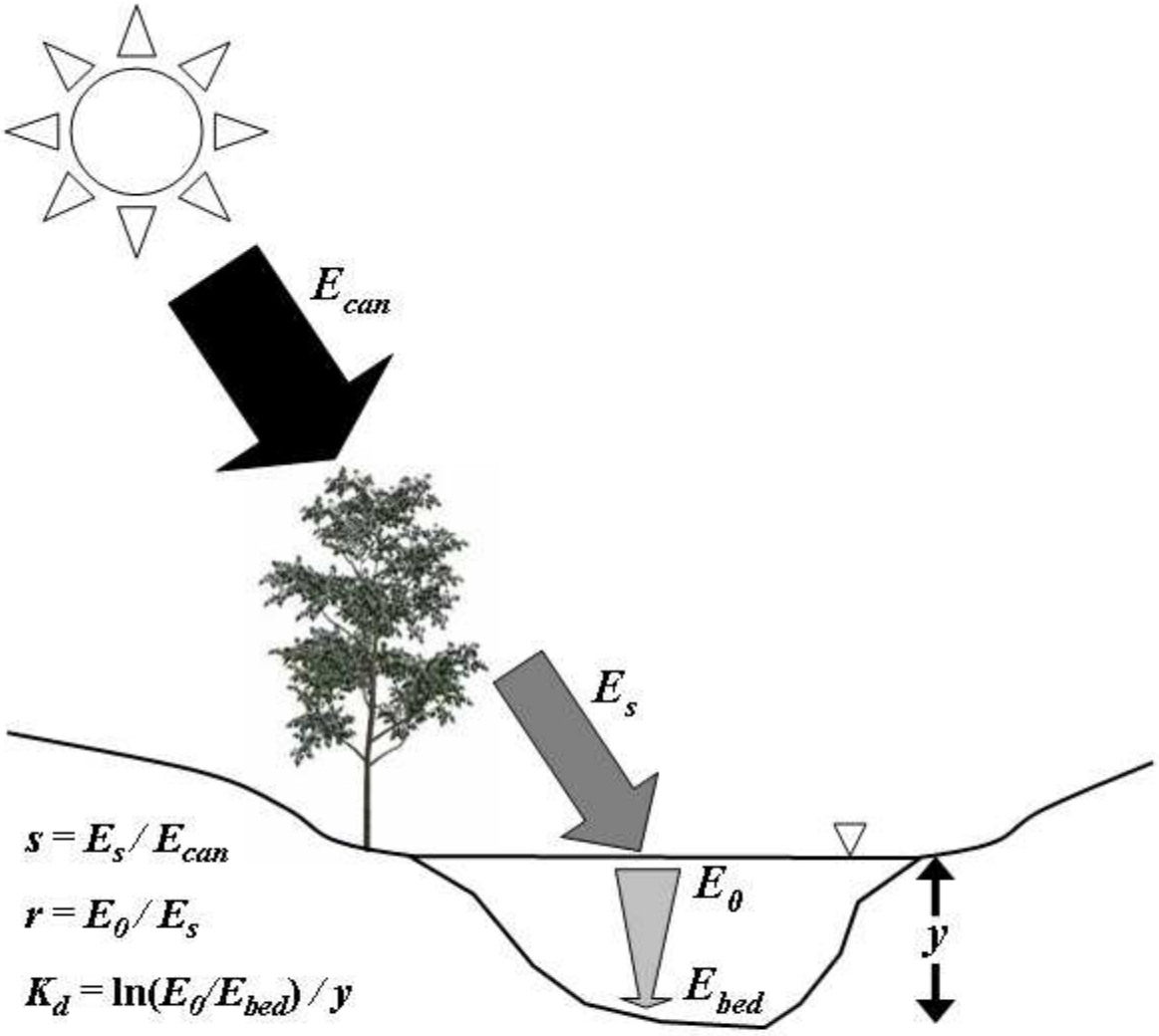

Figure 3.1. Light availability in rivers. E_{can} is the total amount of light that is available to the river before any shading from topography and riparian vegetation. E_s is the amount of light that reaches the water surface after shading from topography and riparian vegetation, where s is the shading coefficient. E_0 is the amount of light that enters the water column after reflection at the air-water interface, where r is the reflection coefficient. E_{bed} is the amount of light that reaches the riverbed after attenuation from the water column, which is dictated by the optical water quality (via the diffuse attenuation coefficient, K_d) and water depth (y).

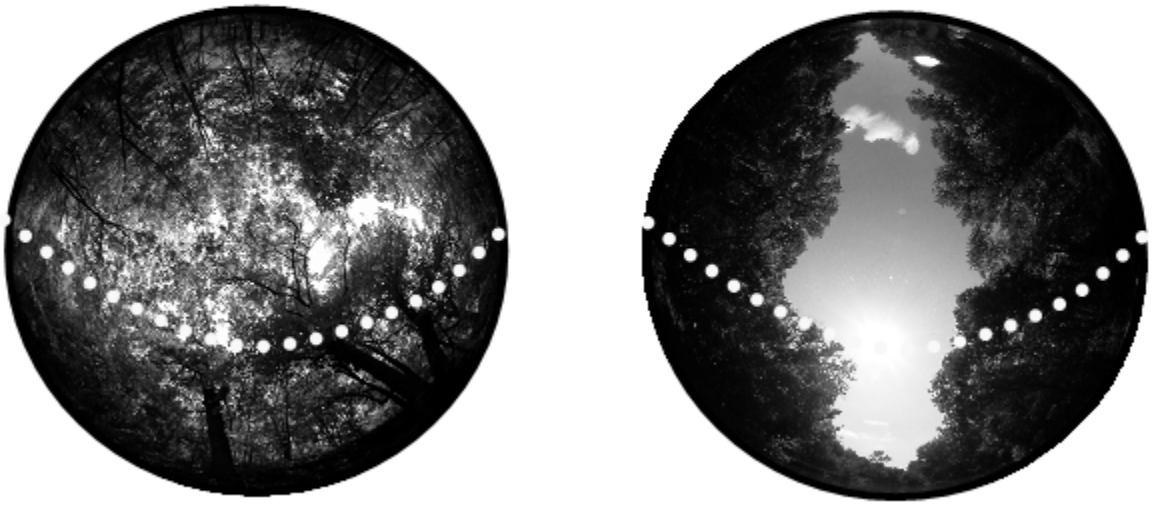

A. BSC- closed canopy

B. DR- open canopy

Figure 3.2. Hemispherical canopy photos of transects at Big Spring Creek (BSC; A) and Deep River (DR; B). The orientation of the BSC transect is West-East (azimuth = 90°) and the orientation of the DR transect is South-North (azimuth = 0°). Both transects are forested. The DR transect has an open canopy because of its greater width, 34 m compared to 6 m for the BSC transect. The dotted white line represents the sunpath.

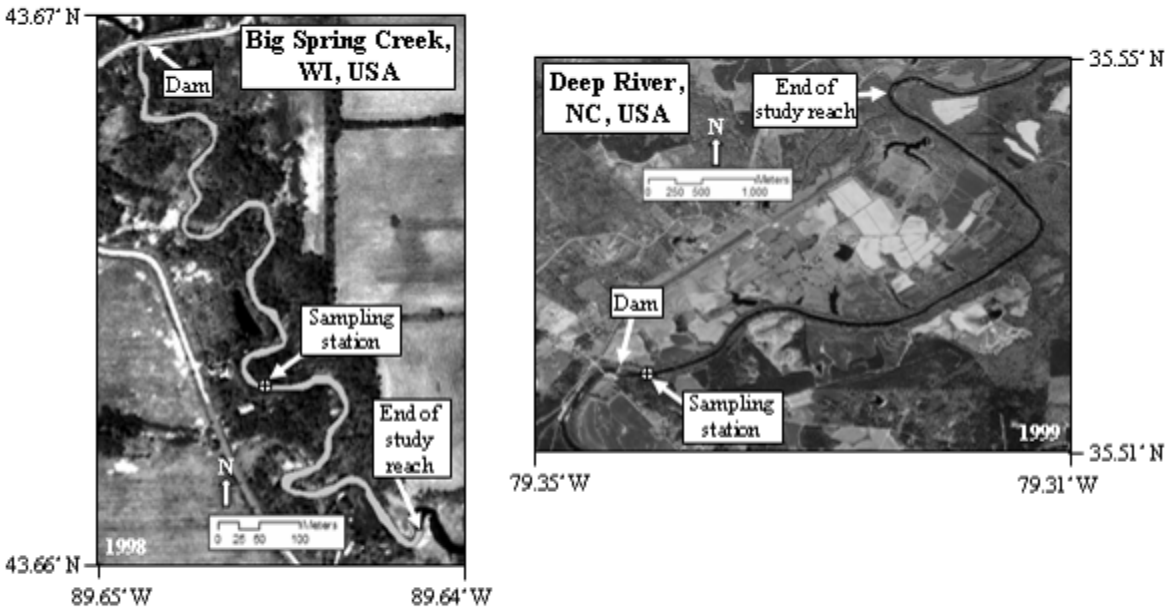

Figure 3.3. Big Spring Creek (BSC) and Deep River (DR) study reaches. BSC's wetted surface is superimposed on the aerial photo to illustrate its width and planform. The dam is the upstream extent of the study reach for both sites. Sampling stations are where discharge was measured and temporal benthic light availability was assessed.

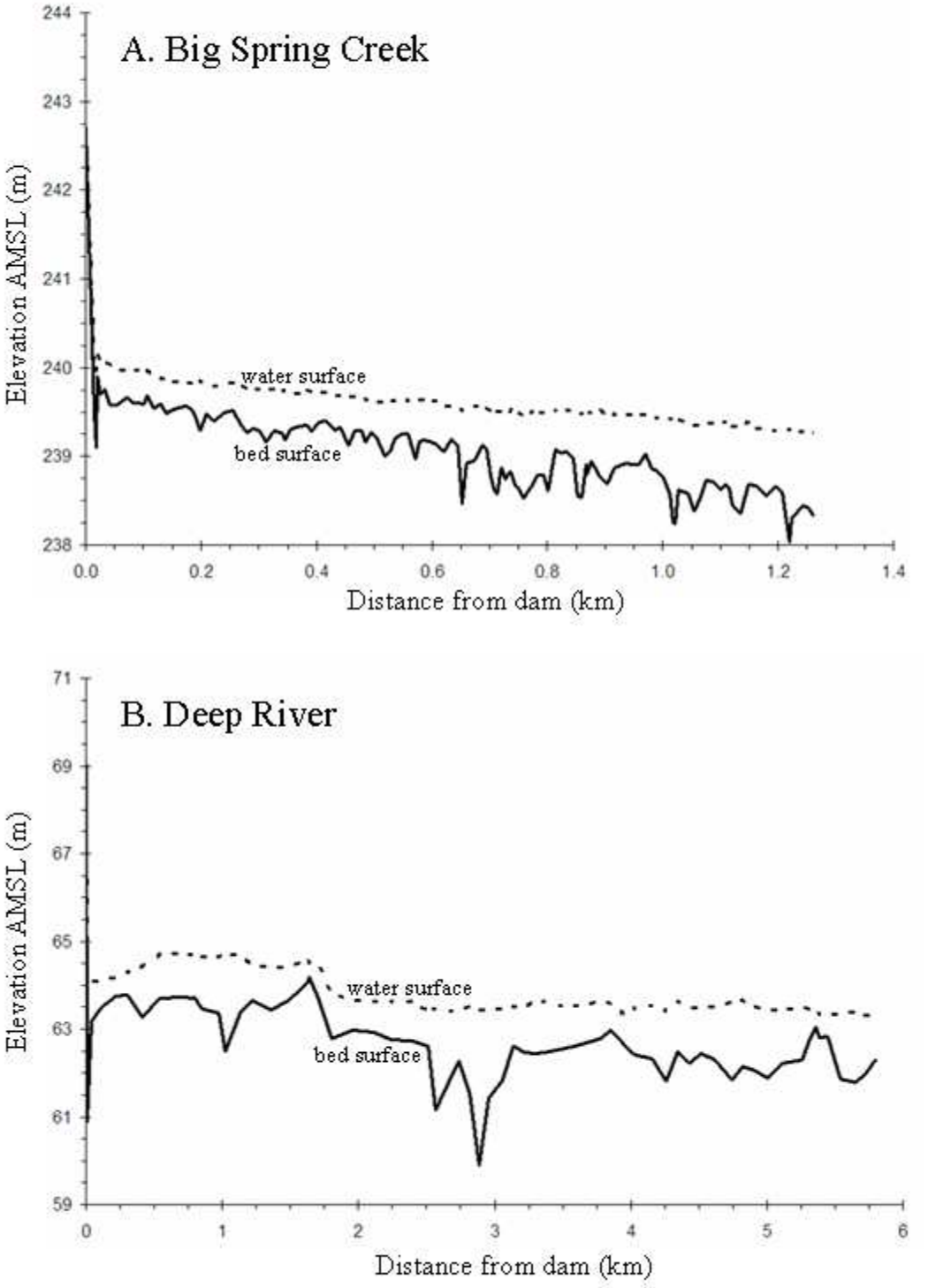

Figure 3.4. Longitudinal profile of Big Spring Creek (A) and Deep River (B). Note the different x- and y-axes between the study sites.

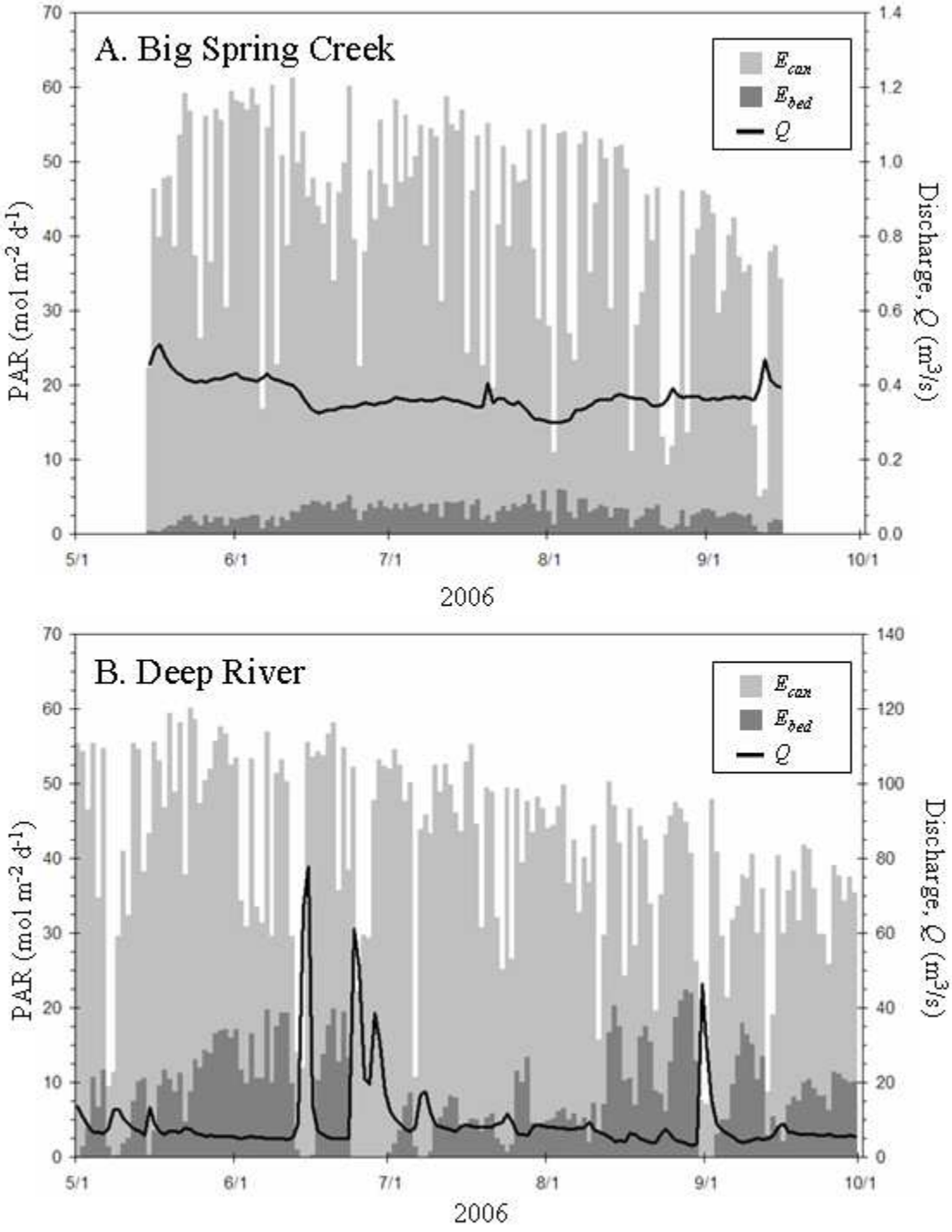

Figure 3.5. Temporal distribution of daily above-canopy PAR (E_{can}), discharge (Q), and benthic PAR (E_{bed}) at Big Spring Creek (A) and Deep River (B). Note the different secondary y-axes for Q between the study sites.

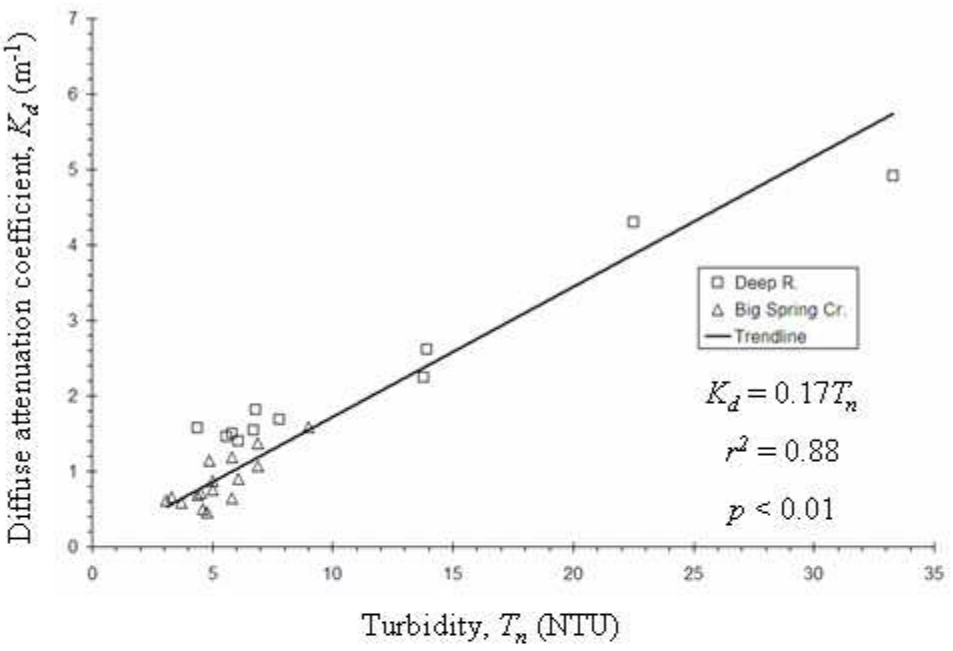

Figure 3.6. Diffuse attenuation coefficient (K_d) vs. turbidity (T_n) for Big Spring Creek and Deep River.

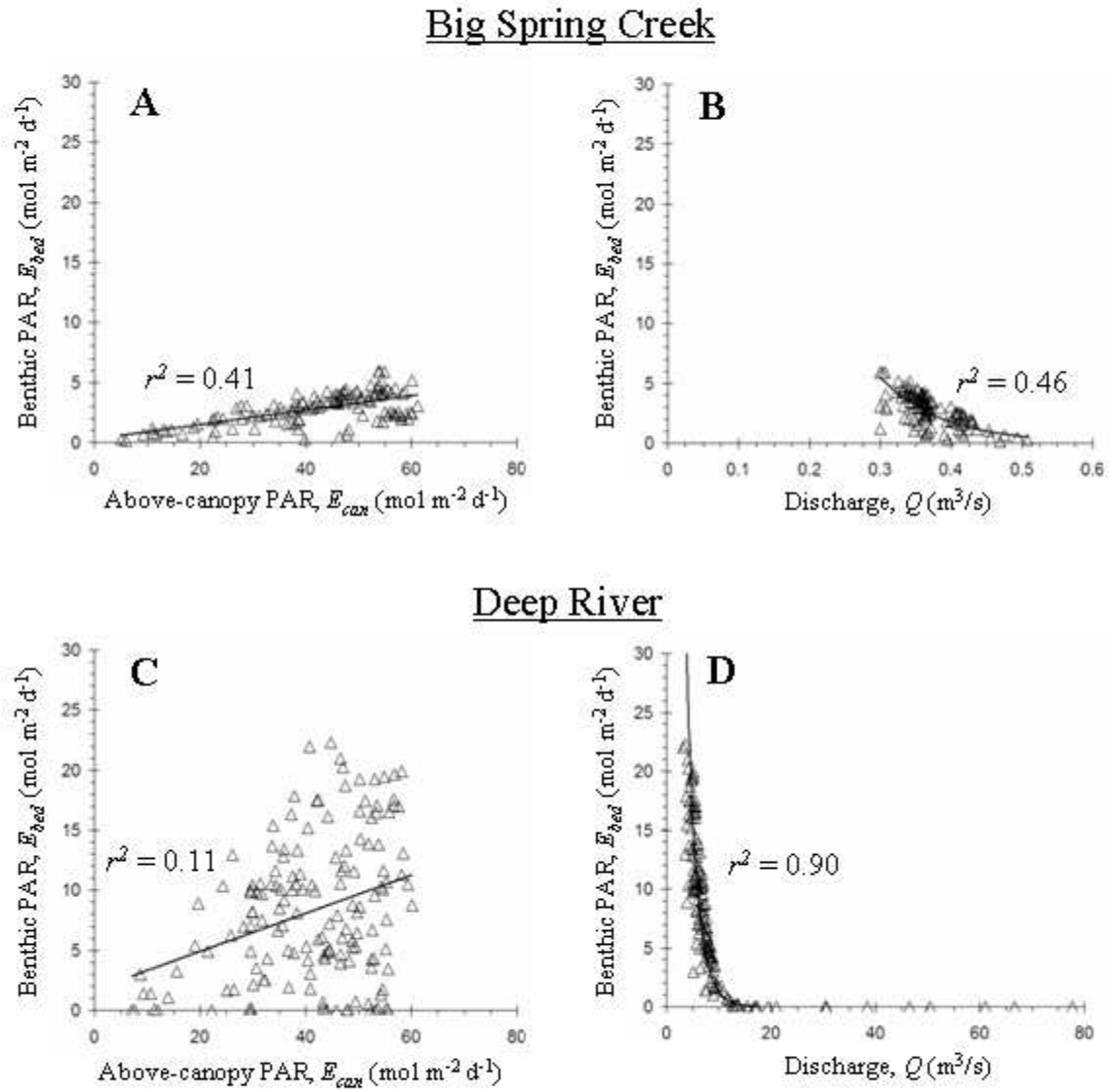

Figure 3.7. Temporal comparisons of benthic PAR (E_{bed}) with above-canopy PAR (E_{can}; A,C) and discharge (Q; B,D) for Big Spring Creek and Deep River, respectively.

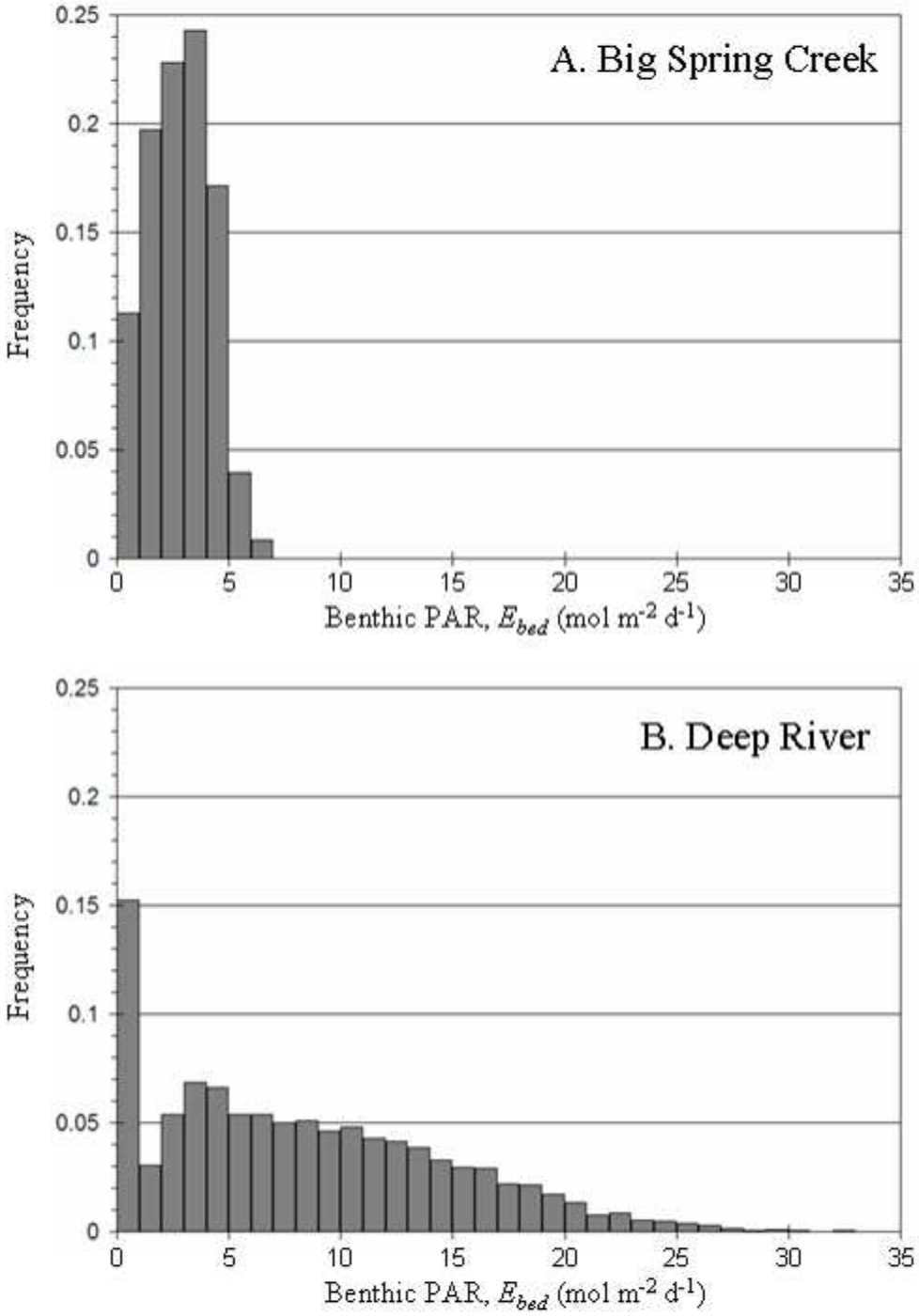

Figure 3.8. Magnitude-frequency distributions of benthic light availability (E_{bed}) at Big Spring Creek (A) and Deep River (B). Histograms were constructed from Monte Carlo simulations using 10,000 iterations for each site.

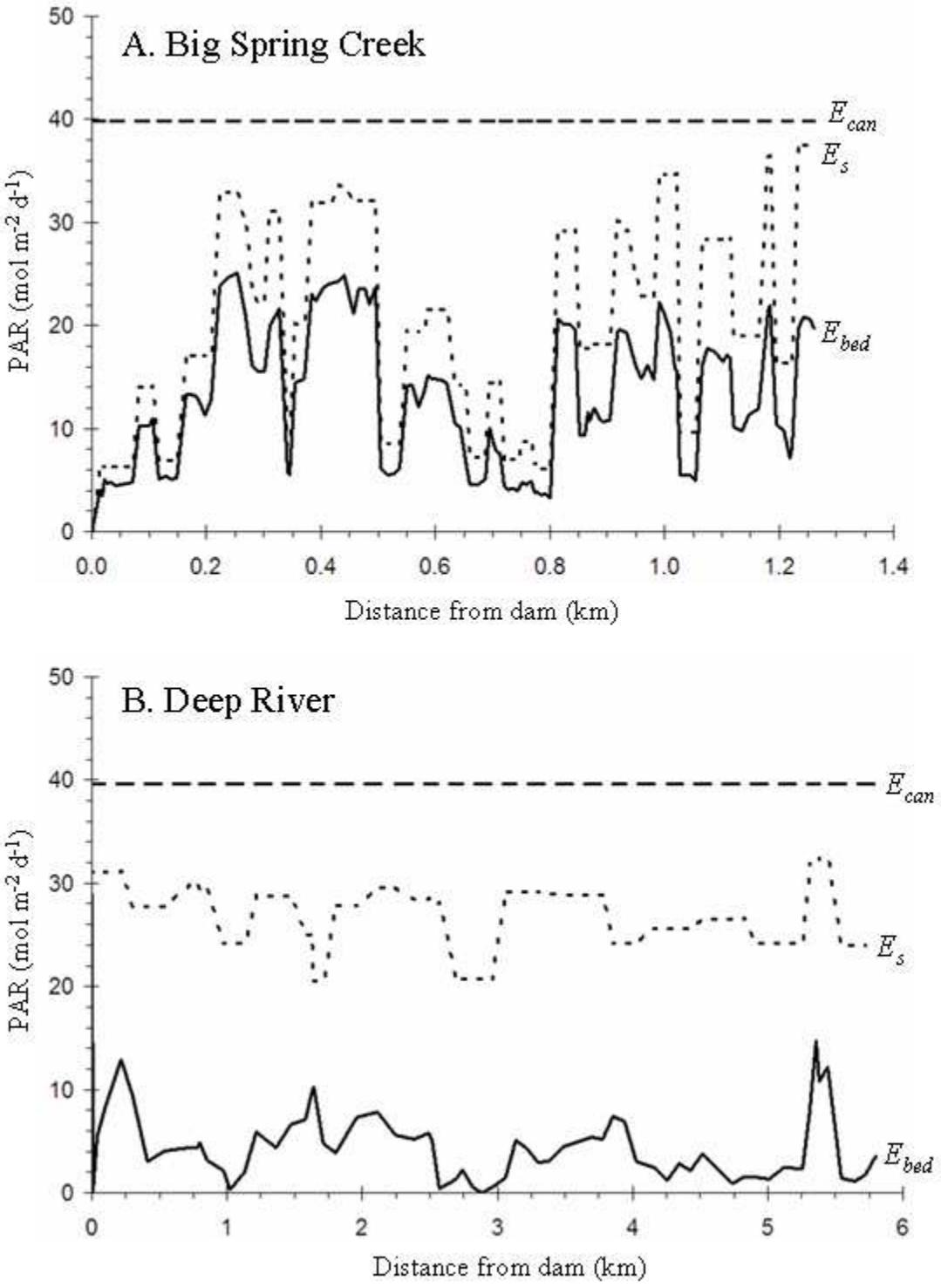

Figure 3.9. Longitudinal distribution of above-canopy PAR (E_{can}), below-canopy PAR (E_s), and benthic PAR (E_{bed}) during baseflow at Big Spring Creek (A) and Deep River (B). Note the different x-axes between the study sites.

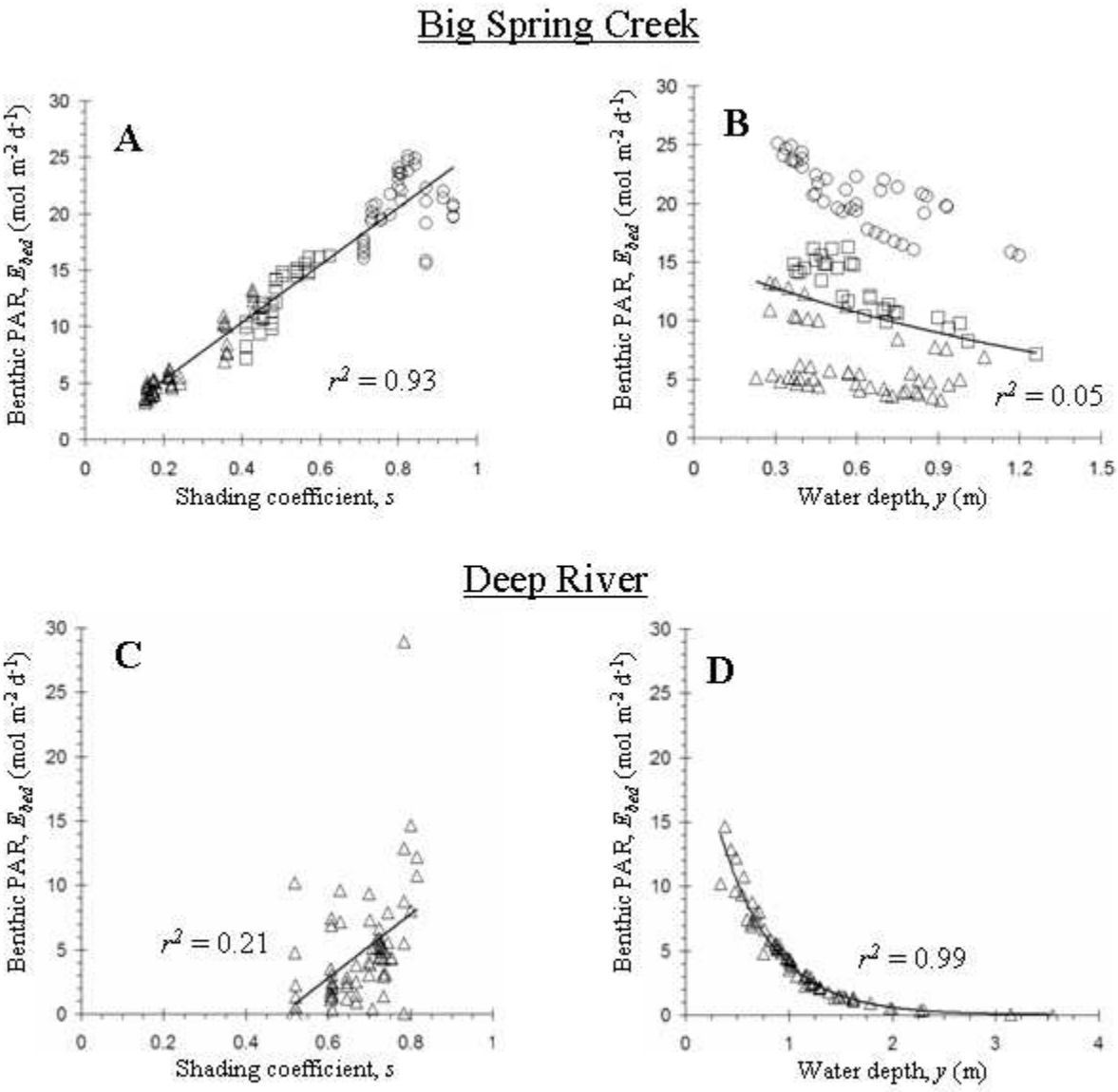

Figure 3.10. Spatial comparisons of longitudinal benthic PAR (E_{bed}) with shading coefficient (s; A,C) and water depth (y; B,D) for Big Spring Creek and Deep River, respectively. Triangles = forest, Squares = mixed, and Circles = grass.

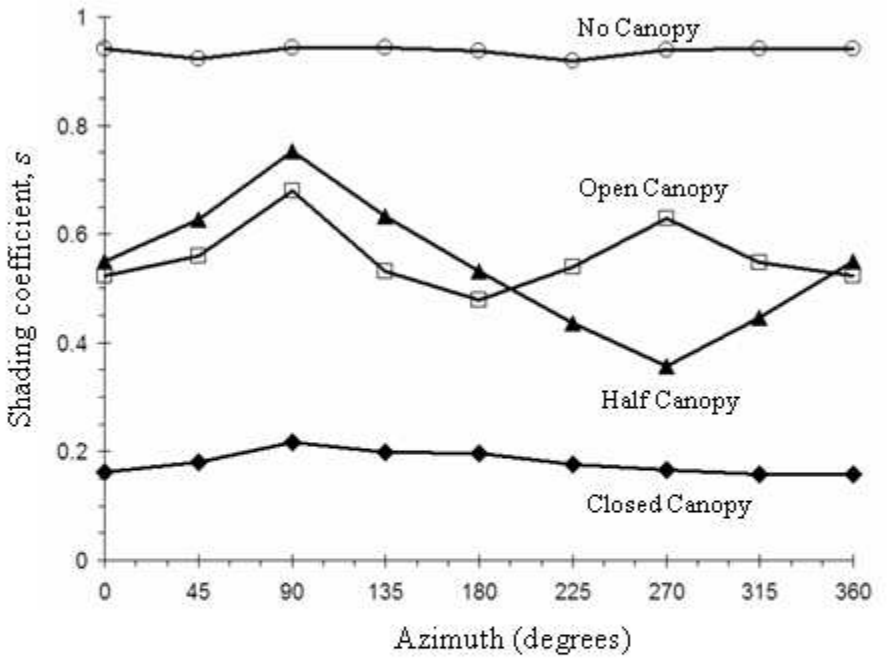

Figure 3.11. Effect of channel orientation (i.e., compass direction) on shading coefficients (*s*), which were derived from Gap Light Analyzer software and canopy photos from Big Spring Creek (BSC) and Deep River (DR). Canopy photos were rotated in 45-degree increments to obtain the entire range of channel orientations. "No Canopy" is a grassed transect at BSC (width = 7 m). "Open Canopy" is a forested transect at DR (width = 34 m). "Half Canopy" is a transect at BSC with the east bank grassed and the west bank forested (width = 8 m). "Closed Canopy" is a forested transect at BSC (width = 6 m).

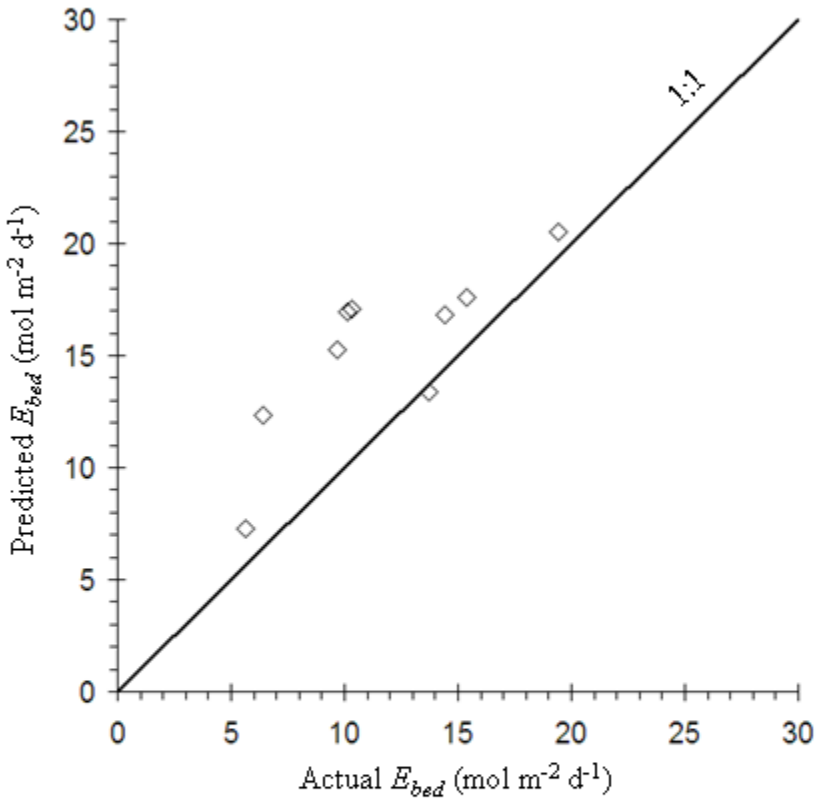

Figure 3.12. Predicted daily benthic PAR (E_{bed}) vs. actual E_{bed} at Big Spring Creek, WI for Jun 16 – 25, 2006. Predicted E_{bed} was modeled using Equation 5. Actual E_{bed} was measured with an underwater PAR sensor located on the bed of a transect 175 m downstream of the sampling station.

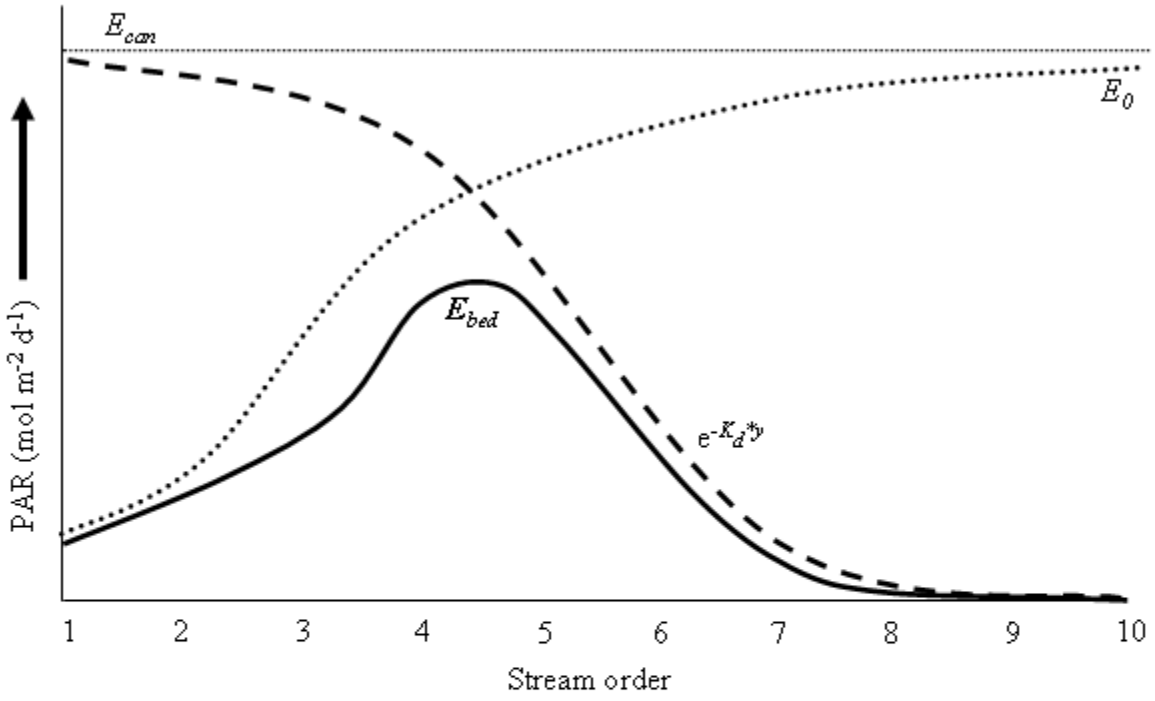

Figure 3.13. Benthic light availability along the river continuum of an idealized 10th-order river with a continuous forested riparian corridor. Benthic PAR (E_{bed}) was derived from Equation 2, where E_{can} is above-canopy PAR, E_0 is the amount of PAR that enters the water column after terrestrial shading and reflection, and $e^{-K_d * y}$ is the inverse exponential product of depth (y) and the diffuse attenuation coefficient (K_d). The product of $e^{-K_d * y}$ is a dimensionless proportion, with a value of ~1 in the headwaters and a value of ~0 at the outlet. The influence of aquatic attenuation thus increases in the downstream direction, whereas the influence of terrestrial shading decreases in the downstream direction.

CHAPTER IV. LIGHT ALONG THE RIVER CONTINUUM

1. INTRODUCTION

Rivers are the ultimate integrator of landscape hydrology, geomorphology, ecology, and anthropogenic land-use. Alterations to the landscape thus result in changes to the river's character, and these changes can be propagated upstream and downstream of the disturbance. This view of the river as a continuum where every point along the channel is inextricably linked through upstream and downstream forcings and feedbacks was first described using a process-based analysis by G.K. Gilbert (1877). Later, Leopold and Maddock (1953) empirically illustrated that certain physical characteristics of a river (width, depth, and suspended sediment concentration) increase along its continuum (from headwaters to mouth) systematically with increasing flow. While Gilbert's work laid the foundation for river continuum studies, it was the hydraulic geometry concept of Leopold and Madddock that demonstrated the utility of using the river continuum framework for applications in geomorphology, hydrology, and ecology.

The hydraulic geometry concept provided the theoretical basis for the River Continuum Concept (RCC; Vannote et al. 1980), which (i) conceptualized rivers as continuous, integrated systems in which the ecology is largely influenced by upstream processes, and (ii) provided generalizations on spatial trends in organic carbon dynamics, ecosystem metabolism, and invertebrate community structure. The RCC shifted the scale

of focus of fluvial ecosystem studies from transects and reaches to the entire river continuum (Minshall et al. 1985). It was also one of the driving forces behind the current paradigm in fluvial ecology of using a landscape (or basin-scale) perspective of rivers (Fisher 1997, Wiens 2002). This landscape ecology perspective has been applied to a multitude of ecological investigations, including the effects of hydrology on primary production (Stanley et al. 2004), land-use change on water chemistry (Lookingbill et al. In review), and channel network configuration on habitat availability (Benda et al. 2004). Yet, the effects of hydrology, geomorphology, and land-use on the primary energy source of fluvial ecosystems – light – have not been quantified at the basin-scale.

The amount of light a river receives constrains its trophic status through photosynthesis and biotic behavioral adaptations (Vannote et al. 1980) and influences temperature fluctuations, photochemical reactions, and photodegradation of suspended matter (Wetzel 2001). Benthic (or riverbed) light availability is mainly governed by terrestrial shading (via topography and vegetation) and aquatic attenuation (via turbidity and water depth) (Julian et al. In review-b). The RCC and other studies (e.g., Bott et al. 1985) suggest that the longitudinal profile of benthic light follows a parabolic trend where benthic light is low in the upper reaches due to terrestrial shading, low in the lower reaches due to aquatic attenuation, and high in the middle reaches where the combined effects of shading and turbidity are lowest (Figure 1). This prediction, however, has not been empirically tested. Further, the effect of landscape alteration on benthic light availability along the river continuum, taking into account both terrestrial shading and aquatic attenuation, has not been quantified.

Spatial and temporal trends in benthic light availability have been altered by various anthropogenic disturbances (Davies-Colley et al. 2003), but most intensively by agricultural practices. Accelerated soil erosion via agriculturalization has been the main contributor of increased turbidity to most rivers around the world (Walling and Fang 2003), which decreases benthic light availability through enhanced aquatic light attenuation. Agricultural land conversion has also caused the widespread removal of considerable portions of riparian forest (MEA 2005), which increases benthic light availability through reduced shading. These alterations are likely to be discontinuous in space and time (Lookingbill et al. In review), further complicating trends in benthic light availability.

Despite the fundamental role of light availability to fluvial ecosystems and its sensitivity to anthropogenic disturbances, light studies in rivers have been mostly neglected because (i) light has not been widely accepted as a limiting resource in riverine ecosystems in comparison to nutrients and habitat, (ii) the optical water quality of rivers is highly variable and difficult to characterize, and (iii) boundary conditions (banks, riparian vegetation) make ambient light measurements difficult (Davies-Colley et al. 2003). There has been a recent increase in riverine light studies, some of which have (i) demonstrated the role of light as a limiting resource in rivers (Davies-Colley et al. 1992, Hill et al. 1995, Rier et al. 2006), (ii) synthesized the controls and spatiotemporal variability of optical water quality over a wide range of rivers (Julian et al. In review-a), and (iii) provided a reach-scale empirical model for quantifying light availability in rivers (Julian et al. In review-b). However, a quantitative landscape perspective on riverine light regimes has not been presented. Because of the primary dependence of many

ecosystem processes on light availability, basin-scale light budgets would provide a useful tool to address many of the current questions in fluvial ecology.

Here, we demonstrate how basin-scale riverine light availability can be characterized using the reach-scale benthic light availability model (BLAM; Julian et al. In review-b) in a GIS framework and incorporating the principles of hydraulic geometry (sensu Leopold and Maddock 1953). We then use this GIS-based model to quantify benthic light availability and gross primary production (GPP) along the continuum of a 6^{th}-order river in an agriculturally-dominated basin and test the predictions of the RCC. Finally, we use this GIS-based model to investigate the effects of agriculturalization on light regimes of rivers.

2. STUDY AREA

The Baraboo River provides an ideal case study to investigate light along the natural river continuum (sensu the RCC) because its entire 187-km mainstem is free-flowing with no impoundments. It historically had nine dams on its mainstem, but all have been removed, the last one in 2001 (*WDNR* 2006). Baraboo River is a 6^{th}-order stream that begins in the Western Uplands of Wisconsin near Kendall, WI and meanders through the Driftless Area of central Wisconsin before it empties into the Wisconsin River near Portage, WI (Figure 2). It drops in elevation from 420 to 235 m above mean sea level over its length of 187 km. Its 1,690-km^2 drainage basin is mostly agriculture (47%), followed by forest (31%), grassland (15%), wetland (5%), urban (1%), and barren (1%) (*WISCLAND* 1993). The pre-settlement landcover was dominated by southern oak forest (white, black, and red oaks) in the uplands and oak savanna (bur oak, white oak,

bluestem) in the lowlands (Curtis 1959). The riparian corridor of Baraboo River is currently composed mostly of mixed-hardwood forest and various grasses. The hydrology of the basin is dominated by thunderstorm frontal systems, resulting in a relatively flashy hydrologic regime, although seasonal flooding is common in spring due to snowmelt events. The flow gage (USGS #05405000) at RK 160 (160 river kilometers downstream of the headwaters) represents the downstream extent of our analysis (Figure 2).

3. METHODS

3.1. Modeling Basin-Scale Benthic PAR

The benthic light availability model (BLAM; Julian et al. In review-b) calculates the amount of photosynthetically active radiation (PAR) at the riverbed (E_{bed}) by incorporating the terrestrial and aquatic controls on benthic light availability:

$$E_{bed} = (E_{can} \times s \times r) \times e^{-K_d \times y} \quad (4.1)$$

where E_{can} is above-canopy PAR in mol m^{-2} day^{-1}, s is the shading coefficient, r is the reflection coefficient, K_d is the diffuse attenuation coefficient for underwater PAR in m^{-1}, and y is water depth in m. This empirical model was designed for the reach scale, where K_d is assumed to remain constant and s collectively includes shading from topography and riparian vegetation. In order to apply this approach to the basin scale, we (i) allowed K_d to vary along the river; (ii) divided s into the topographic shading coefficient (s_t) and the vegetation shading coefficient (s_v), where $s = s_t$ x s_v; and (iii) used a GIS-based analysis.

The conceptual framework of our GIS-based approach for quantifying E_{bed} is presented in Figure 3. We overlaid a hydrography dataset of the Baraboo River onto a digital elevation model (DEM) and landcover classification map (LCM) to calculate s_t and s_v, respectively. We then conducted a synoptic survey of the Baraboo River, measuring channel width and depth, turbidity, and canopy structure. We incorporated these empirical data into our GIS framework and used Equation 1 to derive E_{bed}.

3.2. Model Parameters

3.2.1. Above-Canopy PAR (E_{can})

Above-canopy PAR (E_{can}) is the amount of light available to the river before any terrestrial shading. We modeled E_{can} with *Gap Light Analyzer* (GLA; Frazer et al. 1999), using the parameters in Table 1 and the center of the drainage basin as our location and elevation. We kept E_{can} spatially constant across the basin so that variations in the other parameters could be assessed independently. From GLA, we derived an average daily E_{can} , in mol m^{-2} day^{-1}, for the Baraboo River Basin during May 15 – Sep 15, which corresponds to the period of greater than 90% leaf area index (i.e., at least 90% of the leaves were on the trees). In order to assess the range of E_{bed}, we also obtained actual daily E_{can} values from a USDA weather station located in Dancy, WI (WI02; USDA 2007), which reported 3-min averages of 20-sec readings from a *LI-COR* quantum sensor.

3.2.2. Topographic Shading Coefficient (s_t)

Topography is the first terrestrial control that reduces the amount of light available to the river. We calculated daily average s_t (the proportion of PAR available to

the river after topographic shading) using *Solar Analyst 1.0* (Fu and Rich 2000; Table 1), which uses a view-shed algorithm to compute the proportion of E_{can} that reaches the surface of every cell in a DEM after shading effects from elevation, shadows, and atmospheric conditions. We used a USGS DEM (cell-size: 30 x 30 m) in combination with a raster of the Baraboo River mainstem (cell-size: 30 x 30 m) to extract s_t for each 30-m segment of the river. We created this river raster by converting the DNR hydrogaphy dataset of the Baraboo River (scale: 1:24,000) into a raster using *Arc Hydro* (Maidment 2002). *Arc Hydro* also assigned every cell in the river raster an azimuthal channel orientation (i.e., flow direction) based on the eight compass directions. For example, a river cell flowing into a cell directly below it (N-S) had an orientation of 180°. Because each river cell had some sinuosity, we normalized raster river distance to actual distance by assigning horizontal/vertical cells (0-180°, 90-270°) 33.6 m and diagonal cells (45-225°, 135-315°) 47.5 m. These distances were calculated using the Pythagorean theorem and assuming the total distance adds up to 160 km. From this mainstem river raster, we calculated a longitudinal profile of s_t along the Baraboo River.

3.2.3. Vegetation Shading Coefficient (s_v)

After topographic shading, the next control that reduces the amount of light available to the river is riparian vegetation. We calculated daily average s_v (the proportion of PAR available to the river after vegetation shading) using a LCM of the Baraboo River Basin (WISCLAND 1993) in combination with canopy photos analyzed with *GLA* (Frazer et al. 1999; Table 1), which computes the proportion of E_{can} that reaches the water surface after shading by the canopy. Digital hemispherical canopy

photos were collected using a *Nikon Coolpix 4500* with fisheye lens. We took canopy photos at eight transects along Baraboo River (Figure 2) on Aug 18, 2006. Transects were selected based on changes in channel width and canopy structure. The canopy photos were corrected for topographic shading by dividing the *s* value from *GLA* by s_t ($s_v = s / s_t$), which we obtained from the longitudinal profile of s_t. By performing this correction, we prevented topographic shading from being incorporated twice.

We used the canopy photos to construct empirical relationships between s_v and channel width and orientation (Figure 4). Active channel width (sensu Osterkamp and Hedman 1977) was measured at the transect of each photo location. From these measurements, we constructed a width rating curve based on distance from the headwaters and assigned every cell in the river raster a width based on this rating curve. We calculated the variation in s_v with channel orientation by rotating the canopy photos in 45° increments and then reanalyzing in *GLA* (sensu Julian et al. In review-b). Each curve in Figure 4 was derived from least squares power regression of four canopy photos. Half-canopy s_v curves were derived from transects where one bank was forested and the other deforested. To normalize the half-canopy photos, we rotated each photo so that the forested bank was on the right bank looking downstream (i.e., for a channel orientation of 90°, the south bank was forested). Full-canopy s_v curves were derived from transects where both banks were forested. Due to limited full-canopy photos from the Baraboo River, two of the full-canopy photos were obtained from Deep River, NC, which was also a 6th-order river with a similar riparian corridor (mixed-hardwood forest) and channel width (~40 m; Julian et al. In review-b).

Using the LCM, each cell in the Baraboo River raster was classified as having a full-canopy, half-canopy, or no canopy. Canopy classifications were assigned on the basis of whether or not a forest landcover cell was adjacent to the river cell. For example, a river cell with a forest landcover cell adjacent to its right bank and a non-forest landcover cell adjacent to its left bank was classified as having a half-canopy. Using the river raster's attributes of width, channel orientation, and canopy cover, we calculated s_v for each river cell based on the curves in Figure 4. For cells with no canopy (i.e., neither adjacent cell was a forest landcover), we used an s_v of 1.0.

3.2.4. Reflection Coefficient (r), Diffuse Attenuation Coefficient (K_d), and Depth (y)

After terrestrial shading by topography and riparian vegetation, the amount of available light is further reduced by reflection at the air-water interface. We used a daily average r (the proportion of PAR that enters the river after reflection) of 0.88, which we obtained from a previous study in a nearby basin (Julian et al. In review-b).

Once light enters the water column, it is attenuated exponentially with depth at a rate defined by K_d. We estimated K_d along the Baraboo River from nephelometric turbidity (T_n) measurements, where $K_d = 0.17T_n$ (Julian et al. In review-b). We measured T_n with a HACH 2100P turbidimeter from water samples collected at 22 locations along the Baraboo River on Aug 13, 2006 during baseflow (Figure 2). From these measurements, we constructed a K_d rating curve based on distance from the headwaters.

The amount of light that reaches the riverbed is ultimately dictated by the depth of the river (y). We quantified y at each photo location, using the average of 3 depth measurements taken in the center of the channel and ~3 channel widths apart. From these

measurements, we constructed a *y* rating curve based on distance from the headwaters (sensu Leopold and Maddock 1953). All empirical data collected along the Baraboo River was georeferenced in GIS using a *Garmin* GPS.

3.3. Model Assumptions

We used Equation 1 in conjunction with E_{can} from GLA, the longitudinal profile of s_t, the s_v curves in Figure 4, an r of 0.88, the K_d rating curve, and the y rating curve to calculate E_{bed} for every cell (n = 3980) in the Baraboo River raster. These values of E_{bed} are daily averages, in mol m^{-2} day^{-1}, based on the average daily E_{can} for May 15 – Sep 15, 2006. The cell size of the river raster set the spatial resolution of E_{bed} at ~30 m. Our calculation of E_{bed} assumed that width, depth, and turbidity increased consistently in the downstream direction. Therefore, local variations in width, y, and K_d were not taken into account. Our calculation of s_v assumed (i) the LCM accurately delineated riparian forests, and (ii) canopy structure (height, density) was constant for all forested riparian cells. Because empirical data was collected from the center of the channel during baseflow, E_{bed} is only representative of the channel centerline during baseflow.

3.4. Model Simulations

In addition to characterizing the broad spatial pattern of light regimes along the river continuum, the GIS-based model can be used for sensitivity analyses such as the effect of landscape alteration on benthic light availability. We assessed the effect of agriculturalization on E_{bed} for Baraboo River by conducting three model simulations. The objective of the first model simulation was to reproduce pre-agricultural E_{bed} along

the Baraboo River, where its entire riparian zone was forested and its optical water quality was pristine. We obtained pristine K_d values from a longitudinal survey of water clarity along the Motueka River (Davies-Colley 1990), a relatively undeveloped basin in New Zealand where most of its area was conservation land (55%), followed by production forestry (25%) and low intensity sheep/cattle farming (19%) (Basher 2003). We converted water clarity measurements (via black disk method) to K_d using the conversion factors in Davies-Colley et al. (2003, p. 76). Our justification for using the Motueka River Basin is that it had a similar area (2,180 km^2) and shape (pear-shaped) as the Baraboo River Basin. To simulate a longitudinally continuous riparian forest along Baraboo River, we created a modified LCM where every adjacent cell to the river raster was classified as forest.

The objective of the second model simulation was to generate post-agricultural E_{bed} with a riparian buffer along the Baraboo River, where present-day optical water quality and a continuous forested riparian buffer were used. We simulated the continuous riparian forest using the method above, but used the K_d values from our longitudinal survey of turbidity along the Baraboo River rather than the pristine K_d values. The objective of the third model simulation was to generate deforested post-agricultural E_{bed} along the Baraboo River, where present-day optical water quality and a continuous deforested riparian zone were used. To simulate a completely deforested riparian zone, we created a modified LCM where every adjacent cell to the river raster was classified as non-forest. These three model simulations, along with the actual longitudinal profile of E_{bed} for the Baraboo River, were compared to assess spatial variations of E_{bed} in response to changes in riparian vegetation and optical water quality.

3.5. Primary Productivity

Gross primary production (GPP) can be predicted with PAR measurements and community-specific photosynthesis-irradiance (P-I) relationships (Jassby and Platt 1976). We used the periphyton assemblage of cyanobacteria as our measure of GPP because it is the predominant periphyton in agricultural streams in Wisconsin (Scudder and Stewart 2001). Photoinhibition for benthic cyanobacteria was assumed negligible (Dodds et al. 1999), and therefore the method of Jassby and Platt (1976) was used in combination with the P-I areal parameters for riverine cyanobacteria (Dodds et al. 1999). In this model, GPP was calculated as biomass carbon-specific photosynthesis in g C m^{-2} d^{-1}, with a conversion factor of 0.375*O_2 for C. PAR measurements were obtained from the USDA weather station (WI02; USDA 2007) for the day of Aug. 21, 2006, which was equivalent to the daily average PAR for the study period (39.46 mol m^{-2} d^{-1}) and had varying cloudiness. We calculated GPP in 3-min intervals and then integrated to obtain daily values of GPP for each cell in the river raster (n = 3980).

4. RESULTS

4.1. Empirical Parameters from Synoptic Survey

4.1.1. Channel Geometry

Active channel width along the Baraboo River continuum increased systematically at a rate of $0.23RK^{1.00}$, with a maximum of 40 m at RK 160 (Figure 5A). Baseflow channel depth also increased systematically at a rate of $0.06RK^{0.65}$, with a maximum of 1.5 m at RK 160 (Figure 5B). Vertical channel incision was minimal in the

upper reaches of Baraboo River, but did increase steadily in the downstream direction, attaining a maximum of 4 m at RK 160.

4.1.2. Optical Water Quality

The headwaters of Baraboo River were optically clear with a minimum T_n of 1.44 NTU, which converted to a K_d of 0.24 m^{-1}. Between RK 6 and RK 74, T_n increased rapidly in the downstream direction (Figure 6A). The lower reaches of Baraboo River were very turbid with a maximum T_n of 36.23 NTU (K_d = 6.16 m^{-1}). After RK 74, T_n leveled off and then decreased slightly over the last 18 km of the study area. The spatial trend in T_n was largely dictated by the locations of major tributary junctions (Figure 2), where tributaries were a source of suspended particulates (Julian et al. In review-a). The trend in K_d along the Baraboo River continuum was best characterized by a third-order polynomial (r^2 = 0.93, Figure 6A).

4.2. Modeled Parameters from GIS Analysis

4.2.1. Incoming PAR

Between May 15 and Sep. 15, 2006, daily above-canopy PAR (E_{can}) in central Wisconsin fluctuated considerably in response to varying degrees of cloudiness, ranging from 5.04 (complete overcast) to 59.91 mol m^{-2} d^{-1} (full sun). Average E_{can} was 41.98 $\pm$ 13.88 mol m^{-2} d^{-1} (mean $\pm$ sd). GLA-modeled E_{can} for this same period was 39.85 mol m^{-2} d^{-1}, only a 5% difference than the measured average.

4.2.2. Terrestrial Shading

The topographic shading coefficient (s_t) fluctuated around a mean of 0.94 $\pm$ 0.01 (Figure 7). Most of this 6% shaded PAR occurred at dusk when the Western Uplands blocked incoming PAR from the western horizon. The low values of s_t were associated with high cliffs or hills. For example, the section of river with the greatest topographic shading (RK 32, s_t = 0.75) was located on the north side of Kimballs Bluff, a hill that was 30 m higher than the river's elevation. The extended section with high topographic shading (RK 112-119) traversed through the Upper Narrows of the North Range Baraboo Hills, where high cliffs bordered the river. The high values of s_t, which were mostly located near the headwaters and lower reaches, occurred in relatively flat areas where topographic shading was minimal. Overall, topographic shading along Baraboo River was low, with only locally significant effects.

Riparian vegetation along Baraboo River was highly variable and discontinuous (Figure 8). Along the 160-km study area, 90.5 km had no canopy (neither bank forested), 31.0 km had a half-canopy (one bank forested, one bank deforested), and 38.5 km had a full-canopy (both banks forested). Most of the full-canopy sections were located in the last 50 km of the study area.

The planform of Baraboo River was extremely sinuous, resulting in frequent changes in channel orientation (Figure 2). Of the 3,980 river raster cells, channel orientation changed 1,958 times. A majority of the channel sections had either a 90° (29%) or 135° (25%) orientation, which is consistent with the NW-SE basin orientation. For full-canopy sections, the effect of channel orientation on the vegetation shading coefficient (s_v) was minimal near the headwaters and increased with increasing channel width (Figure 4A). For example, there was no difference in s_v between 90° and 180° at a

width of 1 m, but at a width of 40 m, s_v for 90° was 0.14 greater than for 180°. This divergent trend in s_v for full-canopy sections resulted from closed canopies at small channel widths mitigating the effect of channel orientation (Julian et al. In review-b). Overall, E-W channels (e.g., 90°) had the highest s_v, and N-S channels (e.g., 180°) had the lowest s_v for full-canopy sections.

For half-canopy sections, the effect of channel orientation on s_v was considerable at all channel widths (Figure 4B). For example, there was a 0.20 difference in s_v between 270° and 90° at a width of 3 m, and there was a 0.19 difference in s_v between 270° and 90° at a width of 40 m. This approximate parallel trend in s_v for half-canopy sections resulted from the absence of a closed canopy at any channel width. Overall, channels with northern forested banks (e.g., 270°) had the highest s_v, and channels with southern forested banks (e.g., 90°) had the lowest s_v for half-canopy sections.

4.3. Benthic PAR along Baraboo River

Benthic PAR (E_{bed}) along Baraboo River was highly variable, but generally decreased in the downstream direction (Figure 9A). Maximum E_{bed} (33.05 mol m^{-2} d^{-1}) occurred at RK 0.5, which was deforested (s_v = 1.00) and optically clear (K_d = 0.29 m^{-1}). Minimum E_{bed} (< 0.01 mol m^{-2} d^{-1}) occurred at RK 112 and remained essentially zero for the remainder of the downstream study area. At this point in the river, the high turbidity of the water column (K_d = 5.70 m^{-1}) negated any effects of the terrestrial controls (topography, riparian vegetation, or channel geometry) on benthic light availability.

Upstream of RK 112, riparian vegetation was responsible for most of the spatial variability in E_{bed} along the Baraboo River continuum. For example, two adjacent cells at

RK 0.5 (one with no canopy, one with half-canopy) with the same orientation (90°), width (0.11 m), y (0.04 m), s_t (0.95), and K_d (0.29 m^{-1}) displayed an order of magnitude difference in E_{bed} (33.05 vs. 3.27 mol m^{-2} d^{-1}, respectively). Following riparian vegetation, channel orientation caused the next greatest variation in E_{bed} along the continuum. For example, two nearby cells at RK 15 (one at 90°, one at 180°) with the same riparian vegetation (half-canopy right bank), width (3.48 m), y (0.35 m), s_t (0.94), and K_d (0.59 m^{-1}) displayed a 29% difference in E_{bed} (8.30 vs. 10.73 mol m^{-2} d^{-1}, respectively). Topography caused considerable local differences in E_{bed}. Kimballs Bluff at RK 32, for example, reduced E_{bed} from 15.91 to 12.67 mol m^{-2} d^{-1} over a distance of 0.1 km (s_t was the only parameter that varied over this distance). Because width, y, and K_d were modeled using rating curves, variability in E_{bed} caused by variations in these parameters was not assessed.

Average E_{bed} for the entire 160-km study area of Baraboo River was 5.97 $\pm$ 9.48 mol m^{-2} d^{-1}. This value was calculated using an E_{can} of 39.85 mol m^{-2} d^{-1}, which assumed an intermediate level of cloudiness. Although not illustrated, atmospheric conditions considerably affect E_{bed}. Under full sun conditions (E_{can} = 59.91 mol m^{-2} d^{-1}), average E_{bed} along Baraboo River was 8.97 $\pm$ 14.25 mol m^{-2} d^{-1}. Under complete overcast conditions (E_{can} = 5.04 mol m^{-2} d^{-1}), average E_{bed} along Baraboo River was 0.89 $\pm$ 1.42 mol m^{-2} d^{-1}, a 90% decrease from full sun conditions.

4.4. Benthic PAR under Model Simulations

4.4.1. Pre-agricultural Benthic PAR

The longitudinal distribution of E_{bed} along Baraboo River with a completely forested riparian corridor and pristine optical water quality followed a parabolic trend where E_{bed} was low in the headwaters, high in the middle reaches, and low in the lower reaches (Figure 9B.1). The value of E_{bed} began with 2.80 mol m^{-2} d^{-1} at RK 0, attained a maximum of 17.28 mol m^{-2} d^{-1} at RK 52, and ended with 9.74 mol m^{-2} d^{-1} at RK 160. Because riparian vegetation remained constant along the continuum, this trend of E_{bed} was dictated by the trends of channel width (Figure 5A), depth (Figure 5B), and K_d (Figure 6B). Inter-sectional variability (i.e., vertical scatter around the mean) was caused mostly by channel orientation (Figure 4A) and occasionally by topography (e.g., RK 32). This variation in E_{bed} with channel orientation increased with distance downstream, attaining a maximum difference of 2.36 mol m^{-2} d^{-1} between adjacent cells.

4.4.2. Post-agricultural Benthic PAR with Riparian Buffer

The longitudinal distribution of E_{bed} along Baraboo River with a completely forested riparian corridor and degraded optical water quality followed a parabolic trend where E_{bed} was low in the headwaters, high in the middle reaches, and essentially zero in the lower reaches (Figure 9B.2). The value of E_{bed} began with 2.79 mol m^{-2} d^{-1} at RK 0, attained a maximum of 10.98 mol m^{-2} d^{-1} at RK 11, and reached a minimum of < 0.01 mol m^{-2} d^{-1} at RK 110 where it remained for the last 50 km. Like the previous simulation where riparian vegetation remained constant along the continuum, this trend of E_{bed} was dictated by the trends of channel width (Figure 5A), depth (Figure 5B), and K_d (Figure 6A). The higher K_d values in this simulation due to degraded optical water quality mitigated the effect of channel orientation on E_{bed} (i.e., less vertical scatter around the

mean), with only a maximum difference of 1.24 mol m^{-2} d^{-1} between adjacent cells. Compared to the pre-agricultural simulation, E_{bed} in this simulation had a lower peak that was shifted 41 km upstream.

4.4.3. Post-Agricultural Benthic PAR with No Riparian Buffer

The longitudinal distribution of E_{bed} along Baraboo River with a completely deforested riparian corridor (s_v = 1.00) and degraded optical water quality followed a logarithmic trend where E_{bed} was very high in the headwaters and decreased with distance downstream (Figure 9B.3). The value of E_{bed} began with 33.75 mol m^{-2} d^{-1} at RK 0 and reached a minimum of < 0.01 mol m^{-2} d^{-1} at RK 116 where it remained for the last 44 km. Unlike the two previous simulations, there was no riparian corridor and therefore this trend of E_{bed} was dictated solely by the trends of channel depth (Figure 5B) and K_d (Figure 6A). Without a forested canopy, there was no effect of channel orientation on E_{bed}, and thus inter-sectional variability was caused solely by topography. Compared to the pre-agricultural simulation, E_{bed} in this simulation had a much higher peak that was shifted 52 km upstream all the way to the headwaters.

4.4.4. Longitudinal Primary Productivity

Benthic GPP fluctuated considerably in the headwaters of Baraboo River, ranging from 0.3 to 2.4 g C m^{-2} d^{-1} over the first 0.5 km (Figure 10). This variability resulted from abrupt changes in E_{bed} caused by the discontinuous riparian corridor. As the canopy opening increased with distance downstream (via increased channel width), the variability in GPP decreased. The magnitude of GPP also decreased in the downstream

direction with decreasing E_{bed} (Figure 9A); however, their rates of decline were not longitudinally equivalent. Over the first 30 km, spatially-averaged GPP decreased by 3% whereas spatially-averaged E_{bed} decreased by 32%. Over the next 30 km, the two variables decreased by similar amounts, 78% and 92% for GPP and E_{bed}, respectively. The different trend in GPP over the first 30 km resulted from the asymptotic trend of the P-I curve for riverine cyanobacteria (i.e., above 20 mol m^{-2} d^{-1}, GPP did not increase significantly). GPP was extinguished by RK 107, just 5 km upstream of E_{bed} extinction.

5. DISCUSSION

5.1. Basin-Scale Benthic Light Availability

Along the river continuum, channel geometry (Figure 5; Leopold and Maddock 1953) and optical water quality (Figure 6; Julian et al. In review-a) display a high degree of organization. These longitudinal trends of hydrogeomorphic controls provided the foundation on which our basin-scale benthic light availability model (Figure 3) was built. Using this model and the Baraboo River as a case study, we quantified benthic PAR (E_{bed}) along a 160-km free-flowing mainstem channel located in an agriculturally-dominated basin. Overall, E_{bed} decreased in the downstream direction due primarily to increasing K_d, and there was considerable local variation caused by changes in topography, riparian vegetation, and channel orientation (Figure 9A). The three model simulations revealed that alterations to the riparian community and optical water quality (OWQ) can cause an order of magnitude change in E_{bed}, reduce or increase inter-sectional variability in E_{bed}, and significantly alter broad spatial trends in E_{bed} (Figure 9B).

The RCC predicts that benthic light along a forested river follows a parabolic trend where it is low in the upper and lower reaches, and high in the middle reaches (Figure 1). We found a similar trend for the model simulation with a forested riparian corridor and pristine OWQ; however, the trend was not smooth (Figure 9B.1). There was considerable inter-sectional variability due predominantly to changes in channel orientation. This high variability is liable to cause many more shifts in trophic status than the RCC predicts (Vannote et al. 1980). Additionally, pristine OWQ in rivers is rare. Most landscapes have been affected by some degree of anthropogenic disturbance, which degrades OWQ (Walling and Fang 2003, MEA 2005). Therefore, even rivers with a forested riparian corridor are more likely to have an E_{bed} peak in the upper reaches rather than the middle reaches (Figure 9B.2). The actual values of E_{bed} and the distance at which it is eradicated (e.g., RK 112 for Baraboo River) will depend on basin physiography and level of anthropogenic disturbance. In all, the longitudinal trend in E_{bed} as proposed by the RCC is only valid for rivers with a continuously forested riparian corridor, pristine OWQ, and no sinuosity.

One of the limitations of the RCC concerning light availability is that it only applies to rivers with a continuously forested riparian corridor, which is becoming increasingly rare due to large-scale deforestation (MEA 2005). Because of gaps in riparian forest, most rivers will probably have high spatial variability in E_{bed} with a peak near the headwaters, similar to the longitudinal pattern in Baraboo River (Figure 9A). For non-forested rivers, such as prairie and desert streams (see Wiley et al. 1990), we expect the longitudinal profile of E_{bed} to follow a logarithmic trend where E_{bed} is high in

the headwaters due to lack of riparian shading and decreases along the continuum due to increasing turbidity and depth (Figure 9B.3).

Another limitation of the RCC is that it only applies to a linear, uninterrupted continuum. The non-impounded and non-engineered character of its mainstem channel allowed us to conceptualize the Baraboo River as a seamless continuum, which we acknowledge is not characteristic of most rivers. Most rivers have longitudinal "discontinuities" caused by dams (Ward and Stanford 1983), geomorphic heterogeneity (Montgomery 1999), and confluences (Rhoads 1987, Kiffney et al. 2006). An emerging paradigm in fluvial geomorphology and ecology is conceptualizing the river as a series of network links rather than a continuum (Rice et al. 2001, Benda et al. 2004). Indeed, Julian et al. (In review-a) found that the optical water quality of Baraboo River along its continuum was heavily influenced by tributary inputs. While basin network configuration does influence aquatic light attenuation along the river, terrestrial shading is only dictated by the local controls of topography and riparian vegetation. Therefore, our technique of using DEMs and LCMs to quantify terrestrial shading could be applied to entire river networks. Quantifying aquatic light attenuation for river networks would require more extensive empirical data in order to assess broad spatial variations in y and K_d. In summary, our GIS-based model uses both an empirical and process-based approach to characterize longitudinal trends of E_{bed} along the river continuum, and has the potential to be applied to entire river networks.

5.2. Effect of Agriculturalization on Benthic Light Availability

In this study, we assessed the effect of agriculturalization on benthic light availability at the basin-scale using three model simulations. These three modeled scenarios were (1) pre-agricultural Baraboo River, (2) post-agricultural Baraboo River with a riparian buffer, and (3) post-agricultural Baraboo River without a riparian buffer (Figure 9B). In scenario 1, which represents the Baraboo River before any anthropogenic disturbance, E_{bed} followed a parabolic trend where it was highest in the middle reaches. The peak in this curve at RK 52 is the point along the river where the combined effects of terrestrial shading and aquatic attenuation were at a minimum. This point therefore signifies a threshold where terrestrial shading is the dominant control of E_{bed} upstream of the peak and aquatic attenuation is the dominant control of E_{bed} downstream of the peak. Statistical evidence for this relationship of dominant controls on E_{bed} is presented in Julian et al. (In review-b).

In scenario 2, which represents the Baraboo River after agricultural land conversion and before removal of any riparian forests, the peak in E_{bed} was reduced and shifted upstream. This reduction and upstream shift in E_{bed} is caused by accelerated soil erosion from agricultural land use, which increases water turbidity and consequently the dominance of aquatic light attenuation on E_{bed}. Because of the exceptionally high turbidity values of Baraboo River (Julian et al. In review-a), the longitudinal trend in E_{bed} for most rivers affected by agriculture (assuming a continuous riparian buffer) is likely to fall somewhere between the curves of scenarios 1 and 2 (Figure 9B).

In scenario 3, which represents the Baraboo River after agricultural land conversion and complete removal of riparian forests, the parabolic trend in E_{bed} shifted to a logarithmic trend where E_{bed} was much greater in the headwaters and decreased along

the river continuum. With the absence of riparian vegetation shading, aquatic light attenuation became the dominant control on E_{bed} for the entire continuum. In addition to changing the longitudinal distribution of E_{bed}, this scenario also eliminated all inter-sectional variability caused by channel orientation. For a river with a mixed riparian community such as Baraboo River, the curve in scenario 3 represents the upper limit of E_{bed} while the curve in scenario 2 represents the lower limit of E_{bed}. Comparisons of the four curves in Figure 9 reveal that agriculturalization is likely to (i) increase the magnitude of E_{bed} near the headwaters due to riparian deforestation, (ii) decrease the magnitude of E_{bed} in the lower reaches due to increased turbidity, (iii) shift the peak in E_{bed} upstream due to increased dominance of aquatic light attenuation over terrestrial shading, and (iv) increase reach-scale variability in E_{bed} due to a discontinuous riparian community.

5.3. Other Disturbances on Benthic Light Availability

There are several other widespread anthropogenic disturbances that alter the light regimes of rivers including urbanization, logging, mining, dam construction, and dam removal. Urbanization increases the turbidity of rivers through increased surface soil runoff (Wolman 1967) and decreases terrestrial shading through riparian deforestation and channel widening associated with channel evolution following increased surface water runoff (Hammer 1972). These geomorphic changes from channel evolution usually extend upstream and downstream of the urban-impacted area (Graf 1975, Simon 1992). Before channel widening occurs during channel evolution, channel incision usually occurs (Harvey et al. 1984). This entrenchment not only increases topographic shading

of the channel, but also increases vegetation shading by causing riparian trees to lean towards the center of the channel, which we observed in some of the lower sections of Baraboo River. Overall, urbanization is likely to (i) increase E_{bed} in some reaches due to reduced vegetation shading, (ii) decrease E_{bed} in others due to enhanced aquatic light attenuation or enhanced topographic shading, and (iii) increase the variability of E_{bed} along the river continuum due to spatial discontinuity of the previous two effects, similar to Figure 9A.

Logging has similar effects on E_{bed} as agriculturalization where terrestrial shading is reduced through riparian deforestation and aquatic light attenuation is enhanced through increased surface soil runoff (Garman and Moring 1991, Sabater et al. 2000). Whereas logging and agriculturalization gradually increase turbidity along the river continuum due to non-point source inputs, mining usually is a point source for enhanced aquatic light attenuation because of direct discharges to the river. Mining inputs have been found to increase turbidity by an order of magnitude over distances less than 2 km (Davies-Colley et al. 1992). Dam construction alters both upstream and downstream E_{bed}, where the upstream reach has lower E_{bed} due to increased water depth and the downstream reach has higher E_{bed} due to clearer water being discharged by the dam (Williams and Wolman 1984). Dam removal has the opposite effect on E_{bed}, where the upstream reach has higher E_{bed} due to decreased water depth and the downstream reach has lower E_{bed} due to more turbid water being discharged from the former reservoir (Riggsbee et al. 2007). In addition to anthropogenic disturbances, there are also natural disturbances that can affect E_{bed}, including floods (Julian et al. In review-a) and debris flows (Simon 1992).

5.4. Implications of Altered Riverine Light Regimes

Solar radiation dictates many of the abiotic and biotic processes in rivers (Wetzel 2001), and thus changes in benthic light availability are likely to have far-reaching effects on fluvial ecosystems. The thermal regime of a river is especially sensitive to changes in light availability. Maximum water temperatures in unshaded reaches have been found to be as much as 7°C higher than shaded reaches (Graynoth 1979, Quinn et al. 1997, Rutherford et al. 2004). Because of the effects of water temperature on the behavior of aquatic biota, dissolved oxygen concentrations, biogeochemical reactions, and domestic water use (Walling and Webb 1992, Wetzel 2001), light availability indirectly affects all of these phenomena.

The productivity of riverine ecosystems is driven by the solar energy utilized in photosynthesis (Wetzel 2001), and thus the primary productivity of rivers is greatly affected by changes in terrestrial shading and turbidity. We found that GPP increased by an order of magnitude over just 260 m in response to riparian deforestation in the upper reaches of Baraboo River. Increasing turbidity along Baraboo River decreased GPP from 2.4 to 0 g C m^{-2} d^{-1} over a distance of 107 km. Other studies have found similar relationships. For example, chlorophyll-a biomass (*chl-a*) for unshaded reaches has been found to be as much as 16 times higher than for shaded reaches (Sabater et al. 2000, Kiffney et al. 2004, Rier et al. 2006). Davies-Colley et al. (1992) found (i) E_{bed} and *chl-a* were strongly correlated and (ii) increased turbidity from mining inputs decreased *chl-a* by as much as 57%. Aquatic plant growth, as dictated by light availability, also influences habitat availability (Humphries 1996), food webs (Hill et al. 1995), nutrient

uptake (Sabater et al. 2000, Zahn 2007), particulate matter retention (Horvath 2004), and organic compound degradation (Soda et al. 2007). By quantifying the large-scale spatial variation in benthic light availability, our basin-scale model can be used to understand the nature of all the above phenomena from a landscape perspective.

6. CONCLUSIONS

We coupled readily-available broad spatial data with easily-measured synoptic data to quantify benthic light availability and GPP at the basin-scale. Our model output (Figure 9) displays the spatial variation of benthic light availability along the Baraboo River for a range of boundary conditions. Few rivers have pristine optical water quality and completely forested riparian zones, and therefore the trend of Figure 9B.1 is rare. Rivers are more likely to posses the trend in Figure 9A where discontinuities in terrestrial and aquatic controls cause high inter-sectional variability in E_{bed}. The dramatic differences in E_{bed} between the four scenarios illustrate the sensitivity of riverine light availability to environmental change, whether it is removal of riparian trees causing an order of magnitude increase in E_{bed} or accelerated soil erosion causing an order of magnitude decrease in E_{bed}. Previous studies have demonstrated the consequences of altered light regimes on river ecosystems at the transect and reach-scale. Using our basin-scale benthic light availability model, researchers now have a tool to investigate relationships between light availability and ecosystem processes (e.g., GPP) along the river continuum or throughout the river network.

REFERENCES

Basher, L. R. 2003. The Motueka and Riwaka catchments: a technical report summarising the present state of knowledge of the catchments, management issues and research needs for integrated catchment management. Manaaki Whenua Landcare Research, Lincoln.

Benda, L., N. L. Poff, D. Miller, T. Dunne, G. Reeves, G. Pess, and M. Pollock. 2004. The network dynamics hypothesis: how channel networks structure riverine habitats. Bioscience **54**:413-427.

Bott, T. L., J. T. Brock, C. S. Dunn, R. J. Naiman, R. W. Ovink, and R. C. Petersen. 1985. Benthic community metabolism in four temperate stream systems: An inter-biome comparison and evaluation of the river continuum concept. Hydrobiologia **123**:3-45.

Curtis, J. T. 1959. The Vegetation of Wisconsin. The University of Wisconsin Press, Madison.

Davies-Colley, R. J. 1990. Frequency distributions of visual water clarity in 12 New Zealand rivers. New Zealand Journal of Marine and Freshwater Research **24**:453-460.

Davies-Colley, R. J., C. W. Hickey, J. M. Quinn, and P. A. Ryan. 1992. Effects of clay discharges on streams: 1. Optical properties and epilithon. Hydrobiologia **248**:215-234.

Davies-Colley, R. J., W. N. Vant, and D. G. Smith. 2003. Colour and Clarity of Natural Waters. Ellis Horwood, New York.

Dodds, W. K., B. J. F. Biggs, and R. L. Lowe. 1999. Photosynthesis-irradiance patterns in benthic microalgae: Variations as a function of assemblage thickness anc community structure. Journal of Phycology **35**:42-53.

Fisher, S. G. 1997. Creativity, idea generation, and the functional morphology of streams. J. N. Am. Benthol. Soc. **16**:305-318.

Frazer, G. W., C. D. Canham, and K. P. Lertzman. 1999. Gap Light Analyzer (GLA), version 2.0: Imaging software to extract canopy structure and gap light transmission indices from true-colour fisheye photographs, users manual and program documentation. Simon Fraser University and Institute of Ecosystem Studies, Burnaby, B.C. and Millbrook, NY.

Fu, P., and P. M. Rich. 2000. The Solar Analyst 1.0 Manual. HELIOS Environmental Modeling Institute.

Garman, G. C., and J. R. Moring. 1991. Initial effects of deforestation on physical characteristics of a boreal river. Hydrobiologia **209**:29-37.

Gilbert, G. K. 1877. Report on the Geology of the Henry Mountains. U.S. Geographical and Geological Survey of the Rock Mountain Region, Washington, D.C.

Graf, W. L. 1975. The impact of suburbanization on fluvial geomorphology. Water Resources Research **11**:690-692.

Graynoth, E. 1979. Effects of logging on stream environments and faunas in Nelson. New Zealand Journal of Marine and Freshwater Research **13**:79-109.

Hammer, T. R. 1972. Stream channel enlargement due to urbanization. Water Resources Research **8**:1530-1540.

Harvey, M. D., C. C. Watson, and S. A. Schumm. 1984. Channelized streams: An analog for the effects of urbanization. Pages 401-409 *in* H. J. Sterling, editor. International Symposium on Urban Hydrology, Hydraulics and Sediment Control. University of Kentucky, Lexington, KY.

Hill, W. R., M. G. Ryon, and E. M. Schilling. 1995. Light limitation in a stream ecosystem: Responses by primary producers and consumers. Ecology **76**:1297-1309.

Horvath, T. G. 2004. Retention of particulate matter by macrophytes in a first-order stream. Aquatic Botany **78**:27-36.

Humphries, P. 1996. Aquatic macrophytes, macroinvertebrate associations and water levels in a lowland Tasmanian river. Hydrobiologia **321**:219-233.

Jassby, A. D., and T. Platt. 1976. Mathematical formulation of the relationship between photosynthesis and light for phytoplankton. Limnology and Oceanography **21**:540-547.

Julian, J. P., M. W. Doyle, S. M. Powers, E. H. Stanley, and J. A. Riggsbee. In review-a. Optical water quality in rivers. Water Resources Research.

Julian, J. P., M. W. Doyle, and E. H. Stanley. In review-b. Empirical modeling of light availability in rivers. Journal of Geophysical Research - Biogeosciences.

Kiffney, P. M., C. M. Greene, J. E. Hall, and J. R. Davies. 2006. Tributary streams create spatial discontinuities in habitat, biological productivity, and diversity in mainstem rivers. Canadian Journal of Fisheries and Aquatic Sciences **63**:2518-2530.

Kiffney, P. M., J. S. Richardson, and J. P. Bull. 2004. Establishing light as a causal mechanism structuring stream communities in response to experimental manipulation of riparian buffer width. Journal of the North American Benthological Society **23**:542-555.

Leopold, L. B., and T. Maddock, Jr. 1953. The hydraulic geometry of stream channels and some physiographic implications. USGS Professional Paper **252**:1-57.

Lookingbill, T., S. S. Kaushal, R. H. Gardner, R. P. Morgan, A. J. Elmore, R. H. Hilderbrand, K. N. Eshleman, W. R. Boynton, M. A. Palmer, and W. C. Dennison. In review. Consequences of urbanization in the watershed of a large U.S. river: Blurring ecosystem boundaries. Urban Ecosystems.

Maidment, D. R. 2002. Arc Hydro: GIS for Water Resources. Center for Research in Water Resources, University of Texas, Austin.

Minshall, G. W., K. W. Cummins, R. C. Petersen, C. E. Cushing, D. A. Bruns, J. R. Sedell, and R. L. Vannote. 1985. Developments in stream ecosystem theory. Canadian Journal of Fisheries and Aquatic Sciences **42**:1045-1055.

Montgomery, D. R. 1999. Process domains and the river continuum. Journal of the American Water Resources Association **35**:397-410.

Osterkamp, W. R., and E. R. Hedman. 1977. Variation of width and discharge for natural high-gradient stream channels. Water Resources Research **13**:256-258.

Quinn, J. M., A. B. Cooper, R. J. Davies-Colley, J. C. Rutherford, and R. B. Williamson. 1997. Land use effects on habitat, water quality, periphyton, and benthic invertebrates in Waikato, New Zealand, hill-country streams. New Zealand Journal of Marine and Freshwater Research **31**:579-597.

Rhoads, B. L. 1987. Changes in stream channel characteristics at tributary junctions. Physical Geography **8**:346-361.

Rice, S. P., M. T. Greenwood, and C. B. Joyce. 2001. Tributaries, sediment sources, and the longitudinal organisation of macroinvertebrate fauna along river systems. Canadian Journal of Fisheries and Aquatic Sciences **58**:824-840.

Rier, S. T., R. J. Stevenson, and G. D. LaLiberte. 2006. Photo-acclimation response of benthic stream algae across experimentally manipulated light gradients: A comparison of growth rates and net primary productivity. Journal of Phycology **42**:560-567.

Riggsbee, J. A., J. P. Julian, M. W. Doyle, and R. G. Wetzel. 2007. Suspended sediment, dissolved organic carbon, and dissolved nitrogen export during the dam removal process. Water Resources Research **43**.

Rutherford, J. C., N. A. Marsh, P. M. Davies, and S. E. Bunn. 2004. Effects of patchy shade on stream water temperature: how quickly do small streams heat and cool? Marine and Freshwater Research **55**:737-748.

Sabater, F., A. Butturini, E. Marti, I. Munoz, A. Romani, J. Wray, and S. Sabater. 2000. Effects of riparian vegetation removal on nutrient retention in a Mediterranean stream. Journal of the North American Benthological Society **19**:609-620.

Scudder, B. C., and J. S. Stewart. 2001. Benthic algae of benchmark streams in agricultural areas of Eastern Wisconsin. WRI report 96-4038-E, U.S. Geological Survey, Middleton, WI.

Simon, A. 1992. Energy, time, and channel evolution in catastrophically disturbed fluvial systems. Geomorphology **5**:345-372.

Soda, S., M. Ike, Y. Ogasawara, M. Yoshinaka, D. Mishima, and M. Fujita. 2007. Effects of light intensity and water temperature on oxygen release from roots into water lettuce rhizosphere. Water Research **41**:487-491.

Stanley, E. H., S. G. Fisher, and J. B. Jones. 2004. Effects of water loss on primary production: A landscape-scale model. Aquatic Sciences **66**:130-138.

U.S. Department of Agriculture (USDA). 2007. UV-B Monitoring and Research Program, http://uvb.nrel.colostate.edu/UVB/.

Vannote, R. L., G. W. Minshall, K. W. Cummins, J. R. Sedell, and C. E. Cushing. 1980. The river continuum concept. Can. J. Fish. Aquat. Sci. **37**:130-137.

Walling, D. E., and D. Fang. 2003. Recent trends in the suspended sediment loads of the world's rivers. Global and Planetary Change **39**:111-126.

Walling, D. E., and B. W. Webb. 1992. Water quality: I. Physical characteristics. Pages 48-72 *in* P. Calow and G. E. Petts, editors. The Rivers Handbook: Hydrological and Ecological Principles. Blackwell Scientific, Oxford.

Ward, J. V., and J. A. Stanford. 1983. The serial discontinuity concept of lotic ecosystems. Pages 29-42 *in* T. D. Fontaine and S. M. Bartell, editors. Dynamics of Lotic Ecosystems. Ann Arbor Science, Ann Arbor.

Wetzel, R. G. 2001. Limnology: Lake and River Ecosystems. Academic Press, San Diego.

Wiens, J. A. 2002. Riverine landscapes: Taking landscape ecology into the water. Freshwater Biology **47**:501-515.

Wiley, M. J., L. L. Osborne, and R. W. Larimore. 1990. Longitudinal structure of an agricultural prairie river system and its relationship to current stream ecosystem theory. Canadian Journal of Fisheries and Aquatic Sciences **47**:373-384.

Williams, G. P., and M. G. Wolman. 1984. Downstream effects of dams on alluvial rivers. USGS Professional Paper **1286**:83.

Wisconsin Department of Natural Resources (WDNR). (2006), Wisconsin Dam Database. http://dnr.wi.gov/org/water/wm/dsfm/dams/datacentral.html.

Wisconsin Initiative for Statewide Cooperation on Landscape Analysis and Data (WISCLAND) (1993), Land Cover of Wisconsin. Wisconsin Department of Natural Resources, http://dnr.wi.gov/maps/gis/datalandcover.html#data.

Wolman, M. G. 1967. A cycle of sedimentation and erosion in urban river channels. Geografiska Annaler **49A**:385-395.

Zahn, S. E. 2007. Submerged macrophytes in Big Spring Creek, WI: Distribution and influence on phosphorous dynamics. University of Wisconsin, Madison.

Table 4.1. *Gap Light Analyzer* (GLA) and *Solar Analyst* (SA) user-defined parameters.

Options not available in the software are labeled "na."

Parameter	**GLA**	**SA**
Period	May 15 – Sep 15	May 15 – Sep 15
Projection	Polar	Polar
Orientation	Horizontal	Horizontal
Time step	1 minute	30 minute
Azimuth regions	36	8
Zenith regions	9	8
Solar constant	1367 W/m^2	1367 W/m^2
Cloudiness Index	0.50	na
Spectral fraction	0.45	na
Beam fraction	0.50	0.50
Sky-region brightness	UOC model	UOC model
Clear-sky transmission coefficient	0.60	0.60

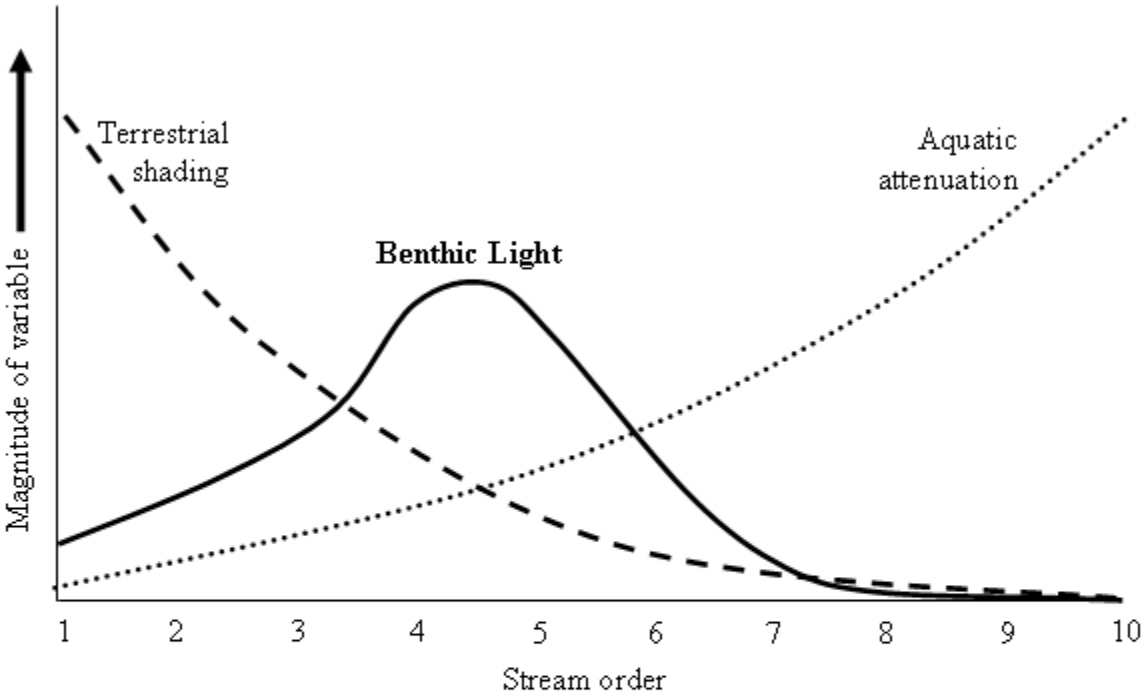

Figure 4.1. Conceptual profile of benthic light availability along the continuum of a forested river. The trends of terrestrial shading and aquatic attenuation were derived from Vannote et al. (1980). The trend of benthic light was derived using the above trends in the benthic light availability model (BLAM; Julian et al. In review-b). Aquatic attenuation (via turbidity and water depth) increases in the downstream direction, whereas terrestrial shading (via topography and vegetation) decreases in the downstream direction. Benthic light reaches a max where the product of riparian shading and aquatic attenuation is the lowest.

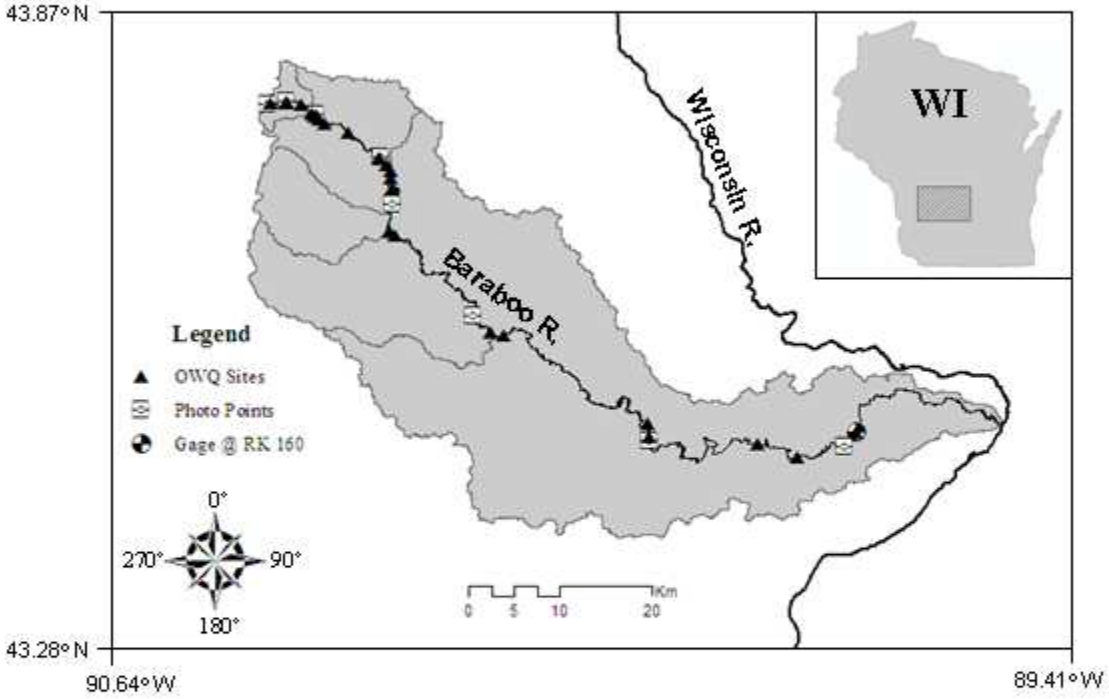

Figure 4.2. Baraboo River Basin. Major tributaries are depicted. Gage represents the downstream extent of this study. Photo points are locations where canopy photos were taken and channel width and depth measured. Optical water quality (OWQ) sites are locations where turbidity was measured. Compass in bottom-left corner provides context for channel orientation.

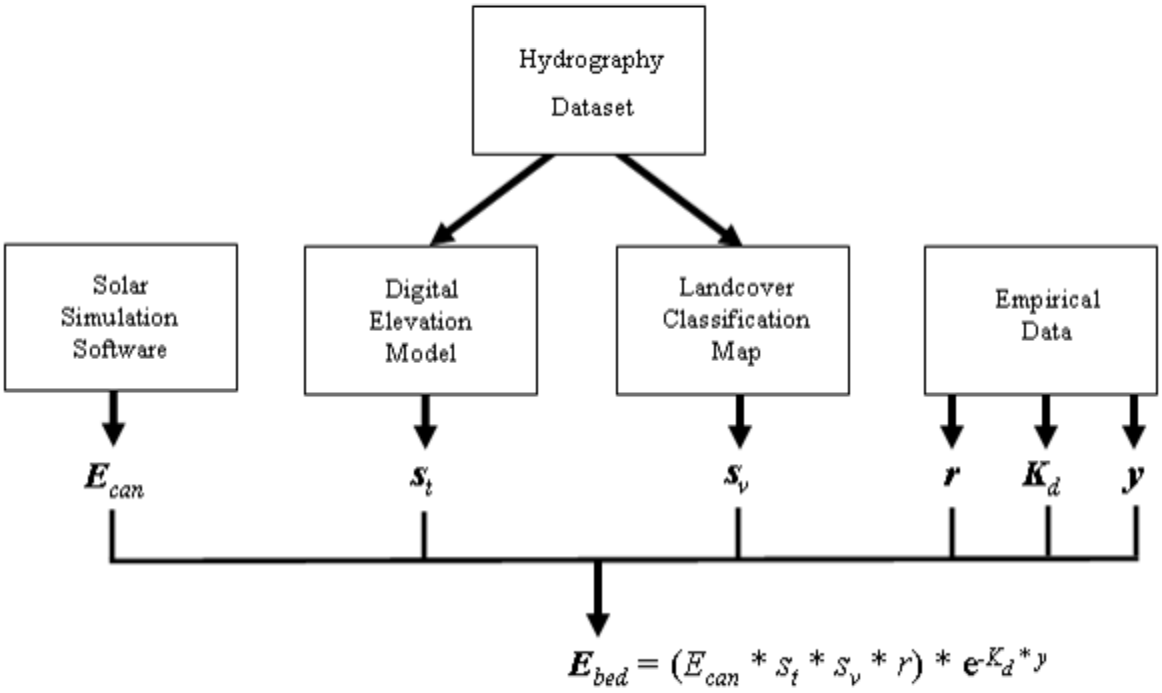

Figure 4.3. Schematic of the GIS framework to model basin-scale benthic light availability.

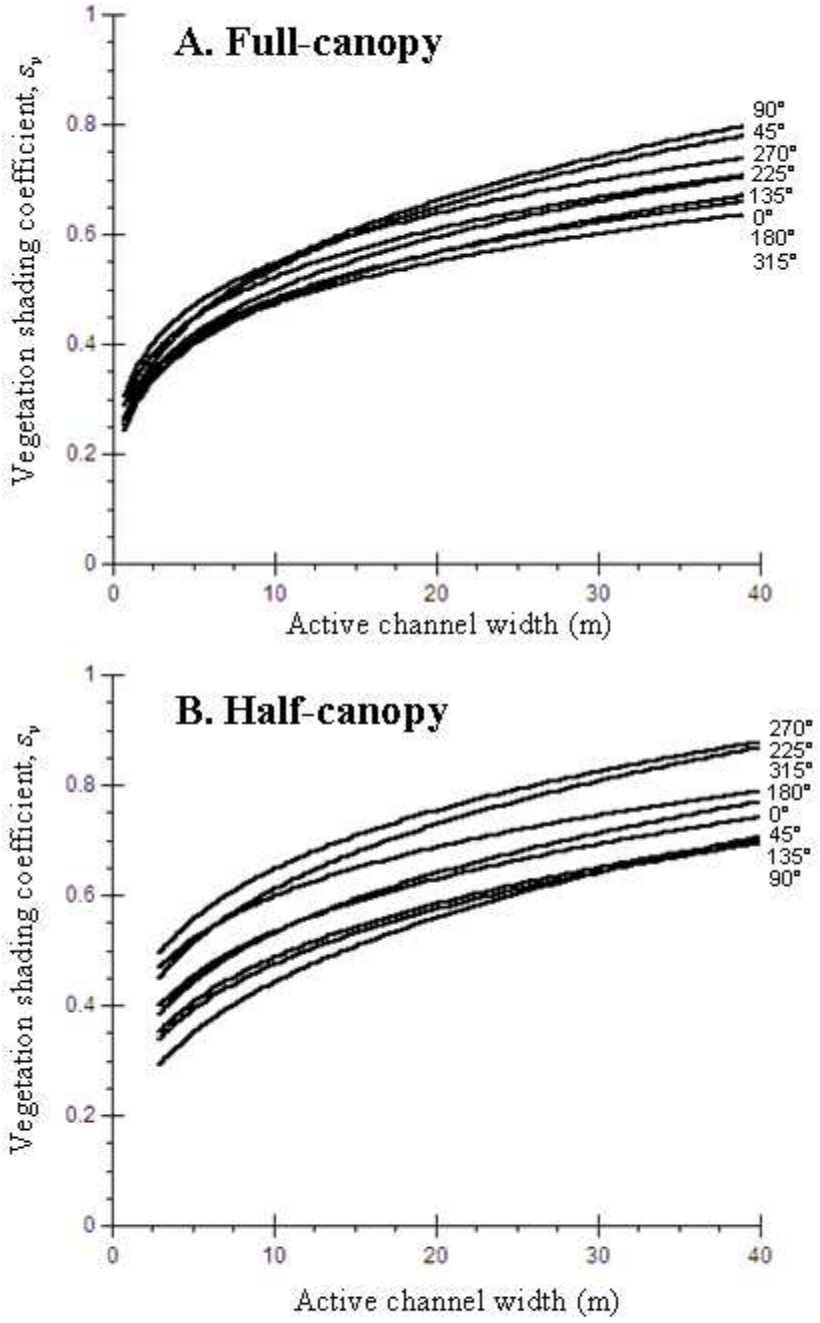

Figure 4.4. Vegetation shading coefficient (s_v) curves based on channel width and orientation. Full-canopy curves (A) are for transects with two forested banks. Half-canopy curves (B) are for transects with one forested bank and one deforested bank. For transects with two deforested banks (no canopy), $s_v = 1.0$.

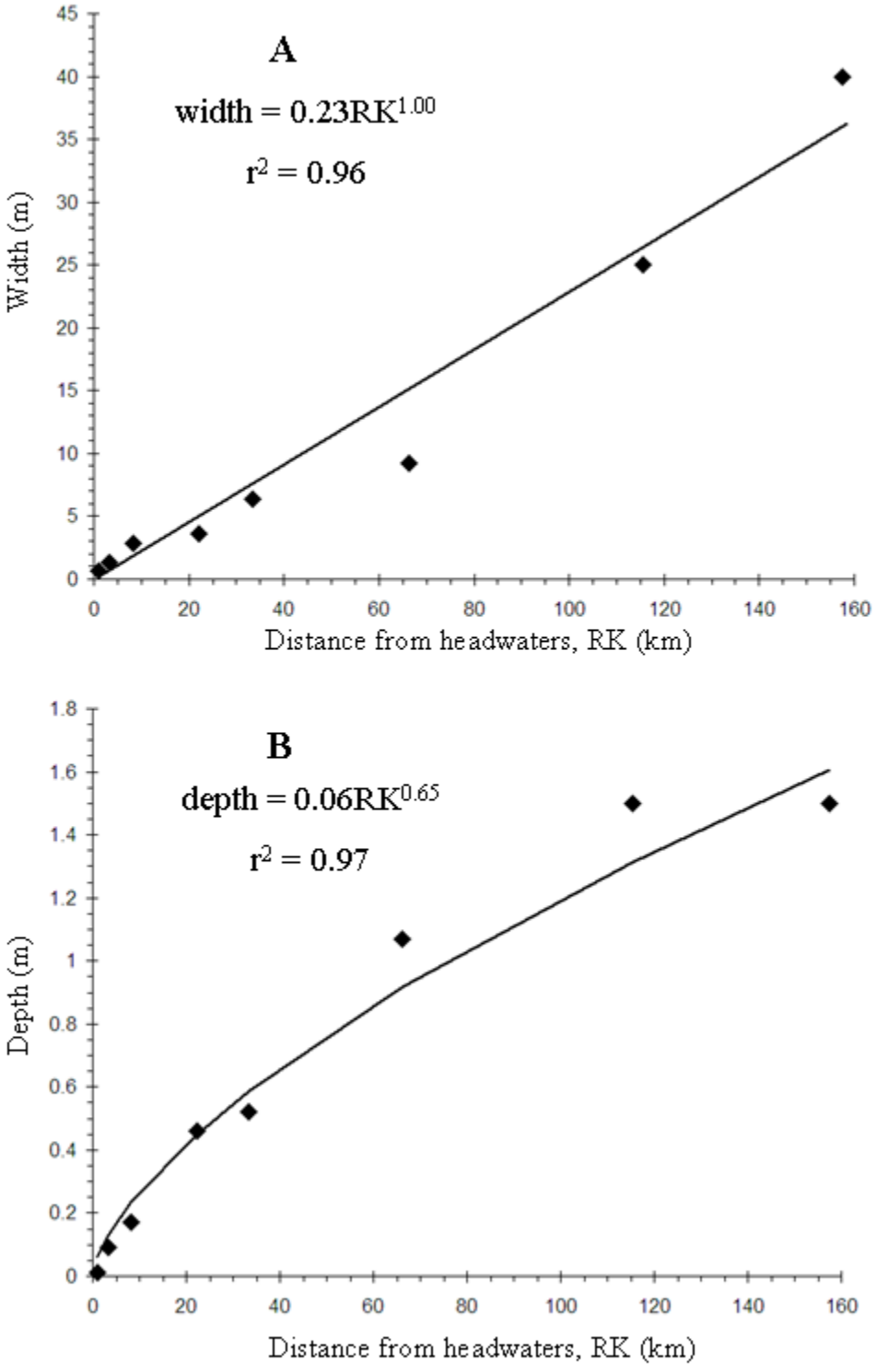

Figure 4.5. Downstream variation in width and depth along Baraboo River.

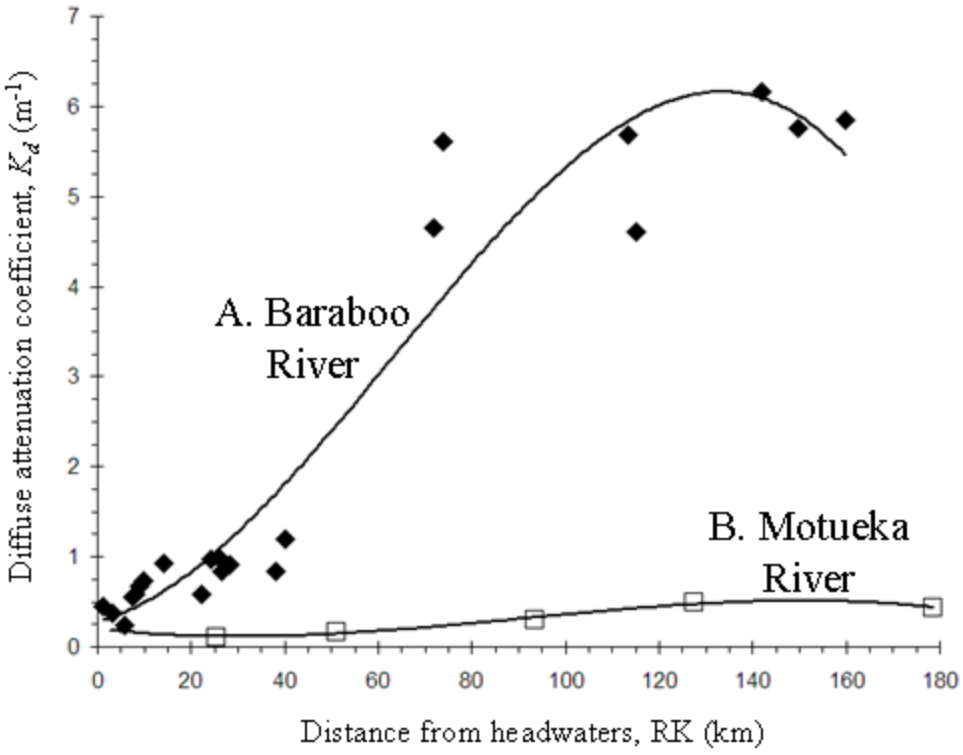

Figure 4.6. Downstream variation in the diffuse attenuation coefficient (K_d) for Baraboo River, WI, USA (A) and Motueka River, NZ (B). Baraboo R. is in an agriculturally-dominated basin, whereas Motueka R. is in a relatively undisturbed basin. Distance for Motueka R. was normalized to that of Baraboo R. Data for Motueka R. adapted from Davies-Colley (1990). Baraboo R.: $K_d = -4.21E\text{-}6RK^3 + 7.93E\text{-}4RK^2 + 0.01RK + 0.29$, $r^2 = 0.93$; Motueka R.: $K_d = -3.57E\text{-}7RK^3 + 9.09E\text{-}5RK^2 - 3.11E\text{-}3RK + 0.12$, $r^2 = 0.99$.

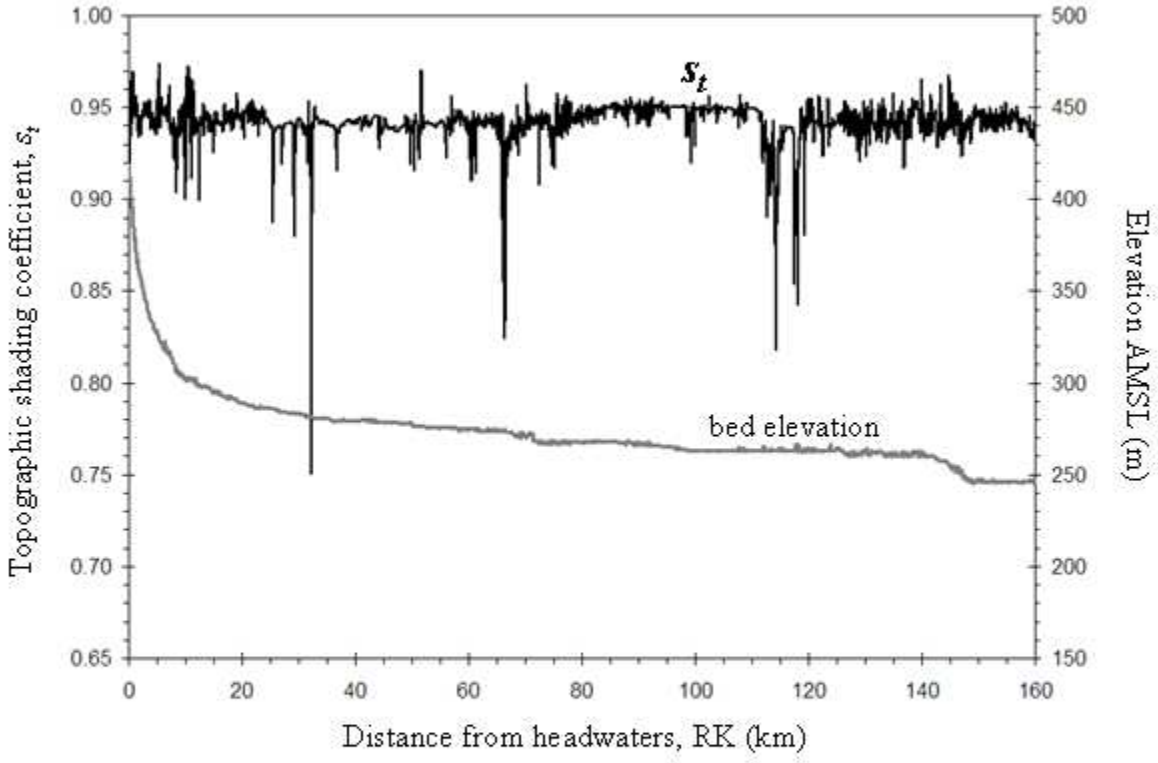

Figure 4.7. Topographic shading and bed elevation along the Baraboo River. Both variables were extracted from a USGS 30-m DEM.

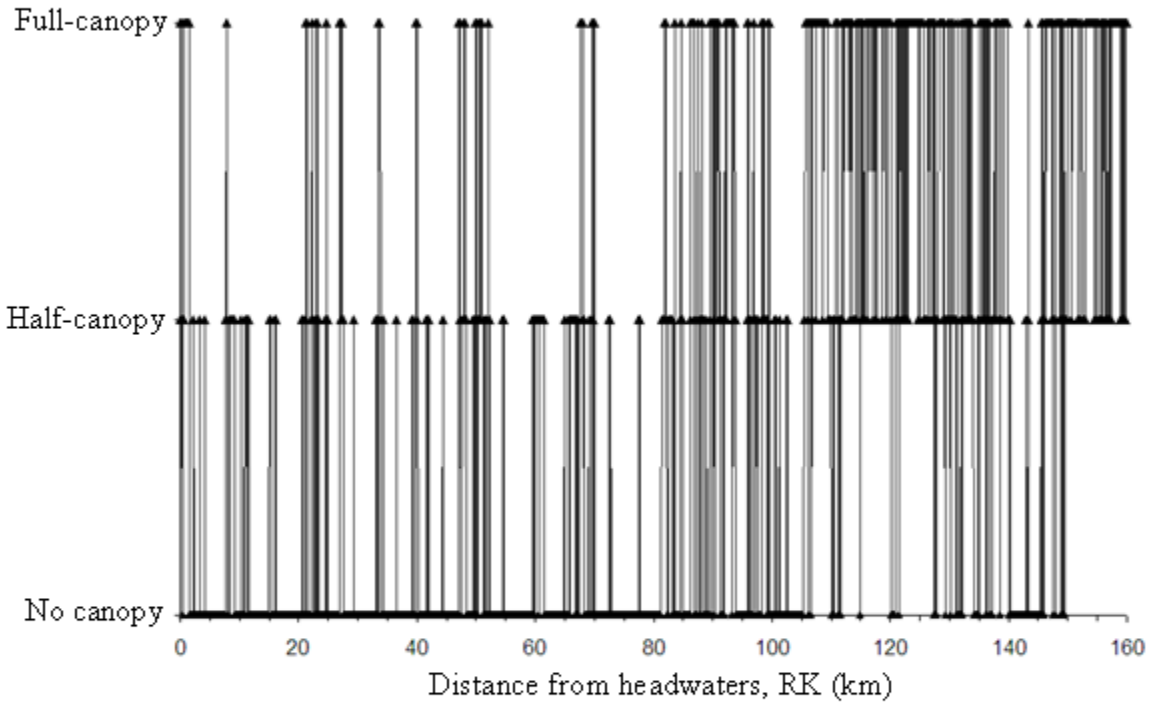

Figure 4.8. Longitudinal distribution of riparian forest along the Baraboo River based on the landcover classification map (WISCLAND 1993). Full-canopy sites are transects with two forested banks. Half-canopy sites are transects with one forested bank and one deforested bank. No canopy sites are transects with two deforested banks. Closely spaced vertical lines denote discontinuities in riparian type, and wide gaps between vertical lines denote continuous patches of riparian type.

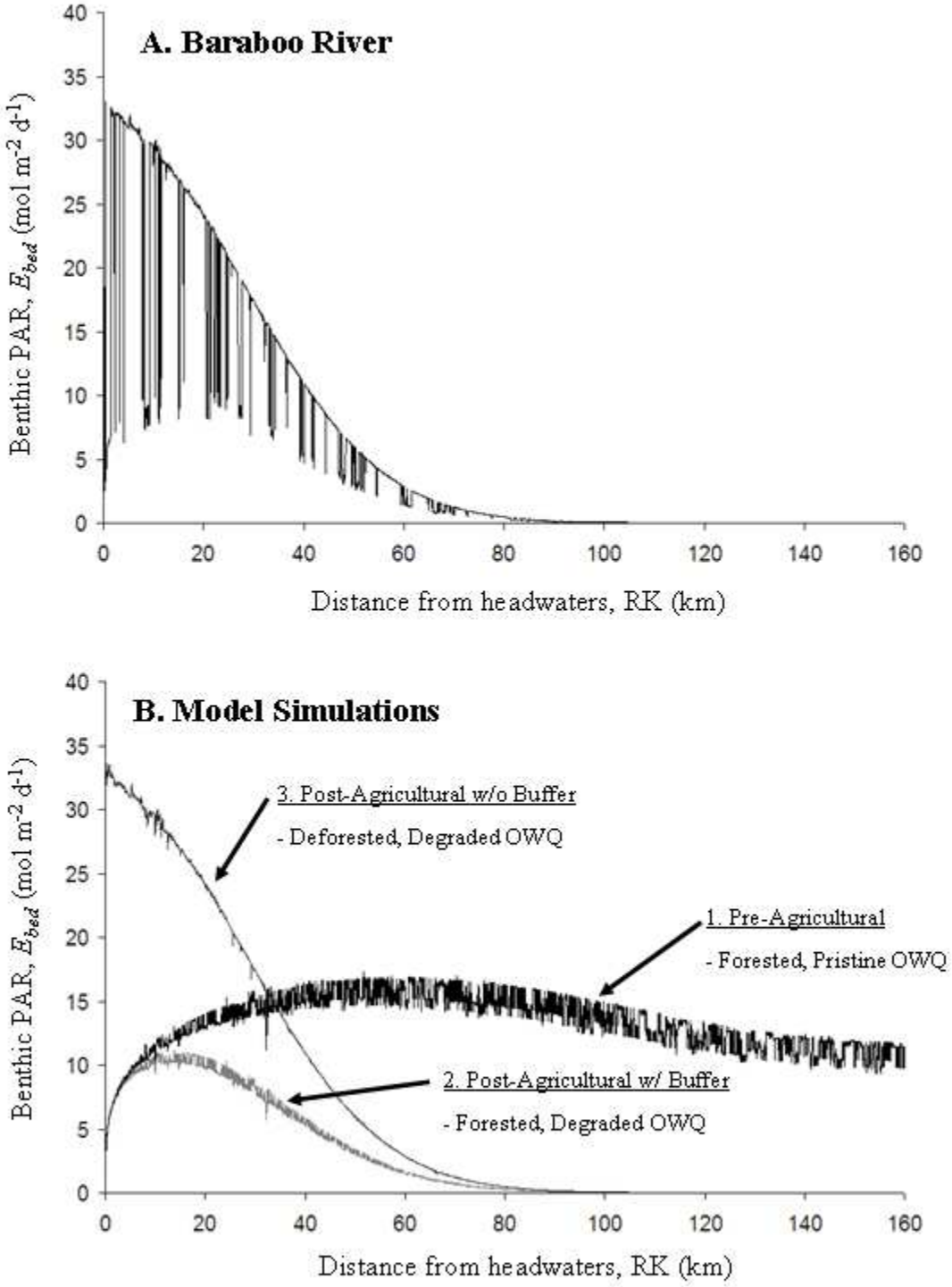

Figure 4.9. Benthic PAR along the Baraboo River (A) and under model simulations (B). The degree of riparian cover and optical water quality (OWQ) is labeled for each simulation. All four curves were calculated using an E_{can} of 39.85 mol m^{-2} d^{-1}.

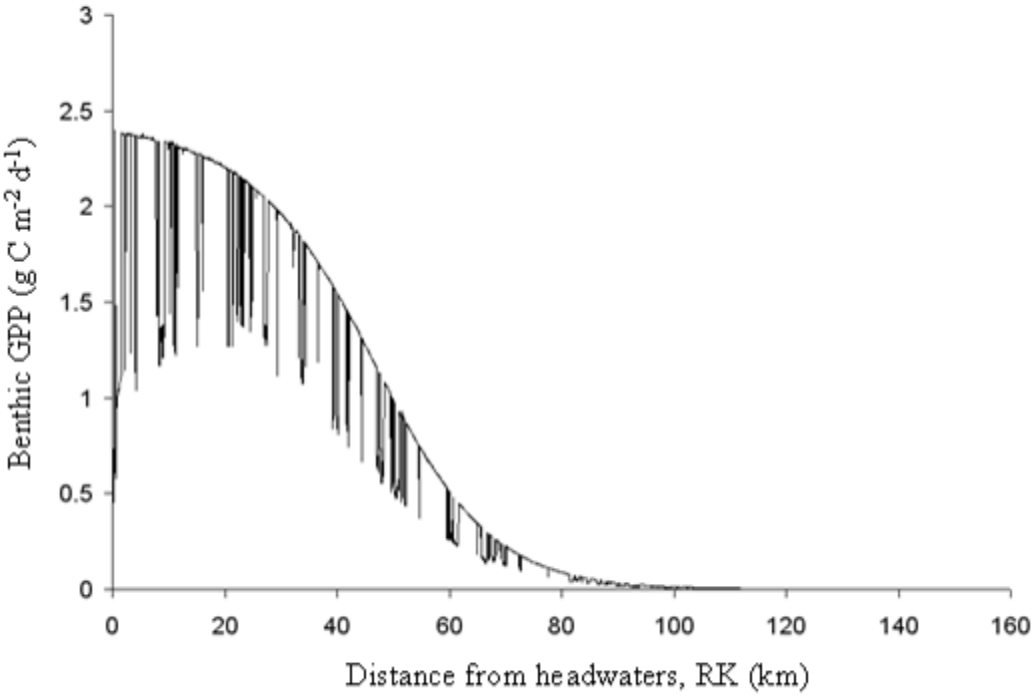

Figure 4.10. Benthic GPP along the Baraboo River. GPP was calculated using the method of Jassby and Platt (1976), the photosynthesis-irradiance curve for cyanobacteria (Dodds et al., 1999), and the E_{bed} distribution of Baraboo River (Figure 9A).

V. CONCLUSIONS

RESEARCH OBJECTIVES AND THESIS STRUCTURE

The main objective of this research was to characterize the spatial and temporal variability of benthic light availability in rivers. The fundamental questions answered were:

1. What are the dominant controls of benthic light availability in rivers?
2. Do spatial and temporal variations in benthic light availability follow general trends?
3. How is benthic light availability affected by anthropogenic influences?

These questions were not dealt with separately in individual chapters, but instead were addressed collectively and hierarchically. The processes that affect benthic light availability in rivers are scale-dependent, and therefore required assessment across a range of spatial and temporal scales. Accordingly, the structure of this thesis followed a transition from small to large spatio-temporal scales.

Investigations began at the transect-scale (i.e., a lateral slice of channel with no longitudinal length). For a river transect at small timescales (hourly-daily), the terrestrial controls on benthic light availability (topography, riparian vegetation, channel geometry) are fixed, whereas the aquatic controls (optical water quality, hydrologic regime) are highly variable (Table 5.1). The first analyses thus dealt with optical water quality and

its variation with hydrologic regime (Chapter II). At the transect-scale, we assessed optical water quality and hydrologic regime over a range of temporal scales, from hourly to monthly. Temporal optical water quality was assessed for a small, 2nd-order river (Big Spring Creek, WI) and a medium, 6th-order river (Deep River, NC) (stream size based on the classification of Vannote et al. 1980). Scaling up to the basin, we assessed optical water quality along the continuum of a medium, 6th-order river (Baraboo River, WI) and a large, 7th-order river (Wisconsin River, WI). We then compared our findings to previous synoptic surveys to characterize broad spatial trends of optical water quality.

Reach-scale (i.e., a length of river with no major tributaries and longitudinally consistent optical water quality) benthic light availability was assessed for a 1.3-km reach in Big Spring Creek and a 5.8-km reach in Deep River (Chapter III). In order to quantify the effect of all five hydrogeomorphic controls on benthic light availability, we developed a model (BLAM) that calculated the amount of above-canopy PAR (in mol/m^2/day) that reached the riverbed (E_{bed}) after terrestrial shading and aquatic attenuation. We used BLAM to characterize E_{bed} spatially (along the reach) and temporally (daily fluctuations in response to changes in water depth and discharge).

Basin-scale (i.e., the entire length of river from headwaters to mouth) benthic light availability was assessed by using BLAM in a GIS framework and incorporating the principles of hydraulic geometry (sensu Leopold and Maddock 1953). We used this GIS-based model to quantify E_{bed} along the continuum of Baraboo River and investigate the effects of anthropogenic disturbances on light regimes of rivers (Chapter IV). In summary, we analyzed the spatial variability of E_{bed} at the transect-, reach-, and basin-scale, and the temporal variability of E_{bed} hourly, daily, and monthly.

SPATIAL AND TEMPORAL TRENDS IN BENTHIC LIGHT AVAILABILITY

From meta-analyses, field studies, laboratory studies, and model simulations, we found that the controls on benthic light availability exhibited general trends, both spatially and temporally. Temporally, optical water quality (i.e., water clarity) decreased with increasing discharge due primarily to greater amounts of particulates in the water column and secondly to greater concentrations of CDOM (Chapter II). Spatially, water clarity generally decreased along the river continuum due to increased particulate inputs from tributaries; however, in most rivers turbidity reached a maximum and then decreased due to increased groundwater discharge and sedimentation in the downstream direction (Chapter II). Benthic light availability is directly proportional to optical water quality (Equation 3.2), and therefore decreases in water clarity resulted in decreases in E_{bed}.

All investigations in this study occurred during the summer when leaf area index was greater than 90%, and therefore temporal trends in riparian vegetation were not assessed (Table 5.1). Temporal variations in topography and channel geometry were also beyond the scope of this study due to their fixed nature within the timescale of our analyses (Table 5.1). Spatial trends in channel geometry generally followed the trends of Leopold and Maddock (1953), where both width and depth increased in the downstream direction due to increasing discharge (Chapter IV). The increase in depth enhanced the effect of aquatic light attenuation in the downstream direction. The downstream increase in channel width indirectly increased E_{bed} by mitigating the shading by riparian vegetation and topography.

While the above trends are fairly intuitive and have been illustrated by other studies (but not collectively quantified), the results presented in this study on the effect of channel orientation on E_{bed} are novel (Chapters III and IV). We found that channel orientation could mitigate or exaggerate the effect of terrestrial shading, depending on the riparian community and size of river. For small rivers with a closed canopy and river sections with no canopy, the change in the shading coefficient (*s*) with channel orientation was minimal. But for large rivers with an open canopy and especially river sections with a half canopy, the change in *s* with channel orientation was considerable. For example, *s* at 270° was 66% higher than *s* at 90° for a 3-m wide half-canopy transect (Figure 4.4). We also found that for all canopy types, North-South orientated channels consistently provided greater shading because of the higher opacity of the channel margins and the smaller window for direct solar radiation transmission (Figure 3.11). Changes in channel orientation, as well as local changes in the other hydrogeomorphic controls, caused considerable variability in the magnitude of E_{bed} over short distances (Figures 3.9).

Model simulations revealed that the broad spatial pattern of E_{bed} for undisturbed forested rivers (i.e., continuous forested corridor and pristine optical water quality) followed a parabolic trend where E_{bed} was low in the headwaters due to terrestrial shading, low in the lower reaches due to aquatic attenuation, and high in the middle reaches where the product of terrestrial shading and aquatic attenuation was lowest (Figure 4.9B). Contrary to previous portrayals of longitudinal light profiles (e.g., Vannote et al. 1980), this trend was not smooth. There was considerable inter-sectional variability due predominantly to changes in channel orientation. Topography also caused

considerable local differences in E_{bed}. Because width, depth, and turbidity were modeled using rating curves, variability in E_{bed} caused by variations in these parameters was not assessed.

Through model manipulations, we found that anthropogenic watershed disturbances could alter E_{bed} by an order of magnitude in the upper reaches and dramatically shift longitudinal patterns (Figure 4.9). The riparian deforestation and degraded optical water quality associated with agriculturalization shifted the longitudinal profile in E_{bed} for Baraboo River from a parabolic to a logarithmic trend, where E_{bed} was much higher in the headwaters and generally decreased in the downstream direction. Selective riparian deforestation also resulted in high inter-sectional variability in E_{bed}. Because of the influence of benthic light availability on water temperature, water chemistry, primary productivity, and biotic behavior, altered light regimes likely impact fluvial ecosystems considerably.

DOMINANT CONTROLS ON BENTHIC LIGHT AVAILABILITY IN RIVERS

The inherent complexity and interdependencies in ecosystems makes it is impossible to quantify every forcing and feedback. Additionally, every landscape possesses a uniqueness in which ecosystem processes and their controls vary greatly from one ecosystem to the next (Phillips 2007). Therefore, our approach to characterizing benthic light availability in rivers was to identify the dominant controls. In this thesis, we have demonstrated that the dominant control on benthic light availability varied across spatial scales (Table 5.2).

The dominant control on spatial variations in E_{bed} for Big Spring Creek, our prototype small river, was riparian vegetation. Its narrow channel width (~7 m) resulted in substantial overhead vegetation shading of incoming PAR, as much as 85% for transects with a full canopy. Topography was not a factor on E_{bed} at Big Spring Creek because of low relief; however, topography is probably a dominant control in mountainous and canyon rivers. The dominance of riparian vegetation on E_{bed} at Big Spring Creek was also due to its shallow depth and relatively clear water (i.e., low aquatic attenuation), which is characteristic of most small rivers (Leopold and Maddock 1953). The lack of aquatic attenuation resulted in above-canopy PAR being the dominant control on temporal variations in E_{bed}.

The dominant control on E_{bed} for Deep River, our prototype medium river, was water depth. Its turbid water resulted in low E_{bed} for deeper sections of the channel due to increased aquatic attenuation. Pools deeper than 2 m had effectively no benthic PAR. The greater width of Deep River (~35 m) mitigated the effect of riparian shading, which accounted for only 32% of the reduction of incoming PAR. For large rivers such as the Amazon River (width ≈ 1 km), the effect of riparian shading on E_{bed} becomes negligible (Table 5.2). This mitigated terrestrial shading resulted in hydrologic regime being the dominant control on temporal variations in E_{bed}. In general, the dominance of the terrestrial controls on E_{bed} decreases in the downstream direction due primarily to increasing width. Conversely, the dominance of aquatic controls on E_{bed} increases in the downstream direction due to increasing turbidity and depth (Table 5.2).

FUTURE APPLICATIONS

This research investigated the link between river hydrogeomorphology and benthic light availability. While many of the general processes and trends in riverine light availability have been presented (Davies-Colley 1990, Kirk 1994, Smith et al. 1997, Davies-Colley and Payne 2000, Vahatalo et al. 2005), this was the first study to quantify the combined effects of all five hydrogeomorphic controls on E_{bed}. This study also presented the first reach-scale model that quantifies benthic light availability, calculating both spatial and temporal variability. Further, we presented a basin-scale version of BLAM, which we used to characterize broad spatial trends in E_{bed}. BLAM provides researchers with a tool to investigate relationships between light availability and ecosystem processes at a transect, along a reach, or throughout the river network.

Despite the many advances in quantitative ecology, most fluvial ecosystem models have been developed for hypothesis-testing rather than predictive tools (e.g., Poole et al. 2006). Because it is both a process-based and empirical model, BLAM has the capabilities to be used for hypothesis-testing and as a predictive tool, and thus has a variety of applications. The application of ecosystem dynamics to stream restoration is an emerging theme with many unanswered questions. BLAM offers to be a tool that can assess the role of riparian structure in river light availability and temperature. Additionally, BLAM has the potential to address some of the limitations of remote sensing applications such as spatio-temporal variability in water column attenuation coefficients and depth. Further, with increasing perturbations (e.g., urban runoff) to rivers progressively decreasing benthic light availability, BLAM offers to be a tool to

establish optical water quality targets. Finally, BLAM provides a framework for future models to assess the role of ultraviolet and infrared radiation in riverine ecosystems.

REFERENCES

Davies-Colley, R., and G. Payne. 2000. A simple approach for characterizing stream and riparian lighting. Pages 499-503 *in* International Conference on Riparian Ecology and Management in Multi-Land Use Watersheds. American Water Resources Association, Portland, OR.

Davies-Colley, R. J. 1990. Frequency distributions of visual water clarity in 12 New Zealand rivers. New Zealand Journal of Marine and Freshwater Research **24**:453-460.

Kirk, J. T. O. 1994. Light and Photosynthesis in Aquatic Ecosystems. Cambridge University Press, New York.

Leopold, L. B., and T. Maddock, Jr. 1953. The hydraulic geometry of stream channels and some physiographic implications. USGS Professional Paper **252**:1-57.

Phillips, J. D. 2007. The perfect landscape. Geomorphology **84**:159-169.

Poole, G. C., J. A. Stanford, S. W. Running, and C. A. Frissell. 2006. Multiscale geomorphic drivers of groundwater flow paths: subsurface hydrologic dynamics and hyporheic habitat diversity. Journal of the North American Benthological Society **25**:288-303.

Smith, D. G., R. J. Davies-Colley, J. Knoef, and G. W. J. Slot. 1997. Optical characteristics of New Zealand rivers in relation to flow. Journal of the American Water Resources Association **33**:301-312.

Vahatalo, A. V., R. G. Wetzel, and H. W. Paerl. 2005. Light absorption by phytoplankton and chromophoric dissolved organic matter in the drainage basin and estuary of the Neuse River, North Carolina (USA). Freshwater Biology **50**:477-493.

Vannote, R. L., G. W. Minshall, K. W. Cummins, J. R. Sedell, and C. E. Cushing. 1980. The river continuum concept. Can. J. Fish. Aquat. Sci. **37**:130-137.

Table 5.1. Effective timescales for the hydrogeomorphic controls on benthic light availability at a river transect, assuming no land-use change.

	Timescale		
Hydrogeomorphic Control	**Hourly-Daily**	**Weekly-Monthly**	**Yearly-Decadal**
Terrestrial Controls			
Topography	Fixed	Fixed	Fixed
Riparian Vegetation	Fixed	Variable	Fixed
Channel Geometry	Fixed	Fixed	Variable
Aquatic Controls			
Optical Water Quality	Variable	Variable	Fixed
Hydrologic Regime	Variable	Variable	Fixed

Table 5.2. Effectiveness of hydrogeomorphic controls on benthic light availability along the river continuum, assuming headwaters are located in mountains and the entire riparian zone is forested.

	Stream size (order)		
Hydrogeomorphic Control	**Small (1-3)**	**Medium (4-6)**	**Large (> 6)**
Topography	dominant	minimal	negligible
Riparian Vegetation	dominant	minimal	negligible
Channel Geometry			
Width	dominant	minimal	negligible
Depth	minimal	dominant	dominant
Planform	minimal	minimal	negligible
Optical Water Quality			
Particulates	minimal	dominant	dominant
CDOM	negligible	minimal	minimal
Phytoplankton	negligible	minimal	minimal
Hydrologic Regime	minimal	dominant	dominant

Notes: Stream size classification based on Vannote et al. (1980).

APPENDICES

Appendix 1. Partitioned OWQ for Wisconsin River (WR).

RK	c	c_w	c_d	c_p	a	a_w	a_d	a_p	b	b_w	b_d	b_p
0	4.100	0.150	0.492	3.458	1.145	0.148	0.499	0.498	2.955	0.002	-0.007	2.960
63	6.183	0.150	1.174	4.860	1.878	0.148	1.143	0.587	4.305	0.002	0.031	4.273
76	5.442	0.150	1.590	3.702	1.829	0.148	1.391	0.290	3.613	0.002	0.199	3.413
112	9.620	0.150	1.123	8.348	1.974	0.148	1.200	0.625	7.647	0.002	-0.078	7.722
155	5.036	0.150	1.042	3.845	1.578	0.148	1.096	0.333	3.459	0.002	-0.055	3.512
167	7.701	0.150	0.946	6.606	1.925	0.148	1.094	0.683	5.776	0.002	-0.149	5.923
177	9.653	0.150	2.119	7.385	3.356	0.148	1.930	1.278	6.297	0.002	0.189	6.107
205	9.650	0.150	2.293	7.207	3.468	0.148	1.926	1.394	6.183	0.002	0.367	5.814
250	8.868	0.150	1.665	7.053	2.463	0.148	1.660	0.656	6.405	0.002	0.006	6.398
292	13.806	0.150	1.596	12.060	3.500	0.148	1.426	1.926	10.306	0.002	0.170	10.134
302	10.351	0.150	1.773	8.429	3.248	0.148	1.643	1.456	7.103	0.002	0.129	6.972
356	11.532	0.150	2.773	8.610	3.995	0.148	2.339	1.508	7.537	0.002	0.433	7.102
444	9.120	0.150	2.422	6.548	3.200	0.148	2.144	0.908	5.920	0.002	0.277	5.641

488	8.860	0.150	1.778	6.933	2.242	0.148	1.347	0.747	6.618	0.002	0.430	6.186
524	13.772	0.150	1.344	12.279	2.773	0.148	0.988	1.637	11.000	0.002	0.356	10.642
548	11.524	0.150	1.115	10.259	2.954	0.148	1.007	1.800	8.570	0.002	0.109	8.460
590	13.861	0.150	1.115	12.596	2.759	0.148	0.959	1.653	11.102	0.002	0.157	10.943
613	15.708	0.150	1.204	14.355	2.582	0.148	0.999	1.435	13.126	0.002	0.205	12.919
639	18.718	0.150	1.202	17.366	3.164	0.148	1.006	2.010	15.554	0.002	0.196	15.356
674	22.777	0.150	1.273	21.355	3.597	0.148	1.013	2.436	19.180	0.002	0.260	18.919

Appendix 2. Partitioned OWQ for Baraboo River (BR).

RK	c	c_w	c_d	c_p	a	a_w	a_d	a_p	b	b_w	b_d	b_p
1	2.439	0.150	0.411	1.879	0.922	0.148	0.590	0.184	1.517	0.002	-0.179	1.695
3	1.593	0.150	0.567	0.877	0.896	0.148	0.684	0.064	0.697	0.002	-0.117	0.812
6	1.169	0.150	0.291	0.728	0.671	0.148	0.449	0.074	0.498	0.002	-0.158	0.655
7	2.492	0.150	0.508	1.835	1.080	0.148	0.694	0.238	1.412	0.002	-0.186	1.597
8	2.906	0.150	0.491	2.265	1.043	0.148	0.664	0.231	1.863	0.002	-0.173	2.034
9	3.281	0.150	0.733	2.398	1.526	0.148	0.879	0.499	1.755	0.002	-0.146	1.899
10	3.141	0.150	0.619	2.372	1.647	0.148	0.879	0.621	1.494	0.002	-0.260	1.751
14	3.547	0.150	0.673	2.725	1.669	0.148	0.874	0.648	1.878	0.002	-0.201	2.077
22	1.987	0.150	0.539	1.298	1.115	0.148	0.760	0.207	0.872	0.002	-0.221	1.091
24	3.996	0.150	0.513	3.333	1.733	0.148	0.793	0.792	2.263	0.002	-0.280	2.541
26	3.579	0.150	0.532	2.898	1.697	0.148	0.790	0.759	1.882	0.002	-0.259	2.139
27	3.817	0.150	0.538	3.129	1.536	0.148	0.772	0.616	2.281	0.002	-0.234	2.512
28	3.624	0.150	0.673	2.802	1.381	0.148	0.848	0.386	2.243	0.002	-0.175	2.416
38	4.237	0.150	0.524	3.563	1.580	0.148	0.714	0.718	2.657	0.002	-0.191	2.846

40	7.460	0.150	0.608	6.703	1.944	0.148	0.775	1.022	5.516	0.002	-0.167	5.681
72	29.265	0.150	0.610	28.505	3.851	0.148	0.789	2.915	25.414	0.002	-0.178	25.590
74	28.589	0.150	0.601	27.838	3.609	0.148	0.814	2.648	24.980	0.002	-0.213	25.191
113	34.281	0.150	0.590	33.542	3.966	0.148	0.757	3.061	30.315	0.002	-0.167	30.481
115	29.463	0.150	0.578	28.736	3.742	0.148	0.702	2.892	25.721	0.002	-0.124	25.843
142	38.293	0.150	0.681	37.462	4.373	0.148	0.809	3.417	33.920	0.002	-0.127	34.045
150	34.738	0.150	0.649	33.940	4.664	0.148	0.789	3.727	30.075	0.002	-0.140	30.213
160	34.489	0.150	0.665	33.674	4.106	0.148	0.728	3.230	30.383	0.002	-0.063	30.444
181	25.248	0.150	0.628	24.471	3.648	0.148	0.681	2.819	21.600	0.002	-0.053	21.652